TRANSPORTATION RESEARCH RECORD 1099

Concrete Pavement Design and Performance

TRB
TRANSPORTATION RESEARCH BOARD
NATIONAL RESEARCH COUNCIL
WASHINGTON, D.C. 1986

Transportation Research Record 1099
Price $9.00
Editor: Lisette Chou
Compositor: Harlow A. Bickford
Layout: Theresa L. Johnson

mode
1 highway transportation

subject area
24 pavement design and performance

Transportation Research Board publications are available by ordering directly from TRB. They may also be obtained on a regular basis through organizational or individual affiliation with TRB; affiliates or library subscribers are eligible for substantial discounts. For further information, write to the Transportation Research Board, National Research Council, 2101 Constitution Avenue, N.W., Washington, D.C. 20418.

Printed in the United States of America

Library of Congress Cataloging-in-Publication Data
National Research Council. Transportation Research Board.

Concrete pavement design and performance.

(Transportation research record, ISSN 0361-1981 ; 1099)
1. Pavements, Concrete—Design and construction—Congresses. 2. Pavements, Concrete—Evaluation—Congresses. I. National Research Council (U.S.). Transportation Research Board. II. Series.
TE7.H5 no. 1099 380.5 s 87-11311
[TE278] [625.8'4]
ISBN 0-309-04120-1

Sponsorship of Transportation Research Record 1099

GROUP 2 COUNCIL
David S. Gedney, Harland Bartholomew & Associates, chairman

Pavement Management Section
R. G. Hicks, Oregon State University, chairman

Committee on Rigid Pavements
Walter P. Kilareski, Pennsylvania State University, chairman
Ernest J. Barenberg, William E. Brewer, Larry Joe Burton, Albert J. Bush III, Richard N. Cochrane, Bert E. Colley, Robert R. Costigan, Raymond A. Forsyth, Ray H. Fowler, James L. Greene, Yang H. Huang, Michael P. Jones, T. J. Larsen, Richard A. McComb, B. Frank McCullough, Dennis W. Miller, John Minor, Robert G. Packard, Surendra K. Saxena, Gary Wayne Sharpe, Joe P. Sheffield, Roger E. Smith, William A. Yrjanson

George W. Ring III, Transportation Research Board staff

The organizational units, officers, and members are as of December 31, 1985.

Transportation Research Record 1099

The **Transportation Research Record** series consists of collections of papers on a given subject. Most of the papers in a Transportation Research Record were originally prepared for presentation at a TRB Annual Meeting. All papers (both Annual Meeting papers and those submitted solely for publication) have been reviewed and accepted for publication by TRB's peer review process according to procedures approved by a Report Review Committee consisting of members of the National Academy of Sciences, the National Academy of Engineering, and the Institute of Medicine.

The views expressed in these papers are those of the authors and do not necessarily reflect those of the sponsoring committee, the Transportation Research Board, the National Research Council, or the sponsors of TRB activities.

Transportation Research Records are issued irregularly; approximately 50 are released each year. Each is classified according to the modes and subject areas dealt with in the individual papers it contains. TRB publications are available on direct order from TRB, or they may be obtained on a regular basis through organizational or individual affiliation with TRB. Affiliates or library subscribers are eligible for substantial discounts. For further information, write to the Transportation Research Board, National Research Council, 2101 Constitution Avenue, N.W., Washington, D.C. 20418.

Contents

New Concepts in Prestressed Concrete Pavement

NEIL D. CABLE, B. FRANK MCCULLOUGH, AND NED H. BURNS

At least three potential benefits of prestressed concrete pavement (PCP) compared with conventional concrete pavement are indicated by previous research and testing. These include (*a*) more efficient use of construction materials; (*b*) fewer required joints and less probability of cracking; and (*c*) reduced overlay thickness that not only reduces the required quantity of concrete, but also would be advantageous where clearance is a problem under bridges, for example. Although several prestressed pavements have been constructed in the United States, the authors believe that the approaches used in these projects do not use the full potential of PCP. Other concepts should be explored that could more fully realize the benefits of PCP in highway construction. Seven new PCP concepts are introduced and developed in this paper: (*a*) central stressing of slip-formed pavement; (*b*) precast joint panels and slip-formed pavement; (*c*) precast joint panels, central stressing panels, and slip-formed pavement; (*d*) composite prestressed concrete pavement Type I (CPCPI); (*e*) composite prestressed pavement Type II (CPCPII); and (*f*) continuous composite concrete pavement (CCCP). The introduction to each new concept includes descriptions of its most important features and the principles involved. In addition, the characteristics of the seven new PCP concepts are compared to determine (*a*) the relative ability of the concept to address the problems encountered on previous projects, (*b*) the relative ability of each concept to effectively utilize the potential of PCP, and (*c*) what, if any, new problems are created with each concept.

In 1983 the Texas State Department of Highways and Public Transportation, commissioned the Center for Transportation Research, University of Texas, Austin, to study the design and construction of prestressed concrete pavement (PCP), with particular emphasis on overlay applications. A thorough review of the available literature to ascertain the current state of the art of PCP and a critical evaluation of the design, construction, and performance of several FHWA sponsored projects constructed during the 1970s led to the need for new concepts for the design and construction of PCP.

BACKGROUND

The objective of this paper is to describe the salient features of the PCP concepts developed by the project staff.

Center for Transportation Research, Department of Civil Engineering, The University of Texas at Austin, Austin, Tex. 78712-1075.

Scope

The PCP concepts are present in the following order: (*a*) central stressing of slip-formed pavement; (*b*) precast joint panels and slip-formed pavement; (*c*) precast joint panels, central stressing panels, and slip-formed pavement; (*d*) composite prestressed concrete pavement Type I (CPCPI); (*e*) composite prestressed concrete pavement Type II (CPCPII); (*f*) segmentally precast prestressed concrete pavement (SPPCP); (*g*) continuous composite concrete pavement (CCCP); and (*h*) others.

In the next section a description of each concept is provided, followed by a detailed comparison of the most important characteristics of the various PCP concepts.

DESCRIPTION OF NEW CONCEPTS

Concept 1: Central Stressing of Slip-Formed Pavement

All of the past FHWA-sponsored PCP projects consisted of consecutive slip-formed slabs separated by short openings to permit posttensioning of the prestressing tendons from the slab ends. Because of the slab lengths and correspondingly high strand and subgrade frictions, it was necessary to stress each strand from both ends. After the posttensioning had been applied and the elastic shortening and most of the creep had occurred, the openings were filled with concrete gap slabs.

One of the objectives was to find a method of posttensioning the strands that would eliminate gap slabs and the problems associated with their use, but still permit taking advantage of the slip-form method of pavement construction. The most promising alternative was central stressing. Central stressing is a procedure by which the strands are stressed at internal blockouts or stressing pockets. The blockouts are filled with concrete after the posttensioning force has been applied.

Another objective was to investigate alternative methods for transversely prestressing pavement. It was believed that transverse prestressing is important to resist the applied wheel loads, prevent longitudinal pavement cracking, and prevent possible separation of separately placed pavement lanes or longitudinal pavement strips.

This concept is illustrated in a plan view of the pavement shown in Figure 1; an enlarged plan view of a stressing pocket is shown in Figure 2. The advantages and disadvantages of using a looped transverse tendon configuration are discussed in detail later in this paper. This design was accepted by the Texas

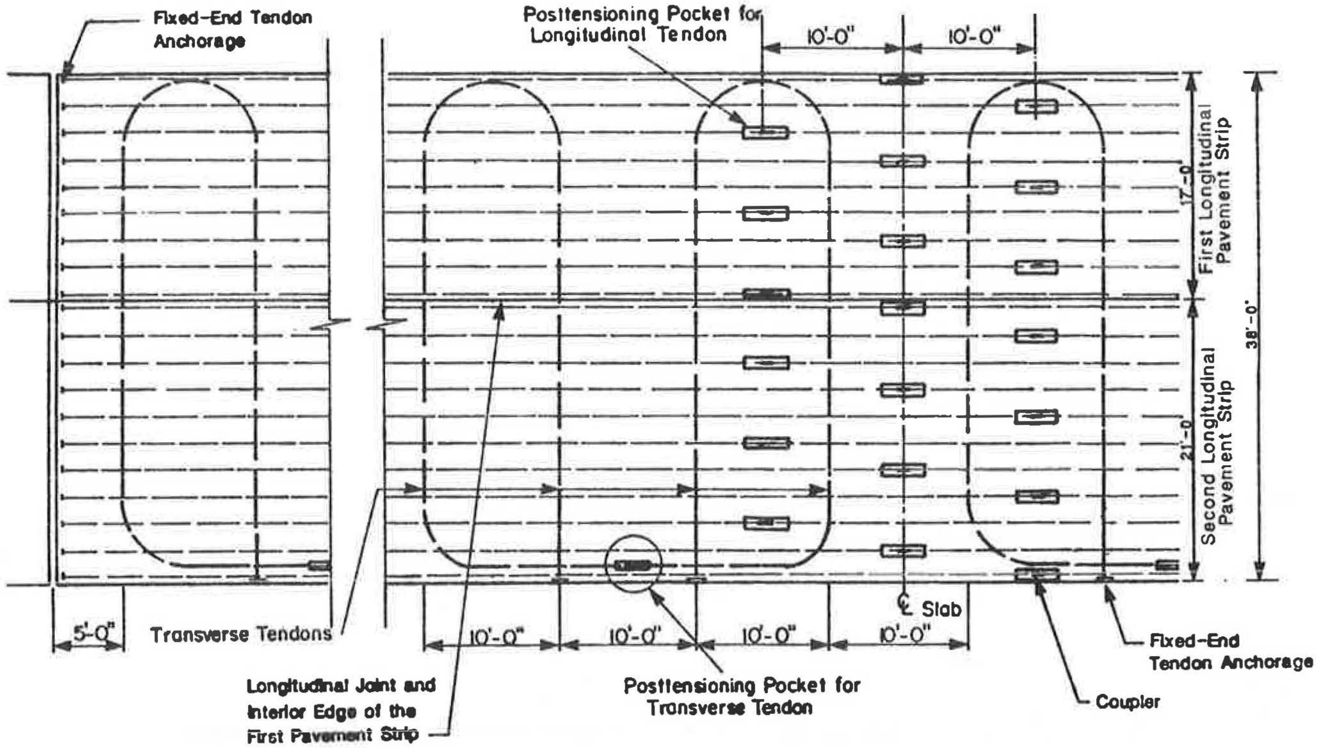

FIGURE 1 Plan view of the pavement during central stressing.

State Department of Highways and Public Transportation (SDHPT) for construction of the 1-mi demonstration overlay project on U.S. Interstate 35. The project will be located near Waco, Texas.

Concept 2: Precast Joint Panels and Slip-Formed Pavement

As implied by its name, precast concrete joint panels are used with precast joint panels and slip-formed pavement. The remainder of the pavement would be slip-formed. Concept 2 is shown in Figures 3 and 4.

The panels would most likely be cast off the job site in a precast plant or in a construction yard nearby and would then be transported to the site and set in place.

The precast panels would be provided in pairs, one on each side of every transverse joint. The same type of transverse joint assembly used in Concept 1 would also be used with this PCP concept. Each pair of joint panels would contain an entire transverse joint assembly, including the steel extrusion into which the neoprene seal is inserted, associated headed studs or deformed bar anchors, base angle (if required) to support the steel extrusion, dowels, and dowel expansion sleeves.

Each panel would contain the pockets for stressing the longitudinal pavement tendons and a single rigid transverse duct that

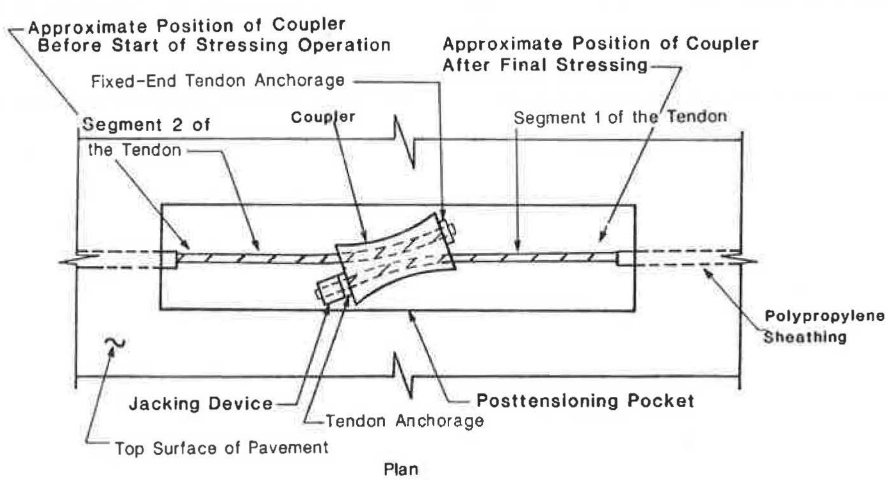

FIGURE 2 Stressing pocket detail.

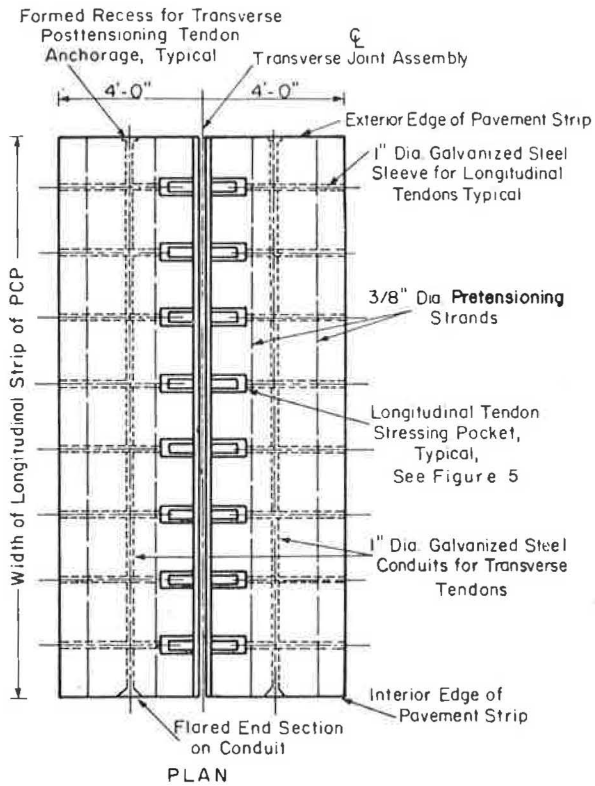

FIGURE 3 Precast joint panels.

would be used for posttensioning the precast joint panels together in the first and second pavement strips.

Each individual panel would be prestressed on the casting bed in the precast plant to a level sufficient to prevent it from cracking as a result of either lifting and handling before placement, or traffic loads after the panel is in its final position in the pavement.

Concept 3: Precast Joint Panels, Central Stressing Panels, and Slip-Formed Pavement

This PCP concept uses precast concrete joint panels as described in Concept 2 (see Figures 3 and 4). In addition, precast concrete stressing pavement are also used. These stressing panels would be located at the midlength of each pavement segment and would contain stressing pockets in which the longitudinal tendons would be jacked (see Figures 5 and 6). They would also contain a rigid transverse duct that would be used to posttension two adjacent stressing panels together. These panels would also permit the use of couplers for stressing the longitudinal tendons.

All the panels would be cast off the job site, transported to the site, and set in place with a truck crane. The remainder of the pavement would be slip-formed.

Concept 4: Composite Prestressed Concrete Pavement Type I (CPCPI)

Precast concrete joint panels similar to those used with PCP Concepts 2 and 3 would also be used with this PCP concept (see Figure 3). These joint panels were described in Concept 2. Central stressing panels similar to those used in PCP Concept 3 could be used with this concept if central stressing is desired (see Figure 5).

In addition, still another type of precast panel used with this PCP concept is the base panel shown in Figures 7 and 8. Like the panels used with the previous concepts, these panels would be cast off the job site. They would be prestressed on the casting beds to compensate for both handling and some in-place stresses. In addition, each base panel would contain a hollow transverse conduit.

All of the various types of precast panels would be transported to the job site and set in place with a truck crane. The

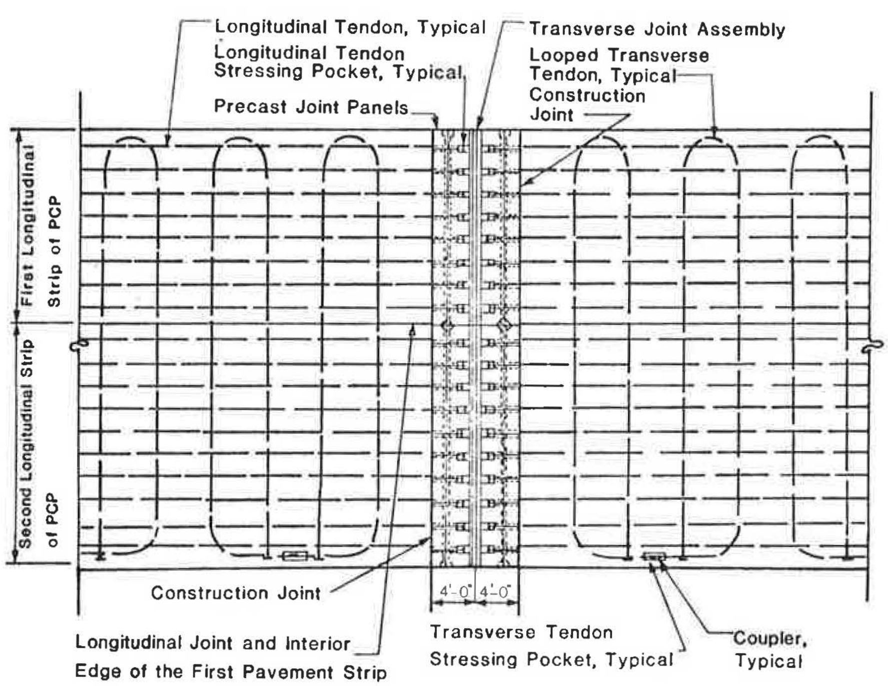

FIGURE 4 Precast joint panels and slip-formed pavement.

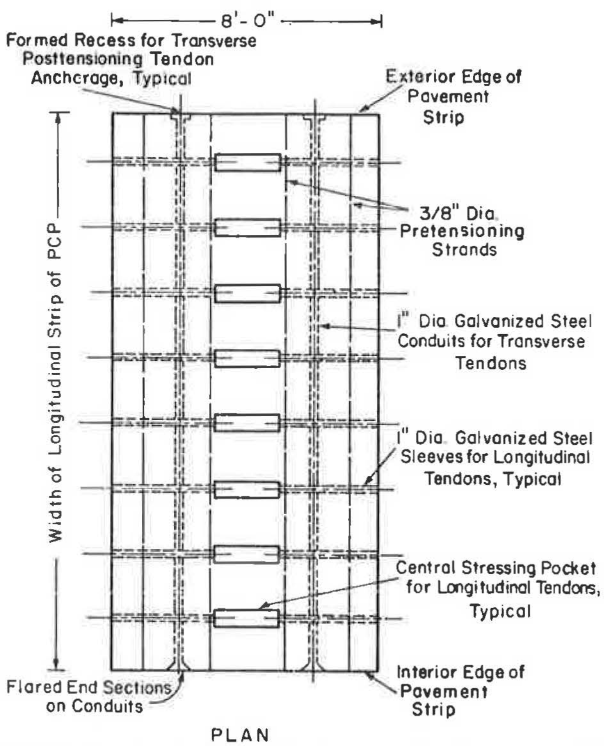

FIGURE 5 Central stressing panel.

concrete wearing course would be slip-formed in place after placement of the precast panels.

Concept 5: Composite Prestressed Concrete Pavement Type II (CPCPII)

Precast concrete joint panels similar to those used in PCP Concepts 2, 3, and 4 would be used for CPCPII. Also, central stressing panels similar to those used in PCP Concept 3 could be used with this concept if the central stressing technique is desired (see Figure 5).

Base panels used for CPCPII would be similar to those used for CCPI in that they would be cast off the job site and contain a hollow transverse conduit. However, the base panels for CPCPII would be thicker than those used for CPCPI; the top surface of the panels would be grooved (which would allow the longitudinal tendons to be located at, or slightly below, the centroidal axis of the panel); and the edge of the panel would be formed to permit grouting of the joints between adjacent panels after they are set in place at the job site (see Figures 9 and 10).

Concept 6: Segmentally Precast Prestressed Concrete Pavement (SPPCP)

Precast concrete joint panels similar to those used in PCP Concepts 2 through 5 would also be used with Concept 6 (see Figure 3). In addition, central stressing panels similar to those used in PCP Concept 3 could be used with this concept if central stressing is desired (see Figure 5).

A panel type, referred to in this section as a full-depth pavement panel would be used with PCP Concept 6. This panel is shown in Figures 11 and 12. Like all the panels used with the previous concepts, these panels would also be cast off the job site. They would be prestressed on the casting beds to compensate for both handling and some in-place stresses. In addition, each full-depth panel would contain hollow longitudinal conduits and a single hollow transverse conduit.

All of the various types of precast panels would be transported to the job site where they would be set in place with a truck crane. No slip-formed concrete wearing course would be used with this concept.

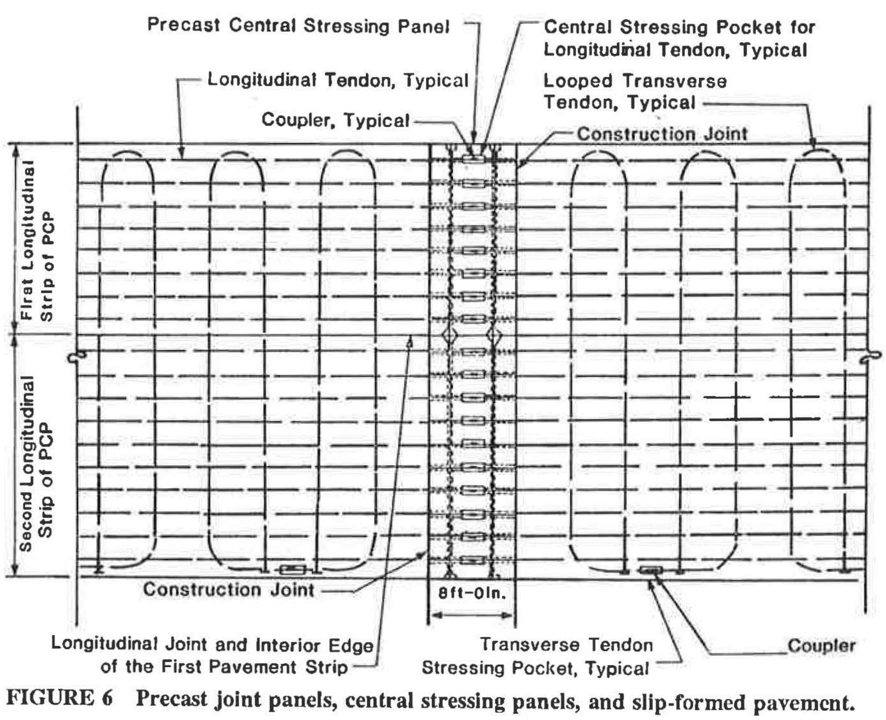

FIGURE 6 Precast joint panels, central stressing panels, and slip-formed pavement.

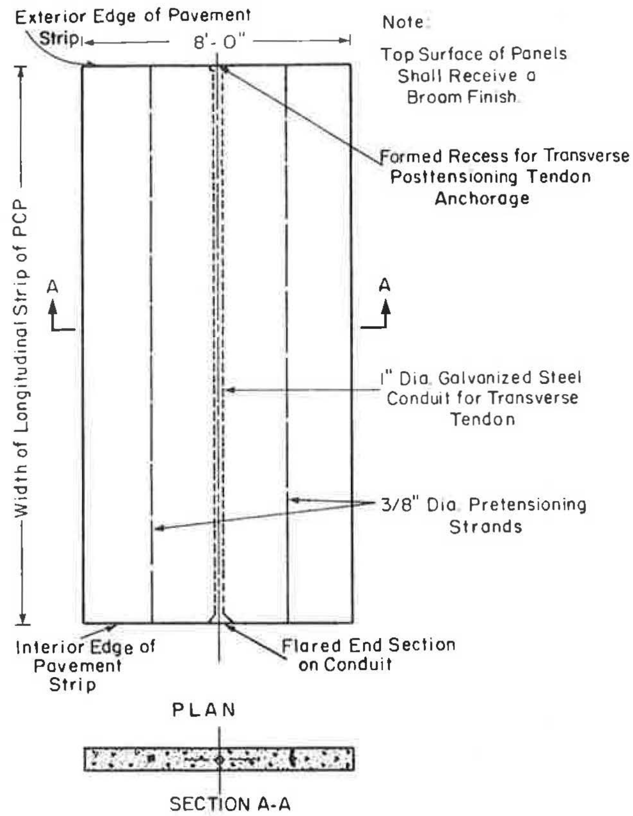

FIGURE 7 CPCPI base panel.

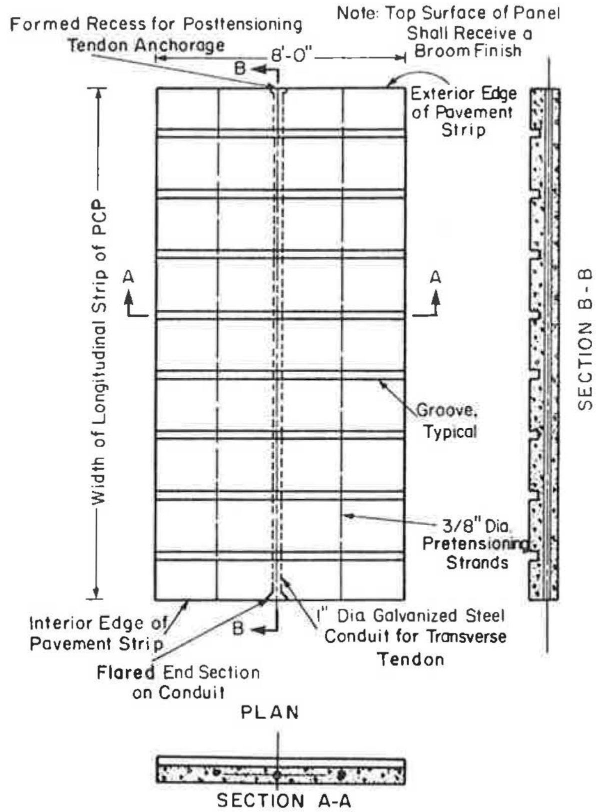

FIGURE 9 CPCPII base panel.

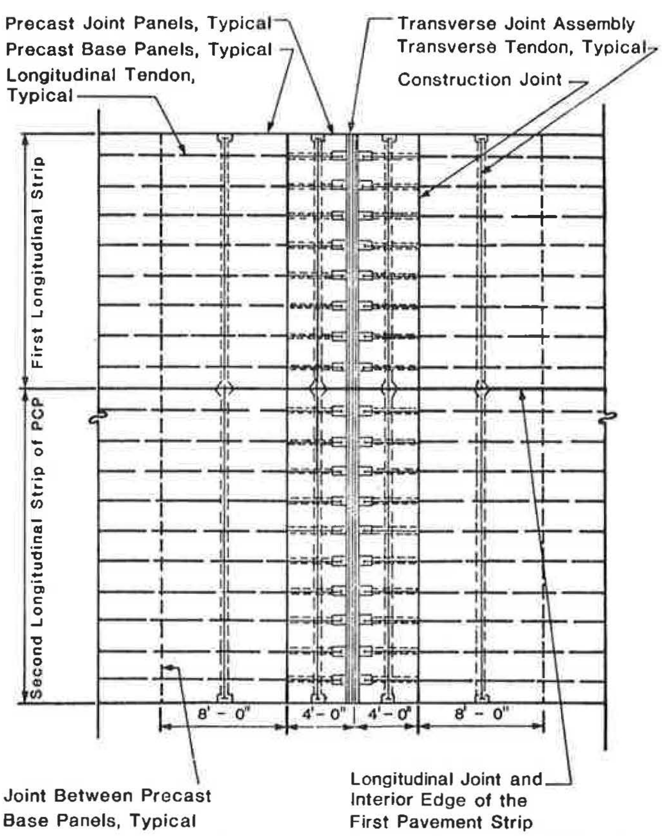

FIGURE 8 Composite prestressed concrete pavement Type I (CPCPI).

Concept 7: Continuous Composite Concrete Pavement (CCCP)

CCCP is very different from any of the concepts discussed thus far, and, in reality, is more similar to the concept of continuously reinforced concrete pavement, as will become apparent in the following discussion.

No joint panels would be used with CCCP because no transverse joints would be required, except where construction joints are needed when the paving operation is interrupted or where expansion joints are needed, for example, at bridges. Only precast concrete base panels (as shown in Figures 13 and 14) would be used in CCCP construction. These panels would be cast off the job site in the same manner as panels used in the previously discussed concepts. They would be prestressed in both directions on the casting bed to compensate for all handling and in-place stresses. In addition, the panels would contain grooves or slots that would be perpendicular to the panel edges. These grooves would accommodate tie bars between adjacent panels.

The precast concrete panels would be transported to the job site to be set in place with a truck crane. The concrete wearing course would be slip-formed in place after placement of the precast panels.

COMPARISON OF CONCEPT CHARACTERISTICS

Summarized in Table 1 is the relative ability of each of the foregoing new concepts to address the problems encountered

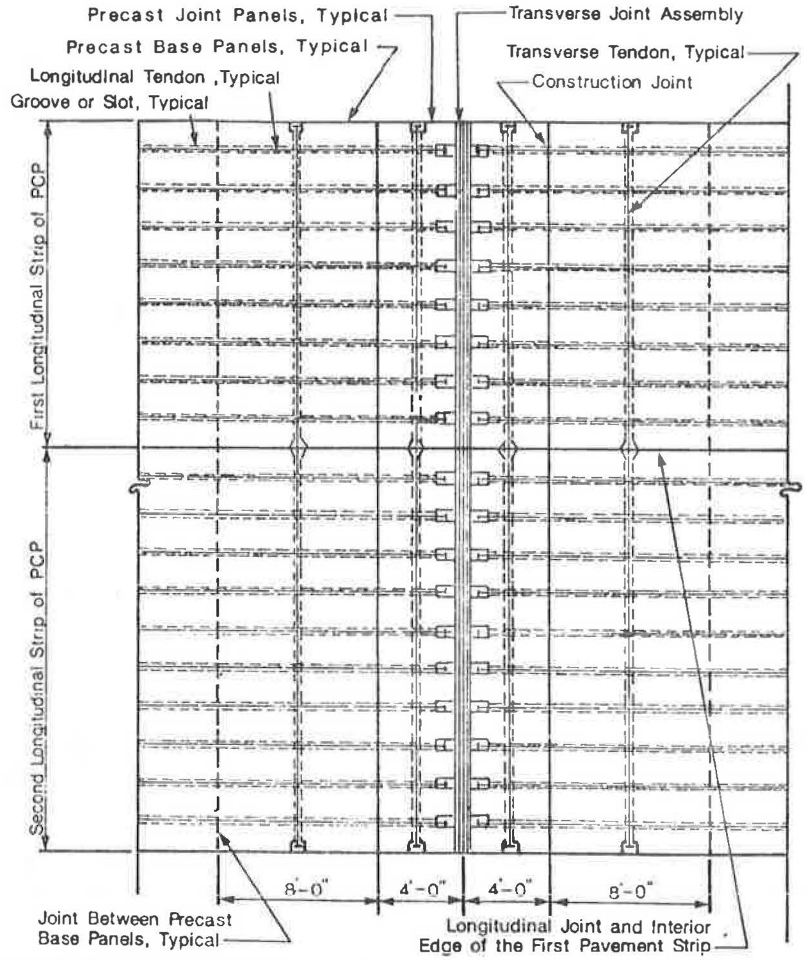

FIGURE 10 **Composite prestressed concrete pavement Type II (CPCPII).**

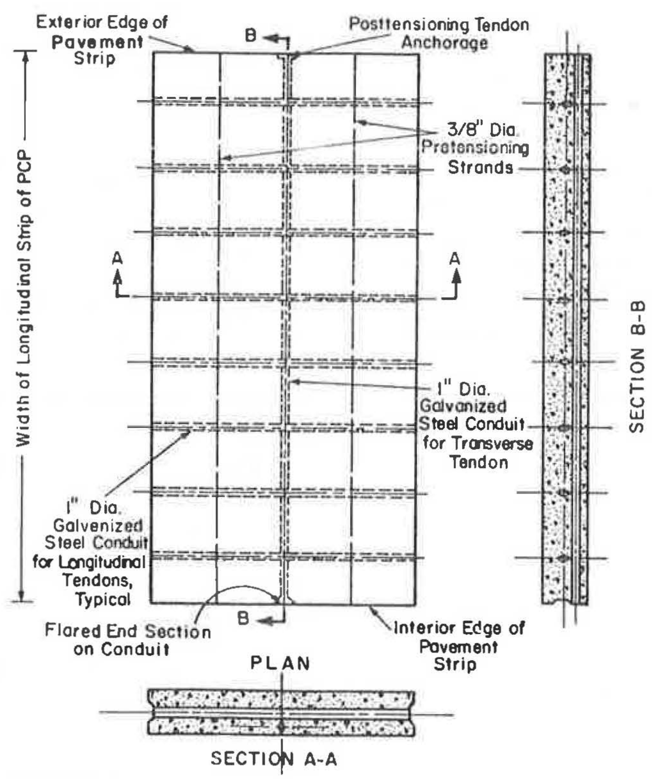

FIGURE 11 **Full-depth pavement panel.**

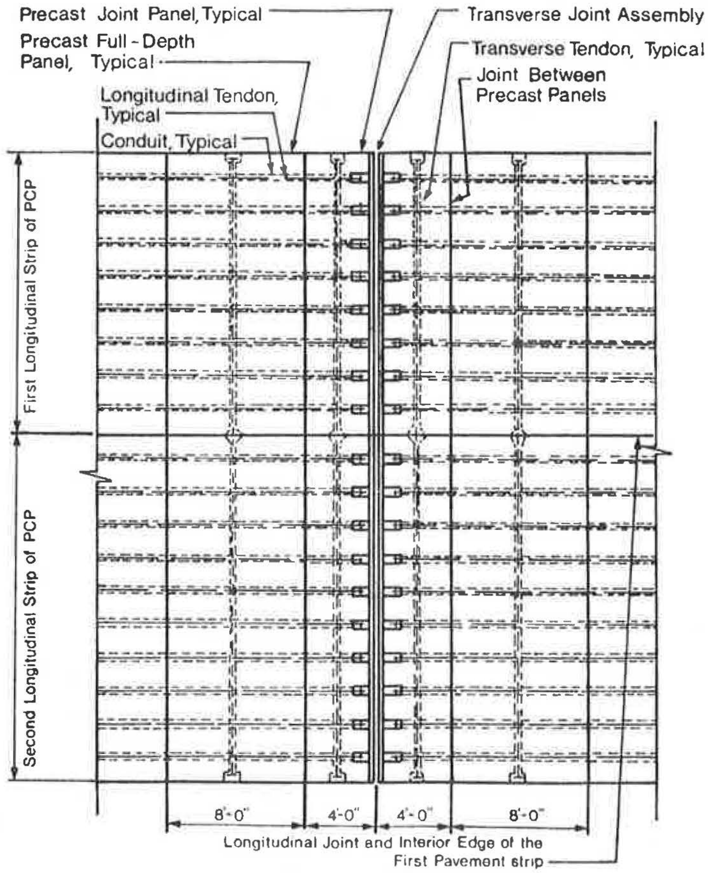

FIGURE 12 Segmentally precast prestressed concrete pavement (SPPCP).

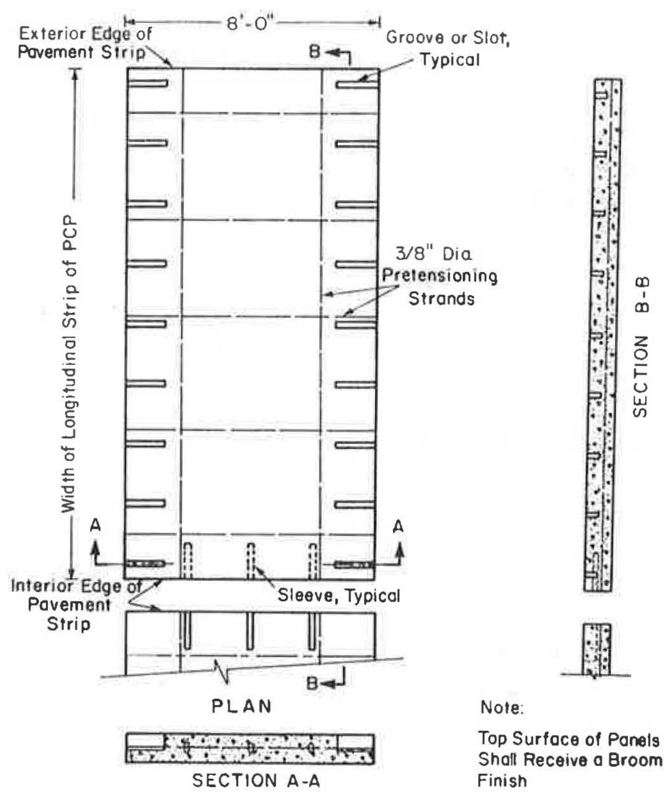

FIGURE 13 CCCP base panel.

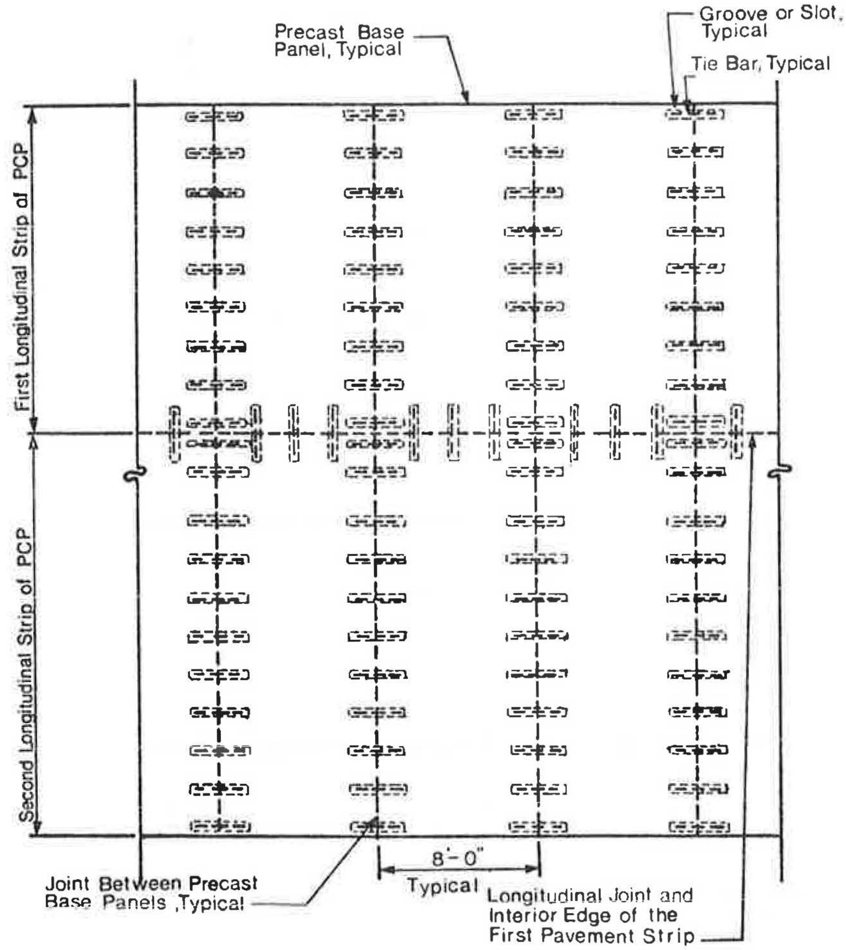

FIGURE 14 Continuous composite concrete pavement (CCCP).

TABLE 1 COMPARISON OF PCP CONCEPT CHARACTERISTICS

CHARACTERISTIC	PCP CONCEPT NUMBER 1	2	3	4	5	6	7
Precast Concrete Panels							
- Utilization of high quality, mass produced, precast, prestressed concrete panels:							
(a) Significant				X	X	X	X
(b) Less significant		X	X				
(c) None used	X						
- Relative importance of the fact that the precast panels must be transported to the job site:							
(a) Significant				X	X	X	X
(b) Less significant		X	X				
(c) Not a factor	X						
Bonded vs. Unbonded Tendons							
- Suited to the use of unbonded tendons	X	X	X	X	X	X	NA*
- Relative difficulty associated with the use of bonded tendons							
(a) Significant	X	X	X				
(b) Less significant				X			
(c) Least significant					X	X	X

TABLE 1 *continued*

CHARACTERISTIC	PCP CONCEPT NUMBER 1	2	3	4	5	6	7
- Number of posttensioning operations required for each longitudinal tendon:							NA
(a) One					X	X	
(b) Three	X	X	X	X			
- Less expensive unsheathed posttensioning strands could be used					X	X	
Transverse Prestress							
- Difficulties associated with laying out and holding the transverse tendons in a looped configuration	X	X	X				
- Pavement transversely prestressed before being subjected to construction traffic				X	X	X	X
- Transverse prestress level in adjacent lanes can be varied in accordance with the anticipated traffic volumes				X	X	X	X
- Eliminate all posttensioning operations in the field							X
Friction-Reducing Mediums							
- Relative difficulty associated with handling and placing polyethylene sheeting:							
(a) Significant	X	X	X				
(b) Less significant				X	X	X	
(c) None							X
- Construction operations (i.e., setting tendon chairs, placing tendons, and slip-forming pavement) would be conducted in direct contact with polyethylene sheeting	X	X	X				
- Polyethylene sheeting would be protected from construction operations				X	X	X	
- Eliminate the need for polyethylene sheeting							X
Gap Slabs vs. Central Stressing							
- Elimination of gap slabs	X	X	X	X	X	X	X
- Number of tendon stressing pockets which must be formed in the field:							
(a) Greatest	X						
(b) Minimal		X	X				
(c) None				X	X	X	X
- Couplers for posttensioning tendons:							
(a) Required	X		X				
(b) Optional				X	X	X	
(c) None used		X					X
- An additional concrete placement operation is required to fill the stressing pockets after completion of final posttensioning operations	X	X	X	X		X	NA
Prestress Force Transference							
- Level of compressive stress which can be applied by posttensioning at early concrete age is dependent on:							NA
(a) Concrete strength	X	X	X	X	X	X	
(b) Tendon anchorage size	X						
(c) Tendon spacing	X						

TABLE 1 *continued*

	PCP CONCEPT NUMBER						
CHARACTERISTIC	1	2	3	4	5	6	7
- Application of initial prestress force:							NA
(a) Prestress force transferred from tendons to immature concrete via individual tendon anchorages, thus limiting the amount of prestress that can be applied at early concrete age	X						
(b) Prestress force transferred from tendons to precast joint panels and then to the immature concrete, allowing greater initial prestress force to be applied at early concrete age		X	X	X	X	X	
- Possible long-term problems due to tensile stresses at the end of each pavement section caused by prestressing							
(a) Possible	X						
(b) Significantly decreased likelihood		X	X	X	X	X	
(c) No likelihood							X
Tendon Placement							
- Chairs required to support tendons during slip-forming	X	X	X				
- No chairs required to support tendons during slip-forming				X	X	X	X
Transverse Joints							
- Relative difficulty associated with holding the transverse joint assembly stationary while applying tension to the longitudinal tendons before the pavement concrete is placed:							NA
(a) Significant	X						
(b) Less significant		X	X				
(c) None				X	X	X	X
- Difficulties associated with concrete placement and consolidation in the vicinity of the transverse joint assembly in the field	X						
Multiple Longitudinal Strip Construction							
- Problems associated with transverse tendons protruding from the first pavement strip	X	X	X				
- Concrete formwork required along the interior edge of the first pavement strip	X	X	X				
Concrete Compaction							
- Reduced difficulty in obtaining good compaction of slip-formed concrete because of reduced cast-in-place concrete depth				X	X	NA	X
Protection of Tendon Anchorages							
- Tendon anchorages completely encased and protected in the concrete pavement	X	X	X	X	X	X	X
Adverse Construction Conditions							
- Reduction in required quantity of cast-in-place concrete which reduces vulnerability to adverse construction conditions:							
(a) Significant				X	X	X	X
(b) Less significant		X	X				
(c) None	X						

TABLE 1 *continued*

CHARACTERISTIC	PCP CONCEPT NUMBER 1	2	3	4	5	6	7
- Problems associated with stopping construction at intermediate points:							
(a) Significant	X	X	X				
(b) Less significant				X	X	X	X
- Possibility of being able to quickly open the pavement to traffic						X	X
Alternate Uses							
- Possibility of being used for a special purpose, temporary, reusable pavement						X	
- Damaged sections easily repaired							X
Alternate Materials and Methods							
- In addition to strand, high-strength bars can be used for transverse posttensioning				X	X	X	
- Possibility of using high-strength bars for longitudinal posttensioning					X		
- Couplers for posttensioning tendons:							
(a) Required	X		X				
(b) Optional				X	X	X	
(c) None used		X					X
- Possibility of using alternate wearing course materials							X
Unfamiliarity							
- Organizations responsible for selecting pavement systems are unfamiliar with the concept	X	X	X	X	X	X	X
- Paving contractors unfamiliar with the concept	X	X	X	X	X	X	X

*NA = Not Applicable

on previous projects and to effectively utilize the potentials of PCP together with possible new problems created with each concept. The comparison is made with regard to the following aspects:

1. Bonded versus unbonded tendons,
2. Transverse prestressing and looped tendons,
3. Friction-reducing mediums,
4. Gap slabs versus central stressing,
5. Prestress force transference,
6. Tendon placement,
7. Transverse joints,
8. Multiple longitudinal strip construction,
9. Concrete compaction,
10. Protection of tendon anchorages,
11. Adverse construction conditions,
12. Alternative uses,
13. Alternative materials and methods, and
14. Unfamiliarity.

SUMMARY

The purpose of this paper was to introduce seven new PCP concepts.

The introduction to each new concept included descriptions of its most important features and discussions of the anticipated sequence that would be used in the construction of a section of PCP utilizing the concept. In addition, the characteristics of the seven new PCP concepts were compared to determine (*a*) the relative ability of each concept to address the problems encountered on previous projects, (*b*) the relative ability of each concept to effectively utilize the potential of PCP, and (*c*) what, if any, new problems are created with each concept.

No attempt was made to identify the best concept because each has its own strengths and weaknesses and different situations may require the use of one concept instead of another. Additional testing is needed to further develop the concepts and determine their viability.

ACKNOWLEDGMENT

The authors acknowledge the combined efforts and support of the Center for Transportation Research at the University of Texas, Austin, and the Texas State Department of Highways and Public Transportation, in cooperation with the Federal Highway Administration, U.S. Department of Transportation. Special thanks are expressed to the staff of the Center for Transportation Research for assistance in the preparation of the figures for this paper.

Mechanical and Environmental Stresses in Continuously Reinforced Concrete Pavements

S. K. SAXENA AND GEORGE T. DOUNIAS

The examination of the combined effects of mechanical and environmental stresses on continuously reinforced concrete (CRC) pavements is accomplished by superimposing the effects of the one onto those of the other. The mechanical stresses are evaluated by a three-dimensional analysis and thermal stresses by two-dimensional analysis. It has been demonstrated that environmental loads constitute the severest loads the pavement is subjected to. Also studied is the comparison of stresses due to one single axle 18-kip load to stresses due to two trucks and a car on a three-lane highway. The ratio of maximum stresses by two loadings may be very useful for a comprehensive understanding of pavement performance when it is designed by the equivalent 18-kip concept.

A major concern in the design of rigid portland cement concrete (PCC) pavements is to control undesirable cracks by using the proper control joints. Despite the efforts to establish the ideal type of joints, most of the undesirable features of natural cracks accompany their use. In response to this problem an effort was made to eliminate the joints and in 1921 the first continuously reinforced concrete (CRC) pavement was constructed by the U.S. Bureau of Public Roads.

On the other hand, to overcome difficulties in maintenance operation, the FHWA proposes the use of zero maintenance pavements which require no maintenance during their first 20 years and only minor repairs during the following 10 years before rehabilitation.

The present study reviews some of the existing methods for pavement stress evaluation and examines a premium pavement using a refinement of a model proposed by Saxena et al. (*1*).

Illinois Institute of Technology, Civil Engineering Department, Chicago, Ill. 60616.

EXISTING ANALYSIS METHODS

Mechanical Loads

Westergaard (*2*, *3*) expanded the theory of slabs created by Hertz (*4*) to include the so-called Winkler foundation. In order to solve the basic differential equation for medium-thick plates, the deflection at any point on the subgrade surface is assumed directly proportional to the vertical stress applied at that point in Winkler foundations; this proportionality is also assumed constant. Therefore, the foundation is represented by individual springs with stiffness k, which is commonly referred to as modulus of subgrade reaction. The values of this constant are determined from plate loads tests.

Some years later Hogg (*5*) and Holl (*6*) solved the same problem with the assumption that the slab is supported by an elastic solid. In their solution, they incorporated the Boussinesq's classic solution for the deflection of an elastic solid resulting from a point load.

Both the aforementioned solutions are available in most of the texts dealing with pavements. Influence charts similar to those prepared by Newmark, solving Westergaard's and Hogg's equations, were presented by Picket and Ray (*7*). Those charts have been extensively used in pavement design and are still the only widely available information for wheel-load stresses.

Hudson and Matlock (*8*) proposed a discrete element model that treats the slab as a set of rigid bars connecting elastic hinges, and with torsion springs connecting adjacent parallel bars. The subgrade was again modelled by the coefficient of subgrade reaction, k (modulus of subgrade reaction K = kb, with B as the width of the slab). This model is capable of handling combination loads that include lateral loads in plane forces and applied couples or moments. Also, discontinuities in the slab and the support and variation of slab thickness can be easily considered to evaluate the effect of cracking, loss of support and nonuniformity in the slab.

The characterization of subgrade by a coefficient of subgrade reaction k is by Winkler and is therefore known as Winkler subgrade. A critical review of the Winkler subgrade and elastic-istoropic solid subgrade has been provided by Vesic and Saxena (*9*). It has been shown that there is no single value of k that can give perfect agreement of all statical influences in a particular case, unless the subgrade thickness is limited to a maximum of 2.5 stiffness radii of the slab. Simple analytical expression for evaluation of k was developed as:

$$k = 0.91\ \{[E_s(1 - \upsilon^2)]/[E(1 - \upsilon_s^2)]\}^{1/3}\ \{E_s/[(1 - \upsilon_s^2)h]\} \qquad (1)$$

where

E, E_s = modulus of elasticity of slab and subgrade, respectively;
υ, υ_s = Poisson's ratio of slab and subgrade, respectively; and
h = thickness of slab.

Good agreement of bending movements or stresses in the slab only are provided by Equation 1.

To obtain a good agreement of deflections, a 2.4 times lower value of k should be used:

$$k = 0.42\ \{[E_s(1 - \upsilon^2)]/[E(1 - \upsilon_s^2)]\}^{1/3}\ \{E_s/[(1 - \upsilon_s^2)h]\} \qquad (2)$$

Saxena (*10, 11*) extended this model by introducing the equilibrium of forces including the subgrade support and by treating the subgrade as an isotropic elastic half space. The subgrade is represented by a modulus of elasticity E_s and Poisson's ratio υ_s. A model test was performed under control conditions to compare the experimental results with those obtained from an elastic solid model as well as a Winkler model. As shown by the results (*11*), the values of deflection computed from Westergaard's formula and those using Winkler subgrade are comparable. These values differ from the elastic solid subgrade and the analytical results using elastic solid subgrade are in remarkable agreement with observed deflections.

All theories based on the classical plate theory have one major drawback. They assume the reaction of the supporting media to be vertical. In modern highway construction practice, various subbase types are used; some have relatively high stiffness and in many cases, the slab–subbase interface develops very good friction. This friction has been ignored and, as a result, the contribution of the subbase in the reduction of slab stresses is considered only as a reinforcement of the subgrade ability to carry vertical loads. Stress reduction due to friction has been proven to be significant, especially in the case of stiff subbase. The plate theory works very well in the case of a very weak or nonexisting subbase, because the assumptions made in the plate theory are well approximated. Many experiments have verified stress reduction by friction and have led to the adaptation of plate theory methods for extensive use. Theories based on the elastic subgrade hypothesis are approximating the problem better; however, they still do not have the ability of modeling the variations in the subbase and natural soil.

Environmental Loads

The stresses caused by temperature variations were divided into temperature-drop and warping stresses, and were examined separately.

Temperature-drop stresses result only when there is friction between the slab and the supporting subgrade that resists the slab shrinkage. Because contraction due to temperature drop can be easily evaluated, the principal concern is to model the friction in the interface. Kelley (*12*) provides a rational friction distribution. Assuming the proposed distribution, evaluation of tensile stresses is relatively easy. Some complications may occur when friction exceeds the shear resistance of the subgrade or when the slab is curled due to temperature differentials (causing discontinuous contact).

In an attempt to deal with the stresses caused by the temperature differential through the slab, Westergaard considered an infinite slab and developed equations representing the curved surface. Based on the stresses found this way, he provided equations for semi-infinite slab and slab with finite width. Furthermore, investigations on Westergaard's equations were conducted by Harr and Leonards (*13*) to compute the stresses, deflections, and loss of support due to warping effects. Lewis and Harr (*14*) further elaborated and extended the work on warping stresses.

The described methods of temperature-drop and warping stress evaluation have the following weak points:

1. Not applicable to slab-subbase separation.
2. The assumption of uniform stress distribution in the slab is not always a good approximation and may result in stress underestimation.
3. Apply only to stresses caused by the slab weight when it resists the curling. Forces transmitted to the subgrade, or friction in the interface between slab and subgrade are not considered.
4. The temperature drop occurs simultaneously with a temperature gradient in the slab which not only causes separation but also some vertical stresses in the interface that change the friction distribution.

Furthermore, the existing methods do not consider the contribution of the subbase-subgrade temperature variations in the general slab performance.

Methods Used in Design Manuals

A study of the widely used design manuals indicated that the only stress incorporated in the pavement design is that due to wheel loads. Environmental loads are considered only indirectly by reducing the strength of the supporting subbase-subgrade system.

For the wheel-load stresses, Westergaard's formula is used. The modulus of subgrade reaction is evaluated by plate load tests, and to account for the subbase contribution, charts are used to modify the subgrade modulus as a composite one. The wheel-load stresses are then evaluated using Westergaard's solution with inputs of wheel load, slab thickness, and composite k-value. This solution is usually provided in charts. The modulus of elasticity for the slab is assumed equal to 4 million psi and the load is distributed over a circular area with contact tire pressure equal to 75 or 80 psi.

The aforementioned method may result in overestimation of the stresses in two ways: (*a*) by excluding the friction factor in the interface between slab and subbase, and (*b*) by frequently considering only the truck load acting on one circular area with contact pressure of 80 psi. This is obviously not correct because the load is transmitted through two or four wheels on the pavement.

Computer Program CRCP-2

CRCP-2 is an extension and revision of the CRCP-1 computer program for analysis of CRC pavements, developed by the Center for Highway Research at the University of Texas, Austin (*15, 16*). The CRCP-2 program incorporates drying shrinkage, temperature drop, and wheel loads. The theoretical model was based on the interaction between steel, concrete, subgradė and the internal forces caused by temperature drop and drying shrinkage. Differences in thermal coefficients of steel and concrete, together with the drying shrinkage of concrete determine the internal stresses in the slab. The friction–movement characteristics of the slab and the soil determine the degree of restraint of the supporting medium. Crack spacing is also determined by comparing concrete stress with concrete strength. If known, wheel-load stresses are input into the model. Alternatively, they are evaluated by Westergaard's equation for interior loading and added to those found by the model. Warping stresses and fatigue due to repetitive loads are not considered.

Inputs are the width and material properties of the concrete slab, type and properties of steel reinforcement, tensile strength data, slab-base friction characteristics, temperature data, and external load. Temperature data consist of minimum temperatures during the first 28 days of construction and minimum temperature expected after the 28th day. The program solves for cracking spacing, crack width, and maximum steel and concrete stresses.

The most important variable in the program is crack spacing. Because all loads contribute in crack spacing they must be considered as acting together.

The CRCP-2 program is a useful tool; however, the formulation of the mathematical model does not consider wheel loads. If no other information is available, Westergaard's solution is used. Also, there is no temperature variation throughout the slab and the resulting stresses due to temperature drop and drying shrinkage are uniformly distributed. The warping effect, perhaps the severest loading, is not considered. The deficiencies of temperature-drop isolation have already been discussed. Finally, steel is assumed to be fully bonded with concrete, and stresses caused by drying shrinkage are not dissipated; in other words, creep effects are not considered. Some analyses of CRCP-2 are also compared in this paper.

APPROACH USED

In this paper an examination is made of the stresses induced by static wheel loads and by temperature drop and temperature gradient into the pavement. The same model that was used by Saxena et al. (*1*) in the study for zero-maintenance anchored pavements will be utilized. A new method of evaluating the wheel-load stresses and some refinement in the model used for thermal stress analysis will be incorporated. The effect of the mechanical loads will be examined by the use of three-dimensional finite-element models and the combined effects of temperature drop and temperature gradient in the slab will be analyzed by two-dimensional finite-element models with two subsequent solutions for heat transfer and thermal stress analysis. The basic tool of analysis will be ANSYS (*17, 18*), a large-capacity finite-element program, capable of solving static, linear and nonlinear dynamic, harmonic response, and thermal analysis. ANSYS can also easily handle nonlinearities in geometry and material properties. The three-dimensional idealization of the pavement-subbase-subgrade system is shown in Figure 1.

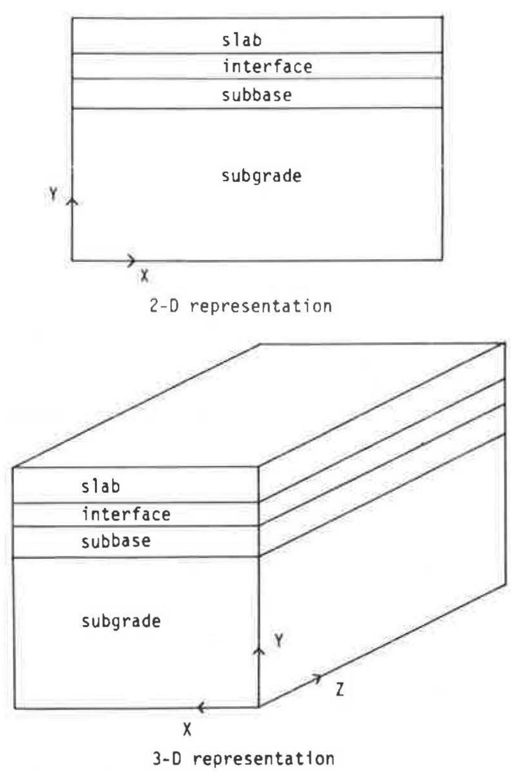

FIGURE 1 Idealization of a pavement–subbase–subgrade system.

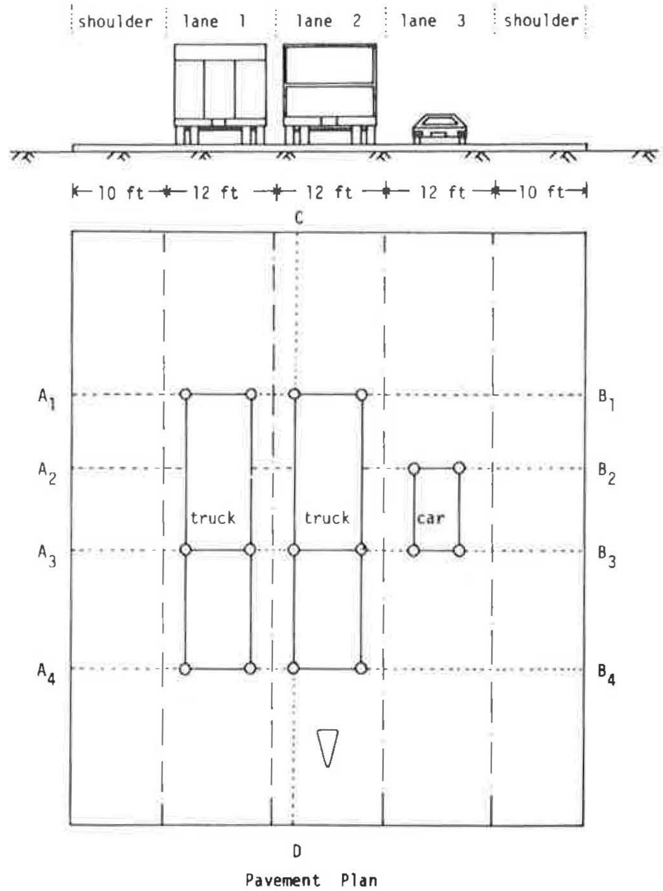

FIGURE 2 Load configuration for a three-lane highway.

Saxena and Militsopoulos (*19*) describe a laboratory experiment used to verify a three-dimensional finite-element model. The results of the two-dimensional heat-transfer model are also verified by the data given by Nordal (*20*) for a road test performed in Norway in 1963. Before the current study, both aforementioned experiments were modeled in a similar way and the results were cross verified.

STUDY OF A PREMIUM PAVEMENT

Mechanical Loads

A pavement system can be idealized as shown in Figure 1; however, the basic objective in examining a three-lane highway model is to study the effects of combined vehicle loads. In the theoretical treatment of the pavement problem, the loading condition usually examined is one load, concentrated or uniformly distributed over a circular area. It provides very useful information for the pavement's performance but does not provide a general view of the pavement's behavior.

Static loads can be input as nodal forces or element surface pressures. For the full-scale model, the nodal forces were used in order to minimize the elements of the mesh, and therefore, the computer cost.

A highway experiences various loading conditions due to infinite possible traffic combinations. A selected loading condition has been adopted for this study, based on a brief investigation of various vehicle configurations. A plan of this load configuration with the pavement's dimensions is shown in Figure 2. Based on that load configuration, the three-dimensional mesh to model a three-lane highway was developed. The boundary conditions used at the base were zero displacements in all directions. For the lateral surfaces, rollers were used. That is, the displacements perpendicular to the surfaces were set equal to zero. The thickness of the slab, used throughout this study, was 10 in. with the material properties provided in Table 1. A thickness of 0.03 in. and a friction coefficient of 1.5, were allotted to the interface element. The stiffness of the interface element was approximated as an average between the slab's and the subbase's stiffness, and the estimated value was 1.0×10^7 lb/in. The subbase was a cement-treated base (CTB), 6-in. thick. Natural soil was extended up to a depth of 50 ft. The three-dimensional mesh is shown in Figure 3.

In pavement design, the concept of an equivalent 18-kip load is widely used. It refers to the load transmitted by a single axle on the pavement. There are many charts and equations designed for equivalent 18-kip load applications (*16*, *21*, *22*),

TABLE 1 MATERIAL PROPERTIES FOR THERMAL STRESS ANALYSIS

Material	T (°F)	E (psi)	ν	α (1/°F)	γ (pci)
Reinforced concrete	120	4.0 × 10	0.15	0.0000055	0.082
	70	4.2 × 10	0.15	0.0000055	0.082
	32	4.5 × 10	0.15	0.0000055	0.082
	0	7.0 × 10	0.15	0.0000055	0.082
Cement-treated base	120	1.0 × 10	0.25	0.0000075	0.070
	70	1.0 × 10	0.25	0.0000075	0.070
	32	1.2 × 10	0.25	0.0000075	0.070
	0	3.0 × 10	0.20	0.0000075	0.070
Clay	120	4,500	0.45	0.000500	0.064
	70	5,000	0.45	0.000009	0.064
	32	5,500	0.45	0.000009	0.064
	0	30,000	0.35	0.000009	0.064
Silt	120	7,000	0.35	0.000500	0.067
	70	7,500	0.35	0.000009	0.067
	32	8,000	0.33	0.000009	0.067
	0	60,000	0.30	0.000009	0.067
Sand	120	9,500	0.30	0.000500	0.070
	70	10,000	0.30	0.000009	0.070
	32	11,000	0.28	0.000009	0.070
	0	80,000	0.25	0.000009	0.070

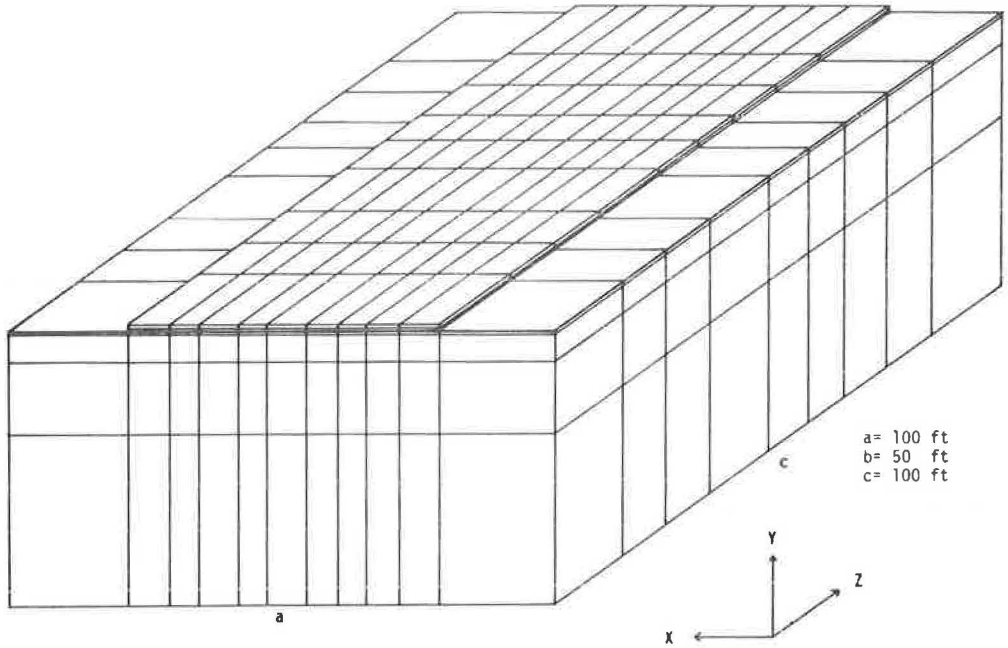

FIGURE 3 Full scale three-dimensional mesh for static analysis.

which can be considered the key term in today's pavement design. The deflected pavement surface for different transverse sections and different subgrades is shown in Figure 4. In Figure 5, the deflections due to total load are compared with those due to one single axle 18-kip load, for clay subgrade.

The need to calculate the stress concentrations directly under the wheel loads led to a refinement of the three-dimensional mesh so that detailed load application and stress evaluation can be made. The representation of the truck load by a nodal force was no longer realistic and, therefore, was replaced by distributed loads. For this analysis, one tandem axle of a heavy truck was isolated in order to study the induced stresses. The detailed geometry of the tandem axle is shown in Figure 6. This loading system has two axles of symmetry, a fact which was considered to reduce mesh dimensions. Only one-quarter of the plan is shown in Figure 7. The mesh is given in Figure 8, where the darkened elements on the top indicate the wheel loads. The boundary conditions used were the same as in a full-scale model. On the two planes of symmetry, displacements perpendicular to them were set equal to zero.

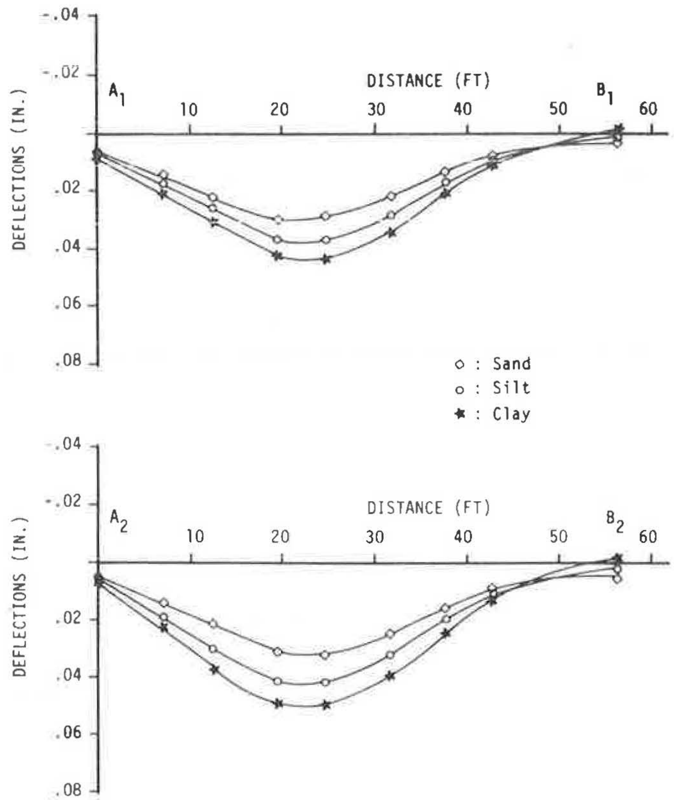

FIGURE 4 Deflection curves for pavement surface (full-scale model).

Environmental Loads

Air temperature follows more or less the same variation as pavement's surface. Soil's temperature is affected by the heat transfer on the surface and by the internal heat sources. The soil profile at some depth maintains a fairly constant temperature while the layers close to the surface have varied temperatures. Changes in surface temperature are directly reflected on the temperature variations of the shallow soil layers. The information about the air temperature variations during the day (diurnal) and during different seasons are adequate to create an input model for use with heat transfer analysis.

The diurnal temperature variation more or less follows a known pattern so that with known extreme values of variation, it is relatively easy to create the model for the heat transfer analysis. The models used for the freeze region for summer and winter are shown in Figure 9. The model selected for this analysis is two-dimensional plane strain because the pavement is very long and the air temperature uniform throughout. The

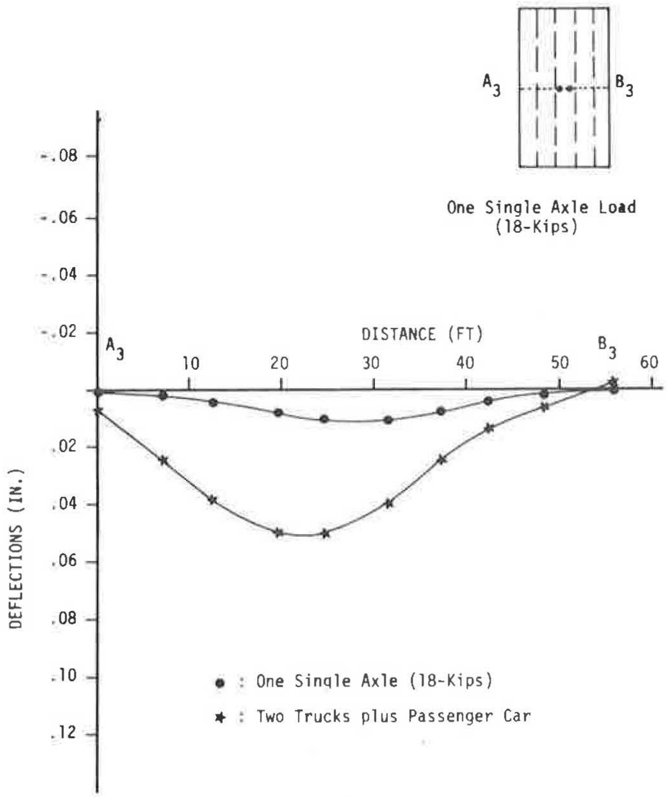

FIGURE 5 Pavement deflections in transverse section due to (*a*) one axle (18 kip) and (*b*) two trucks plus a passenger car.

dimensions of the pavement are the same as those for the three-dimensional full-scale model for mechanical loads. Temperature at a depth of 50 ft was set equal to 50°F, a realistic boundary condition. Lateral boundaries were simulated by constraining nodes along peripheral nodal lines so that the temperature variation with depth is the same.

Nodal temperature histories are used as input for the heat transfer analysis. An initial load step sets all temperatures equal to 50°F and the daily variations follow. Usually 2 days are enough to generate a constant change in the pavement's temperature distributions. The duration of every load step is 6 hr, but two iterations are performed per step. This transient heat transfer analysis was performed for freeze and nonfreeze regions in summer and winter. The subgrade used was a typical clay. Material properties are given in Table 2. Some of the resulting temperature distributions for different daytimes are shown in Figures 10 and 11. Those results correlate well, both in shape and magnitude, with typical field data. A lag in temperature peaks can be observed with increasing depth because of thermal damping. A comparative study of the obtained temperature distributions with the monthly average temperature gradients provided by Darter (*23*) led to the adaptation of representative temperature distributions.

The mesh used for the heat transfer analysis can be used for the thermal stress analysis if the elements used are altered. Boundary conditions will be fixed bottom and rollers for lateral boundaries. Inputs for the thermal stress analysis are the material properties, the temperature distribution, and the reference temperature (temperature of zero expansions). The reference temperature for reinforced concrete (curing temperature) is assumed to be 70°F for this investigation. ANSYS thermal stress analysis can incorporate only one reference temperature for all materials and elements used. Because reference temperature cannot vary, input temperature distributions should be modified to count for this effect. This can be simply done, as shown in Figure 12, by increasing the soil's input temperature by the difference between the reference temperature of soil and concrete. Deflection curves for the pavement for day and night times for the freeze region in different seasons are shown in Figure 13. The maximum thermal tensile stresses at the bottom of the slab for extreme and representative conditions during different seasons for two regions are given in Table 3.

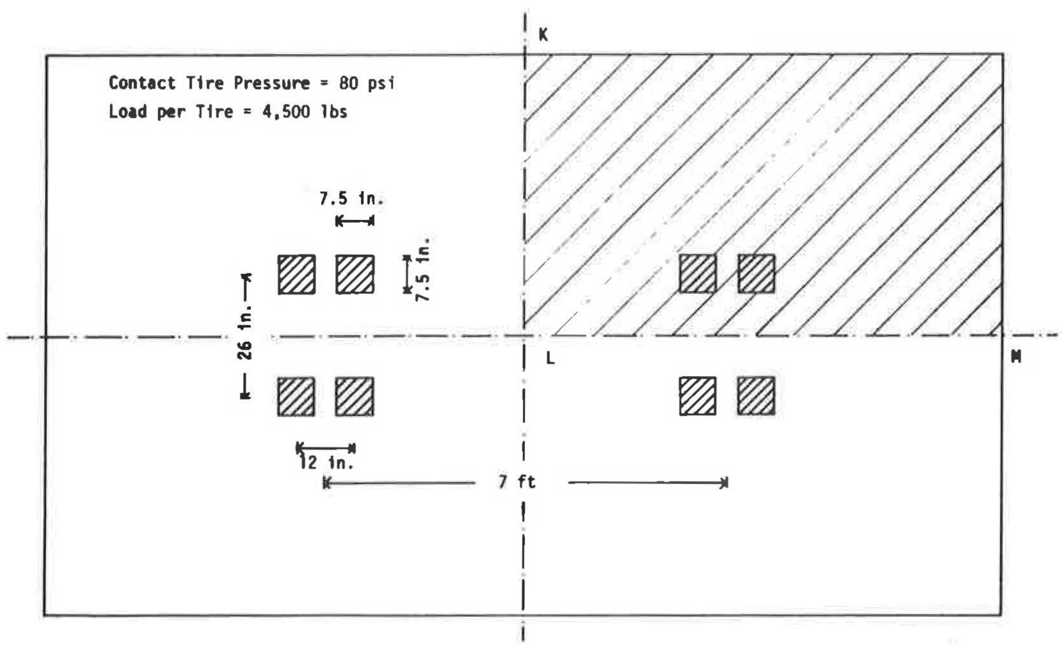

FIGURE 6 Plan of truck's tandem axle.

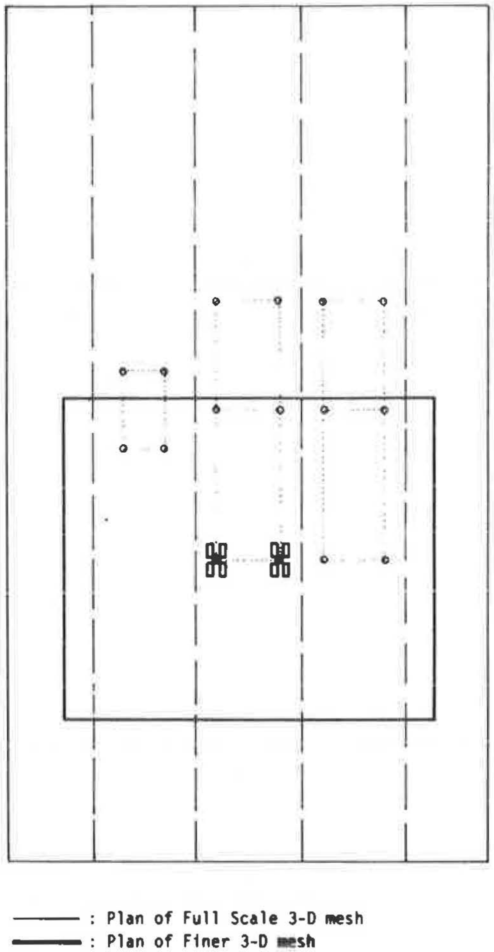

FIGURE 7 Plan comparison of the two three-dimensional models.

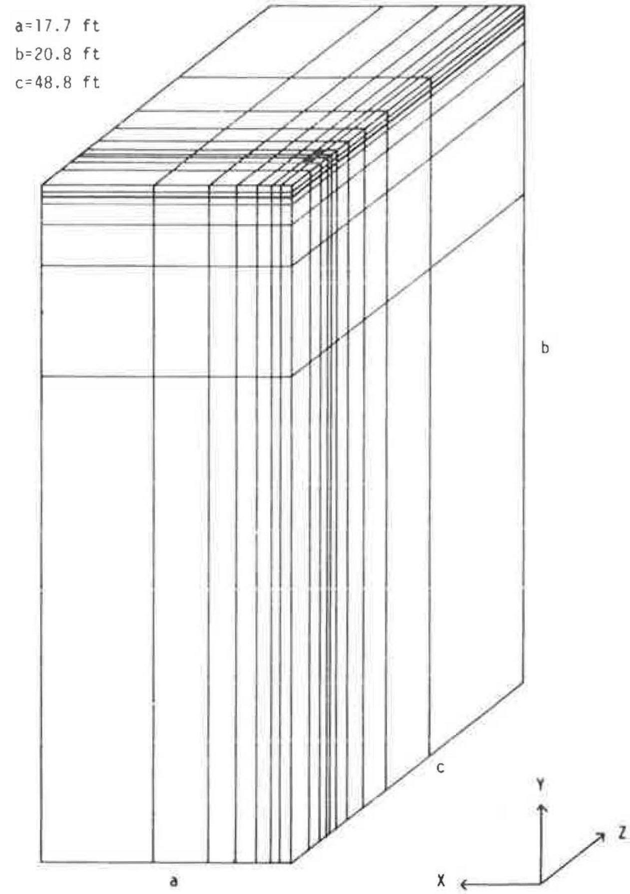

FIGURE 8 Three-dimensional finer mesh for stress evaluation.

TABLE 2 MATERIAL PROPERTIES FOR HEAT TRANSFER ANALYSIS

Material	T (°F)	K (Btu/Hr-In.-°F)	C (Btu/lb-°F)	γ (pci)
Reinforced concrete	70	0.073	0.156	0.082
	32.5	0.073	0.156	0.082
	31.5	0.073	0.156	0.082
	0	0.073	0.156	0.082
Cement-treated base	70	0.075	0.20	0.07
	32.5	0.075	0.20	0.07
	31.5	0.080	0.25	0.07
	0	0.080	0.25	0.07
Clay	70	0.067	0.22	0.064
	32.5	0.067	0.22	0.064
	31.5	0.091	0.3	0.064
	0	0.091	0.3	0.064
Silt	70	0.067	0.22	0.067
	32.5	0.067	0.22	0.067
	31.5	0.091	0.3	0.067
	0	0.091	0.3	0.067
Sand	70	0.08	0.2	0.07
	32.5	0.08	0.2	0.07
	31.5	0.14	0.3	0.07
	0	0.14	0.3	0.07

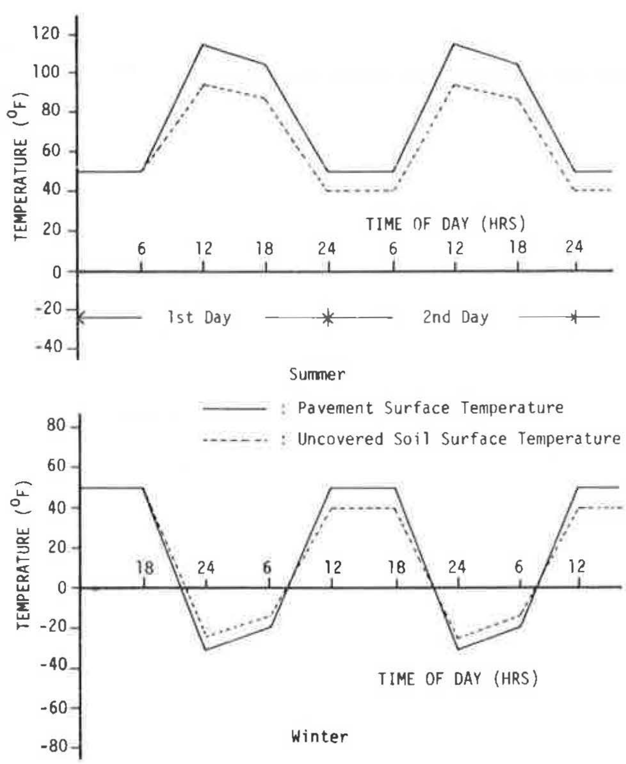

FIGURE 9 Diurnal temperature variation used as input for heat-transfer analysis in a freeze region.

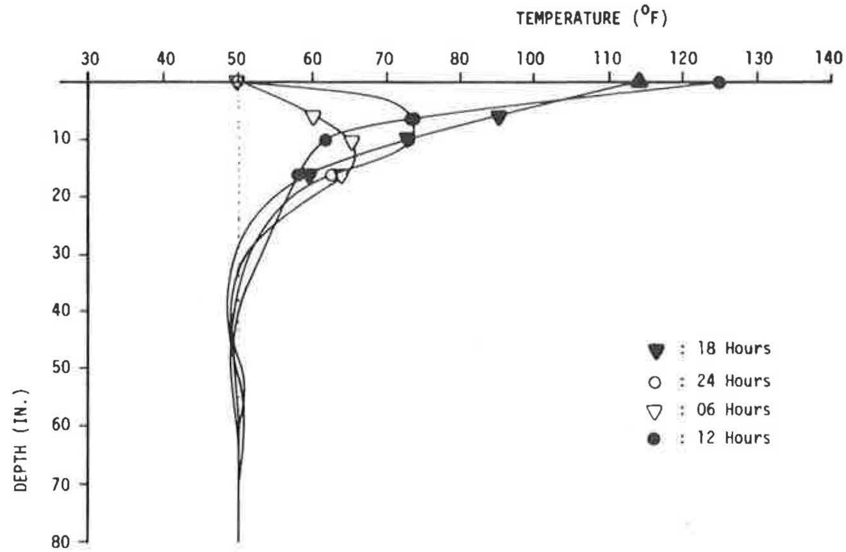

FIGURE 10 Summer tautochrones at middle lane in a freeze region.

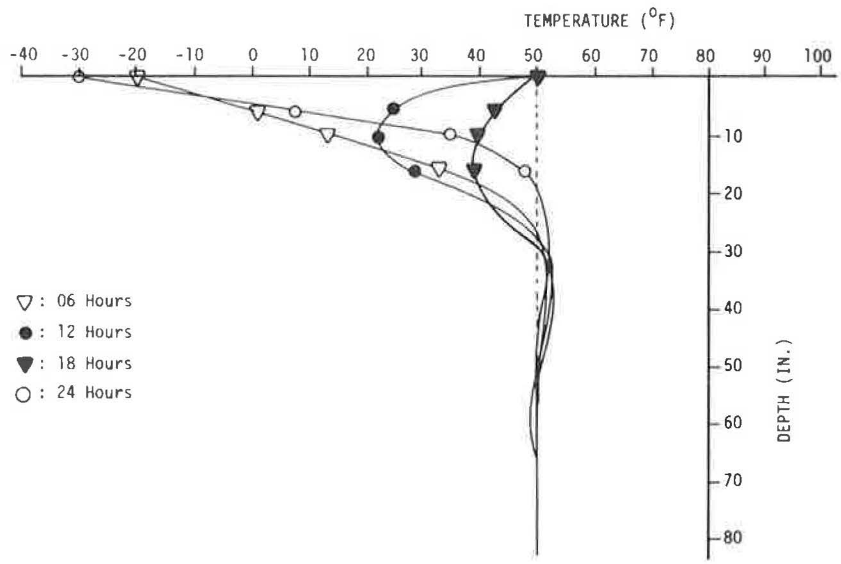

FIGURE 11 Winter tautochrones at middle lane in a freeze region.

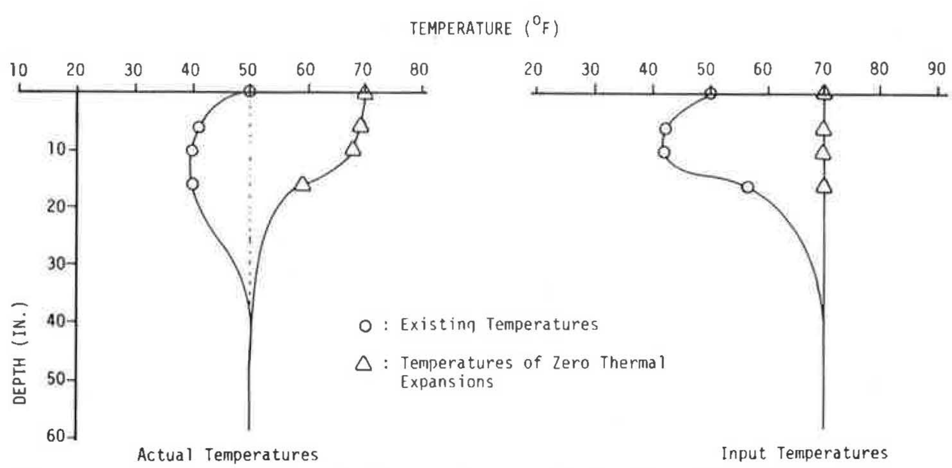

FIGURE 12 Illustrative example of temperature modification for use in thermal-stress analysis.

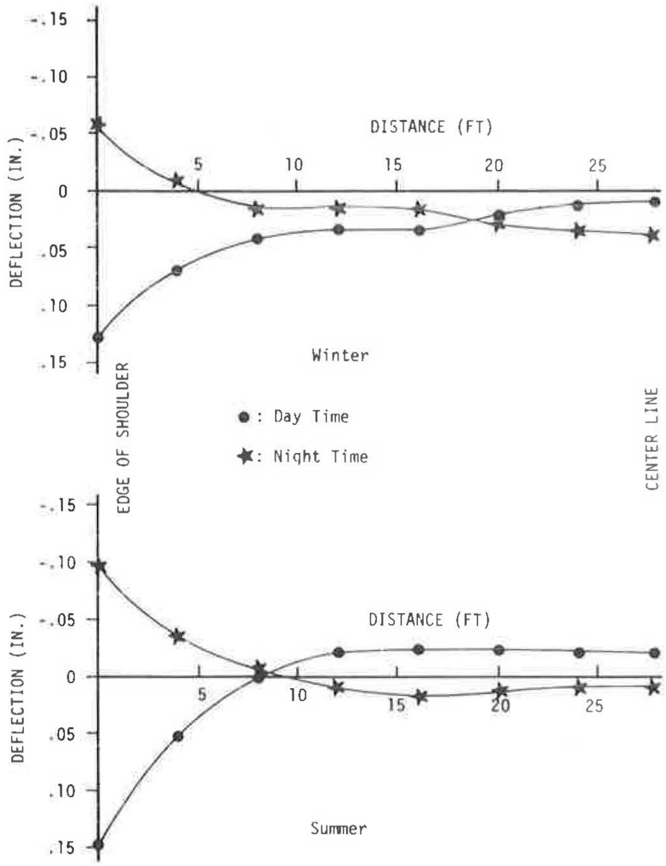

FIGURE 13 Pavement deflections due to thermal loads in freeze region clay subgrade.

Results From CRCP-2

A reexamination of combined mechanical and environmental effects on pavements was conducted using the CRCP-2 program with the following input parameters:

- Slab thickness, 10 in.;
- Curing temperature, 70°F;
- Maximum temperature drop, 70°F; and
- Wheel-load stress, 80 psi.

The problem was solved for four different steel percentages, 0.65, 0.70, 0.75 and 0.80. Material properties used were typical for concrete and steel used in highway construction. At the end of the analysis period, the following values were found, where the four different values are related to the four different steel percentages:

	Steel Percentages			
	0.65	*0.70*	*0.75*	*0.80*
Crack spacing (ft)	4.36	3.75	3.22	2.88
Crack width (in.)	0.035	0.030	0.026	0.023
Maximum concrete stress (psi)	556	556	556	556
Maximum steel stress (psi)	64600	59200	54300	59000

TABLE 3 MAXIMUM TENSILE STRESSES AT THE BOTTOM OF THE SLAB DUE TO THERMAL LOADS

	Extreme (psi)	Representative (psi)
Freeze Region		
Spring	–	193
Summer	429	259
Autumn	–	193
Winter	670	382
Nonfreeze Region		
Spring	–	131
Summer	–	132
Autumn	–	131
Winter	–	312

CONCLUSIONS

An easy and direct way of examining the combined effects of mechanical and environmental stresses on CRC pavements may be to superimpose the effects of one onto those of the other. A useful observation about the nature of the considered loads is that thermal loads act for relatively long periods (some hours), while mechanical loads have a very transient application. The maximum slab bottom tensile stresses found by the three-dimensional fine mesh, superimposed with those found by the two-dimensional thermal stress analysis are given in Table 4. The maximum stress is encountered in freeze regions during wintertime. Stresses for representative conditions, for often encountered detrimental cases, do not seem to pose any problem. Extreme stresses, which occur rarely, will cause a decrease in crack spacing.

TABLE 4 MAXIMUM TENSILE STRESSES AT THE BOTTOM OF THE SLAB DUE TO COMBINED MECHANICAL AND ENVIRONMENTAL LOADS

	Extreme (psi)	Representative (psi)
Freeze Region		
Spring	–	273
Summer	509	339
Autumn	–	273
Winter	750	462
Nonfreeze Region		
Spring	–	211
Summer	–	212
Autumn	–	211
Winter	–	392

Creep and relaxation effects have not been considered here. These effects will considerably reduce the pavement stresses in real life. Maximum stresses found by the analysis described can be considered rather conservative and may constitute the upper limit.

A more illustrative method of studying the superimposition of loads is to add the deflections caused by mechanical loads (as found by the three-dimensional full-scale model for total load configuration) to the deflections caused by thermal loads (as found by the two-dimensional thermal stress analysis) (Figure 14). Contributions of mechanical and thermal stresses are candidly understood by this approach.

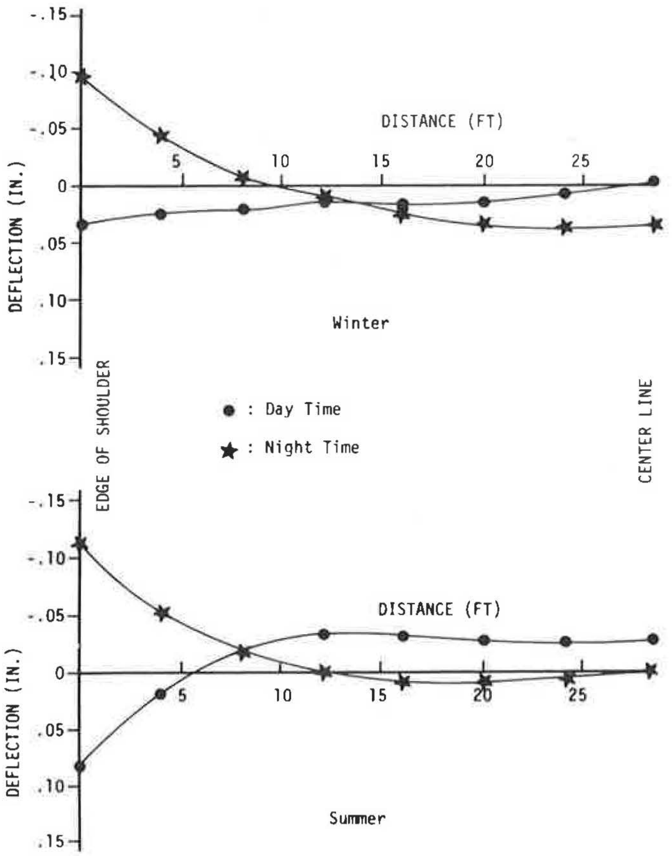

FIGURE 14 Pavement deflections due to thermal loads in nonfreeze region clay subgrade.

The results indicate that a dangerous condition may be created when separation occurs between the slab and the subbase due to curling. Mechanical loads applied at that instant may cause dangerous stress reversals. In the current study, separation was observed only for the edge of the shoulders. Because shoulders are usually confined or continuous, this effect may not occur in real life.

The environmental loads constitute the severest loads the pavement is subjected to. Deflections can be of the same order, perhaps even higher, than those caused by wheel loads. Stresses are many times higher than those caused by mechanical loads. Furthermore, the daily reversal of a pavement's curvature may cause fatigue and deterioration. Mechanical loads may overload or relieve stresses by thermal loads depending on the temperature distribution.

Maximum vertical stresses in the soil were found to be 1.5 psi for this type of premium pavement. This value is lower than what is usually considered as critical (10 psi).

Investigation of different subgrades indicated that soil's contribution in reduction of stress and deflection is very significant. Wheel-load deflections for sand (E = 10,000 psi), were 40 percent lower than those found for clay (E = 5,000 psi). Wheel-load stresses for sand were 39 percent lower than those for clay. Nevertheless, thermal stresses and deflections are only slightly affected by the subgrade type.

The comparison between the one single axle 18-kip load and the total load configuration (Figure 2) was intended to yield two ratios. The ratio for the maximum deflections was 1 to 5 and for the maximum stresses 1 to 3. Those ratios may be very useful for a comprehensive understanding of a pavement's performance when it is designed by the equivalent 18-kip concept.

The CRCP-2 computer program results cannot be directly compared with the results found by the proposed model, because they account for different loading conditions. Stresses revealed by CRCP-2 are in the same range with those obtained by the current model. CRCP-2 yielded maximum concrete stress equal to 556 psi, while maximum concrete stress revealed by the current model was 750 psi. CRCP-2 does not solve for deflections. The estimation of crack spacing and crack width made by CRCP-2 is very useful for a better understanding of pavement performance. Both crack spacing and crack width are decreasing as steel percentage increases. Regional and serviceability factors will define the required steel percentage.

REFERENCES

1. S. K. Saxena, W. J. Rosenkranz, and S. T. Militsopoulos. *Model Study and Analytical Investigations of Anchored Pavement.* Report FHWARD-80-26. Office of Research, FHWA, U.S. Department of Transportation, 1980.
2. H. M. Westergaard. Stresses in Concrete Pavements Computed by Theoretical Analysis. *Public Roads*, Vol.. 8, No. 3, 1921, pp. 54–60.
3. H. M. Westergaard. New Formulas for Stresses in Concrete Pavements of Airfields. In *Papers and Reports of Committees Published in Proceedings, ASCE, November 1946 to September 1947 Inclusive, Not Published in Transactions, Vol. 112.* ASCE, New York, N.Y., 1947.
4. H. Hertz. Uber das Gleichgewicht Schwinnender elastischer platten. *Wiedermann's Annalen cler Physik und chemie.*, Vol. 22, 1884, pp. 449–455.
5. A. H. A. Hogg. Equilibrium of a Thin Slab on Elastic Foundations of Infinite Depth. *Philosophical Magazine*, Vol. 35, 1944, pp. 2654–276.
6. D. L. Holl. "Thin Plates on Elastic Foundations." *Proc., 5th International Congress on Applied Mechanics*, Cambridge, Massachusetts, 1938.
7. G. Picket and G. K. Ray. "Influence Charts for Concrete Pavement." Paper 2425, ASCE, New York, N.Y., 1951, p. 49.
8. W. R. Hudson and H. Matlock. *Discontinuous Orthotropic Plates and Pavement-Slab.* Research Report-56-6, CFHR, The University of Texas, Austin, 1966.
9. A. S. Vesic and S. K. Saxena. *NCHRP Report 97: Analysis of Structural Behavior of AASHO Road Test Rigid Pavements.* HRB, National Research Council, Washington, D.C., 1970, 35 pp.
10. S. K. Saxena. *Foundation Mats and Pavement Slabs Resting on an Elastic Foundation—Analyzed Through a Physical Model.* Ph.D. dissertation, Department of Civil Engineering, Duke University, Durham, North Carolina, 1971.
11. S. K. Saxena. "Pavement Slabs Resting on Elastic Foundations." In *Highway Research Record 466*, HRB, National Research Council, Washington, D.C., 1973, pp. 163–178.
12. E. F. Kelley. Applications of the Results of Research to Structural Design of Concrete Pavements. *Public Roads*, Vol. 20, No. 5–6, 1939, pp. 83–126.
13. G. A. Leonards and M. E. Harr. Analysis of Concrete Slabs on Ground. *Journal of Soil Mechanics and Foundations Division, Proceedings, ASCE*, June 1959.
14. K. H. Lewis and M. E. Harr. "Analysis of Concrete Slabs on Ground Subjected to Warping and Moving Loads." In *Highway Research Record 291*, HRB, National Research Council, Washington, D.C., 1969, pp. 194–211.
15. J. Ma and B. F. McGullough. *CRCP-2, and Improved Computer*

Program for the Analysis of CRC Pavement. Research Report 177-9, CFHR, The University of Texas, Austin, 1977.
16. B. F. McGullough, J. Ma, and C. S. Noble. *Limiting Criteria for the Design of CRCP*. Research Report 177-17, CFHR, The University of Texas, Austin, 1979.
17. G. J. De Salvo and J. A. Swanson. *ANSYS Examples Manual*. Swanson Analysis Systems Inc. Houston, Pennsylvania, 1972.
18. G. J. De Salvo and J. A. Swanson. *ANSYS User's Manual*. Swanson Analysis Systems Inc. Houston, Pennsylvania, 1978.
19. S. K. Saxena and S. G. Militsopoulos. "Model Study of Anchored Pavement." In *Transportation Research Record 814*, TRB, National Research Council, Washington, D.C., 1981, pp. 55–62.
20. R. S. Nordal. "The Thermal Regime of the Pavement and the Subgrade at the Vormsund Test Road." *Proc., Symposium on Frost Action*, Norwegian Road Research Laboratory, Oslo, Norway, Oct. 1973.
21. *AASHTO Interim Guide for Design of Pavement Structures*. AASHTO, Washington, D.C., 1972.
22. *Design of Continuously Reinforced Concrete for Highway*. Associated Reinforcing Bar Producers. Chicago, Illinois, 1981.
23. M. I. Darter. Design of Zero Maintenance Plain Jointed Concrete Pavements. In *Development of Design Procedures, Vol. 1., 1977*. Report FHWA-RD-77-111, 253 pp.

Concrete Pavement Joint Stiffness Evaluation

JAMSHID M. ARMAGHANI, JOHN M. LYBAS, MANG TIA, AND BYRON E. RUTH

Concrete pavement distress is often associated with the effectiveness of load transfer at joints and contributing factors such as pumping. Current analytical methods attempt to simulate load transfer, curling, and load effects in the modeling of pavement response. In general these analytical models do not accurately define load transfer and thermal effects. Therefore, research has been initiated to develop improved methods for analysis and design of concrete pavements. The initial results of tests conducted on a Florida Department of Transportation test pavement indicate that pavement and joint response can be effectively modeled using a three-slab, two-joint, finite-element computer program (FEACONS III). Besides conventional layer parameter input, the program requires spring constants for pavement-edge friction, joint shear, and joint moment. The analysis of plain concrete pavement was performed using the falling weight deflectometer (FWD). Data were collected during different seasons, when the differential (ΔT) and average slab temperatures varied substantially. Generally four different load levels were used in the FWD to assess load-deflection linearity. Temperature-curling and contraction–expansion effects were also monitored independently. Spring stiffnesses were varied in the FEACONS III analyses until the predicted deflection basins matched those measured for different temperature and loading conditions. The results obtained with a downward curling ($\Delta T \simeq 9°F$ or $5°C$) indicated that spring stiffnesses representing edge friction, joint shear, and moment at the joint remained constant regardless of loading position. This suggests that differential drying shrinkage or a moisture differential had produced upward warping, which was offset by the 9°F (5°C) downward curling. At other differential temperatures, the spring stiffness varied according to slab lift-off and load position. The average slab temperature (seasonal) was found to have a pronounced effect on joint stiffness. At high temperatures, the shear and moment stiffnesses were very high, providing close deflections for loaded and unloaded sides of the joint. When mean slab temperature was lowered, the analyses indicated a significant reduction in joint stiffness.

The critical element of a concrete pavement is the joint that influences load transfer and pavement performance. Pavement engineers should therefore be primarily concerned with the analysis of joints to better describe their behavior. A thorough understanding of the effects of thermal and load conditions on concrete joints should provide for an improvement in design methodology and durability.

Thermal conditions imposed on concrete pavements influence the joint stiffness that affects load transfer characteristics. The average temperature of the concrete pavement influences load transfer of undowelled joints according to the degree of aggregate interlock. On the other hand, the temperature differential between the top and bottom surfaces determines the degree of warping and the curling conditions at the joint that, in effect, cause the variability in the stiffness along the joint.

A number of finite-element computer programs have been developed to analyze the structural behavior of jointed pave-

Civil Engineering Department, College of Engineering, University of Florida, Gainesville, Fla. 32611.

ments. Among these programs, WESLIQUID (*1*), ILLI-SLAB (*2*), and the model developed by Huang (*3*), have been widely used for analysis. In these programs the joint stiffness is related to joint efficiency, which is a physical property of the joint. The joint efficiency is defined as the percent ratio of deflections between the unloaded and the loaded sides of a joint. For any loading position, the joint efficiency as defined may vary for different locations along the joint. Moreover, the thermal condition may also influence the value of joint efficiency regardless of loading position. Therefore, relating the stiffness to joint efficiency may, in many cases, result in an inaccurate modeling of joint behavior.

Described in this paper is a procedure to determine the stiffness of an undowelled joint in a concrete pavement using a finite-element program, FEACONS III, as an analytical tool, and the results from the loading tests using the falling weight deflectometer (FWD). Tests were conducted on a specially prepared test pavement. The test pavement was constructed to be representative of in-service concrete pavements in the state of Florida. Load tests were performed at different slab positions such as, center, edge, corner, and two other locations along the undowelled joint. The tests were conducted at different temperature differentials of the pavement and at different seasonal concrete temperatures. Deflection profiles of the pavement at the undowelled joint were also measured for different temperature differentials to determine the warping conditions at the joint.

This study is a part of an ongoing research program between the University of Florida and the Florida Department of Transportation (FDOT) to evaluate

1. Behavior of dowelled and undowelled joints,
2. Effects of thermal conditions of the pavements on the response to the applied FWD loads, and
3. Effects of voids and their locations on the pavement response.

The goal of this research is to accurately model the response of the test pavement when it is subjected to different thermal and loading conditions. Some early findings of this research were presented in a previous paper by Lybas et al. (*4*). Since then, extensive work has been done toward accomplishing the three aforementioned objectives of the main research. The information presented in this paper is a part of the findings of this ongoing research.

FEACONS III COMPUTER PROGRAM

The finite-element analysis of concrete slabs (FEACONS III) computer program was developed at the University of Florida (*5*) to analyze the response of a concrete pavement subject to concentrated or uniform vertical loads.

The program considers the following factors in the analysis:

1. Weight of the concrete slabs,
2. Voids beneath the concrete slabs,
3. Effects of joints and edges, and
4. Effects of temperature differentials between the top and bottom surfaces of the slabs.

FEACONS III models a concrete pavement as a three-slab system. A concrete slab is modeled as an assemblage of rectangular plate finite elements with three degrees of freedom at each node. Load transfer across the joints between the adjoining slabs are modeled by linear and rotational springs connecting the slabs at the nodes of the elements along the joint. Frictional effects at the edges are modeled by linear springs at the nodes along the edges. The subgrade is assumed as a Winkler foundation modeled by a series of vertical springs at the nodes. Subgrade voids are modeled as initial gaps between the slab and the springs at the specified nodes.

There are four input parameters for the program:

1. Subgrade spring stiffness (K_s) in kips per cubic inch modeling the subgrade stiffness of a pavement;
2. Edge spring stiffness (K_{EG}) in kips per square inch modeling the frictional resistance at the edge of the pavement;
3. Joint linear spring stiffness (K_L) in kips per square inch modeling the shear stiffness of the joint; and
4. Joint rotational stiffness (K_R) in kips per inch modeling the moment stiffness of the joint.

DESCRIPTION OF TEST PAVEMENT

A six-slab concrete pavement test road incorporating two dowelled and four undowelled joints was constructed at the FDOT Bureau of Materials and Research. Each slab is 6.1-m (20-ft) long, 3.66-m (12-ft) wide, and 23-cm (9-in) thick. The test road, as shown in Figure 1, incorporates voids of two different depths and various sizes. Slab 4 is a control slab, cast with no voids, and has been used for comparison of response with the slabs with voids.

TESTING SYSTEMS AND DATA COLLECTION

FWD Measurements

FWD loads were applied at the center, edge, and corner of Control Slab 4. Two other locations along the undowelled joint were also tested; their locations were at 75 cm (30 in.) and 165 cm (66 in.) from the edge, respectively. Magnitudes of the testing loads ranged from 250 kPa (36 psi) to 950 kPa (138 psi). The tests were conducted at various temperature differentials (ΔT) that occurred during the test day. The tests were repeated during summer, fall, and winter. A typical load deflection relation at various temperature differentials for corner loading is shown in Figure 2.

For each joint loading, deflections were measured with sensors along the loaded and unloaded sides of the joints. Thus the measured deflection basins on both sides of the joints were obtained.

Temperature Measurements

Air and concrete temperatures were measured using thermocouples. Thermocouples were embedded in Slabs 3 and 4 as shown in Figure 1. Thermocouple Locations a and b in Slab 3

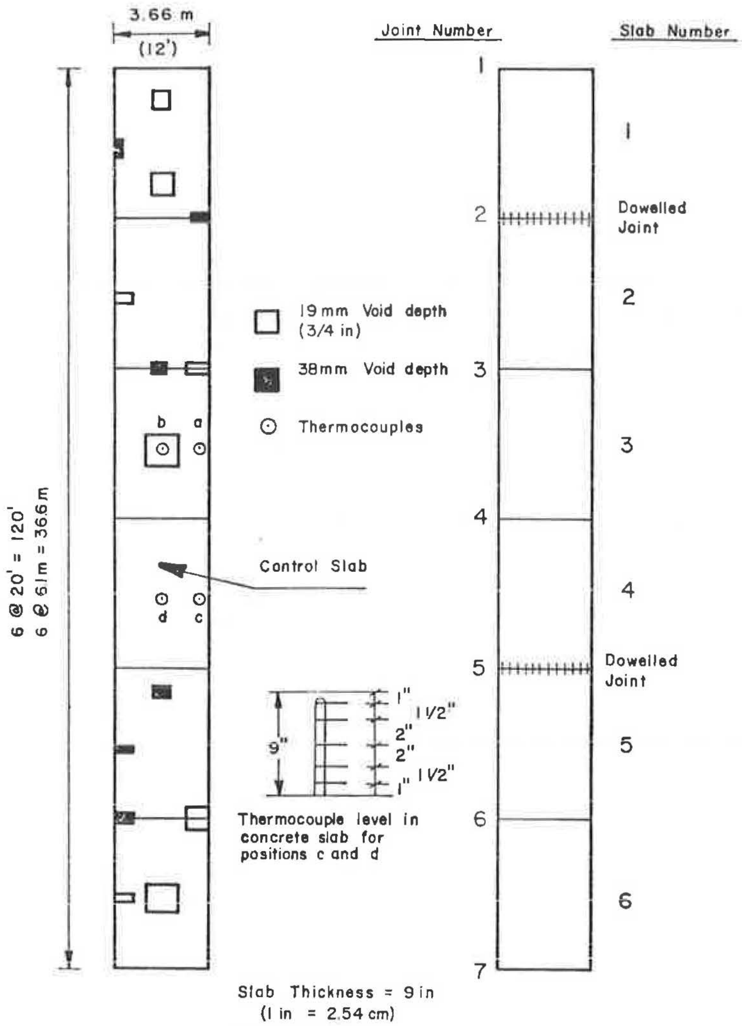

FIGURE 1 Details of test road.

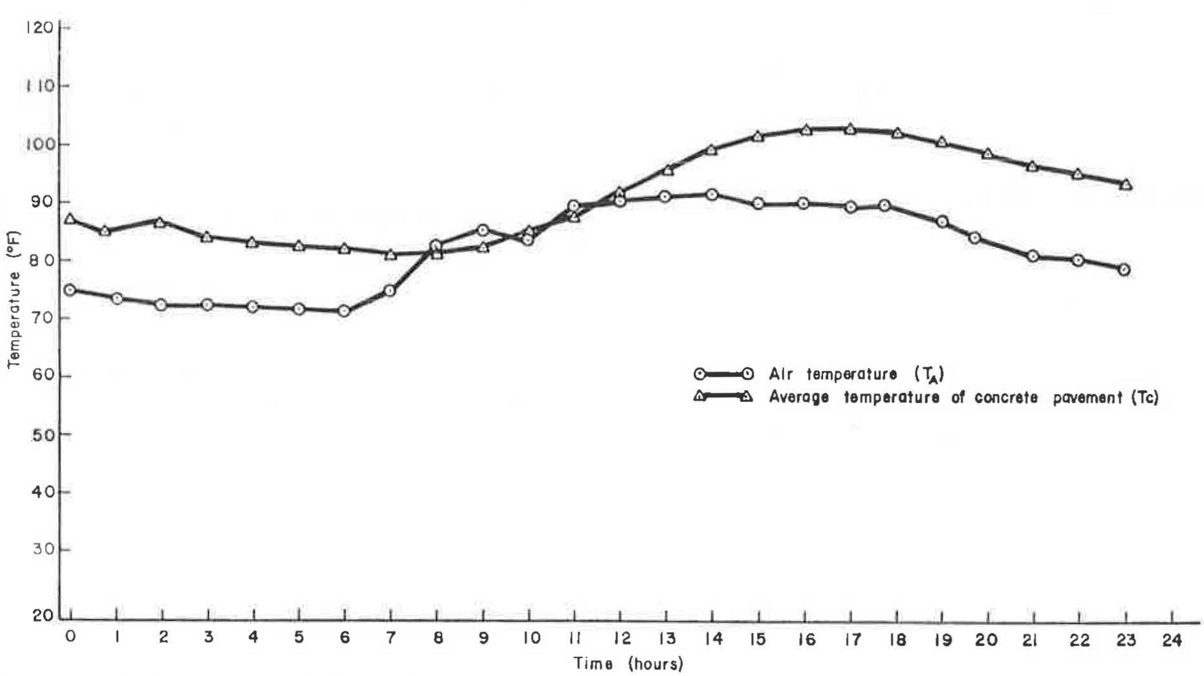

FIGURE 2 Typical load–deflection relations at the slab corner.

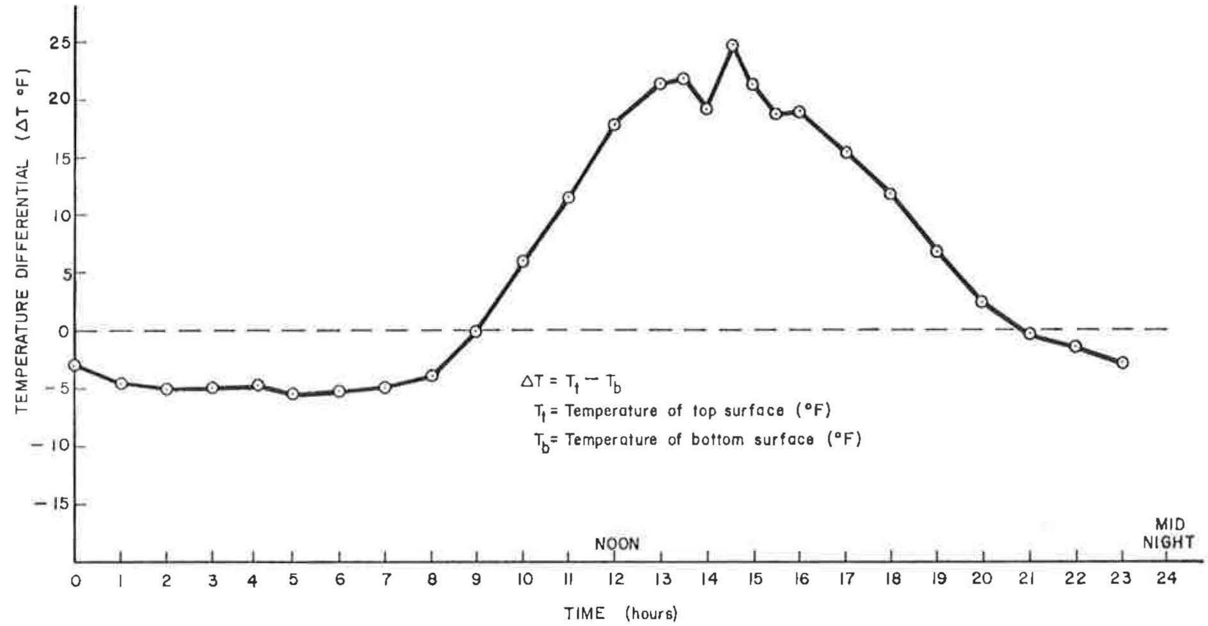

FIGURE 3 Typical hourly temperature records of air and of the concrete pavement for the summer season.

include a thermocouple 1 in. below the top and 1 in. above the bottom surface of the concrete. Thermocouple Locations c, and d in Slab 4 include five thermocouples positioned at different levels in the concrete as shown in Figure 1.

Concrete and air temperatures were recorded every 15 min during the FWD loading tests. The temperatures were also recorded every hour before and after the FWD tests for the complete 24-hr cycle. A typical hourly air temperature (T_A) and average concrete temperature (T_c) are shown in Figure 3. The average concrete temperature represents the average of the measured temperatures from all thermocouples in the pavement. Typical hourly values of temperature differentials (ΔT) computed as the difference between the temperatures of the top and bottom surfaces of the pavement are shown in Figure 4.

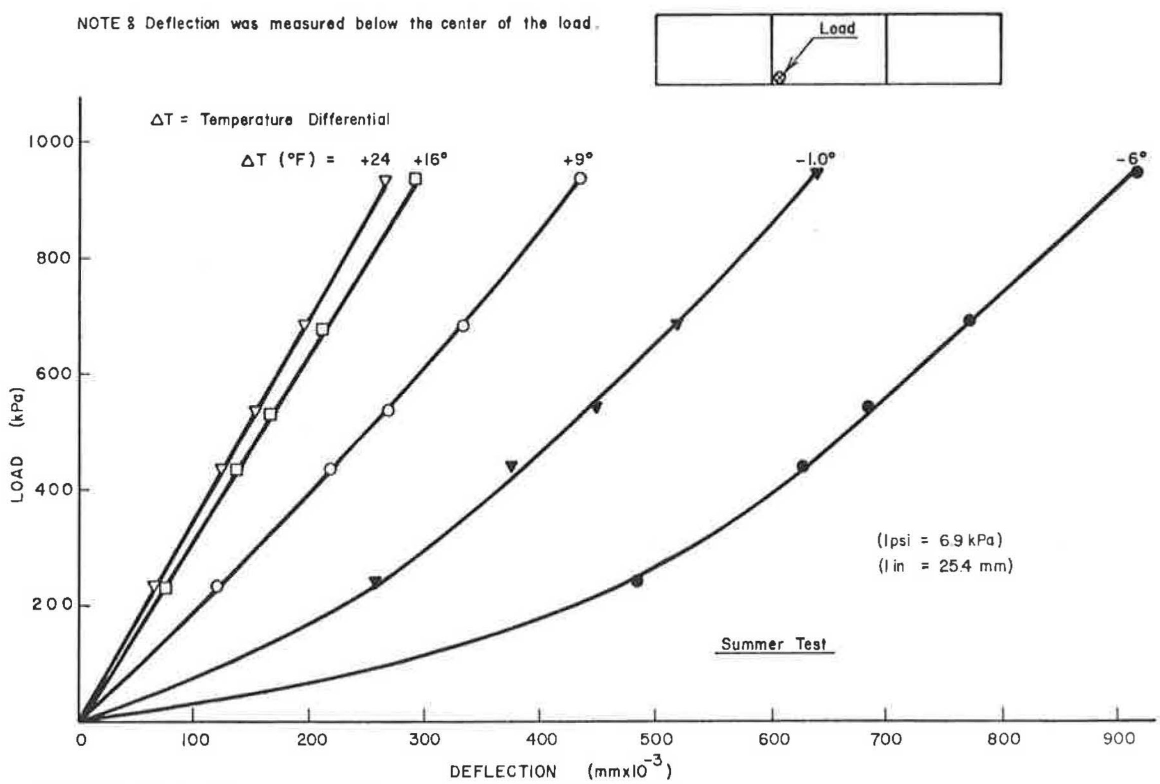

FIGURE 4 Typical 24-hr cycle of temperature differential for the pavement during the summer season.

Deflection Profiles at the Joint

Deflection profiles of the pavement along the undowelled joint (Joint 4) were measured at various temperature differentials using linear variable differential transducers (LVDTs). A timber frame was placed over the pavement width to hold the LVDTs. Seven LVDTs were used to record the surface elevations along the undowelled joint. A data acquisition unit HP3497 controlled by an HP9825A computer, was programmed to record LVDT readings and store them in the computer every 30 min. Another data control unit was programmed to record temperature measurements from the thermocouples simultaneously with the LVDT readings. The deflection profiles from the LVDT measurements at various temperature differentials are shown in Figure 5.

SELECTION OF INPUT PARAMETERS FOR FEACONS III

In order to use the FEACONS III program to evaluate joint stiffness, the main input parameters of the model had to be determined first. The main assumption in the model was that uniform subgrade support existed with no voids beneath the slabs. All test results for the analysis presented in this paper were obtained from Control Slab 4.

Selection of Subgrade Spring Stiffness (K_s)

Different subgrade spring stiffnesses (K_s) were assumed in the FEACONS III program. Predicted deflection basins representing the different subgrade spring stiffnesses were compared with the measured deflection basin for loading at the slab center. The actual deflection basin in this comparison represented the linear response of the pavement or the condition of full contact between the center of the slab and the subgrade.

The predicted deflection basin that best correlated with the measured deflection basin was considered to represent the subgrade spring stiffness of the pavement.

Selection of the Edge Spring Stiffness (K_{EG})

With the subgrade spring stiffness (K_s) evaluated, predicted and measured deflections from the edge loading were correlated to determine the edge spring stiffness (K_{EG}). Different K_{EG} values were assumed in the program. Comparisons were made between the predicted and the actual deflection basins.

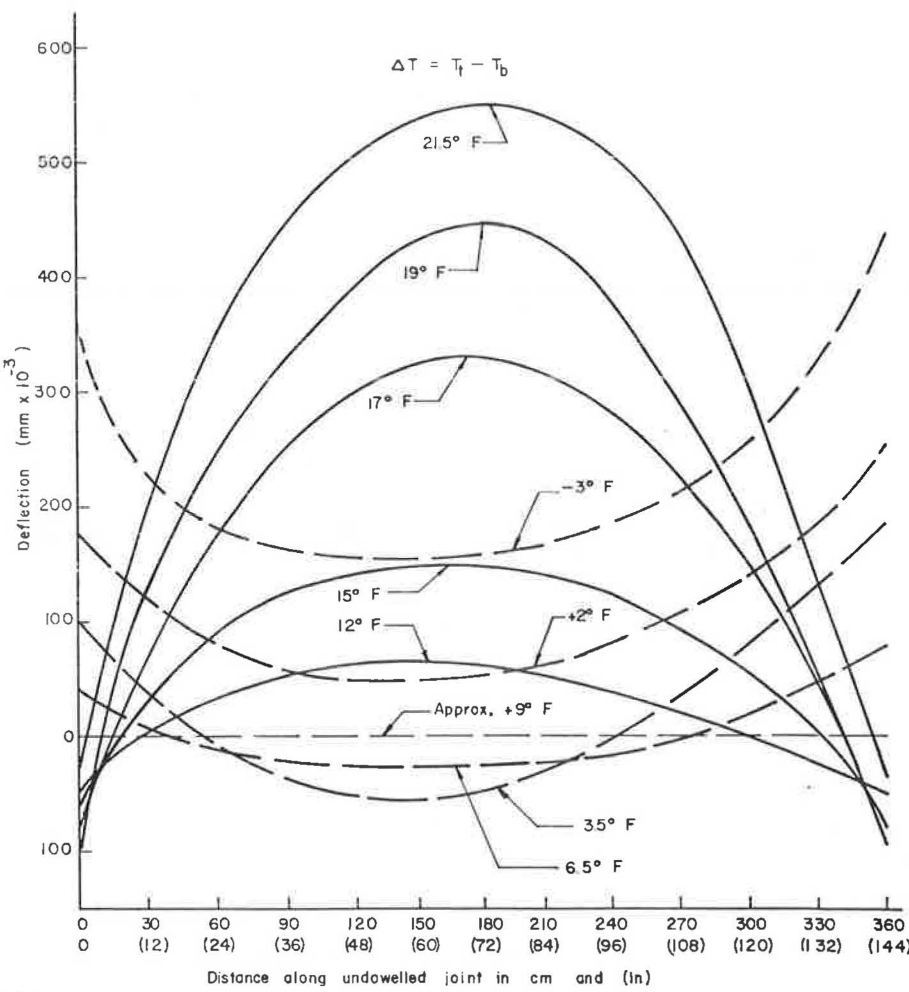

FIGURE 5 Deflection profiles along the joint due to the change in the temperature differential (ΔT) in concrete pavement.

The predicted deflection basin that correlated closely to the actual deflection basin represented the edge spring stiffness that best modeled the frictional resistance at the pavement edges.

Selection of the Linear and Rotational Spring Stiffnesses at the Joint (K_L), (K_R)

Linear spring stiffness (K_L) representing the shear stiffness, and the rotational spring stiffness (K_R) representing the moment stiffness had to be determined individually to assess the actual joint stiffnesses. With the load applied at the joint, the predicted deflection basins were compared with the measured deflection basins. This comparison was made for deflection basins on the loaded and on the unloaded side of the undowelled joint. As in the center and edge loading case, only measured deflection basins exhibiting linear load response were used in the analyses.

Different combinations of K_L and K_R values were assumed in the FEACONS III program. The combination of K_L and K_R, that resulted in deflection basins that best correlated with the measured deflection basins on both sides of the joint, represented the joint stiffness for the specified loading condition.

ANALYSIS OF THE FWD LOAD–DEFLECTION DATA

The test results from corner loading at Slab 4 were analyzed. Figure 2 shows the load–deflection relation for various temperature differentials (ΔT). This relation is nonlinear at ΔT of –6°F, representing an upward curling of the corner, as is evident from the deflection profiles in Figure 5. As the temperature differential (ΔT) became more positive, the condition of the slab corner changed from upward to downward curling as shown in Figure 5. This change is reflected in the load–deflection relation as it became linear at ΔT of +9°F and above, and the pavement system response to loads became uniform. In Figure 5, the +9°F temperature differential represents a flat position of the joint. The load–deflection relation was also determined for the other two load positions along the joint, and the condition of linear pavement response was selected for comparison with the predicted deflections. The linear load–deflection relations at the three load positions along the undowelled joint are shown in Figure 6.

Typical load–deflection relations at the slab center are shown in Figure 7. At ΔT of –3°F the load–deflection is linear, indicating linear response of the pavement system to the applied loads. This temperature differential (–3°F) represents a downward curling position of the slab center, where the slab may be in full contact with the subgrade. However, at ΔT of +11°F and more, the response is nonlinear; this is due to the upward lifting of the slab center from the subgrade.

In order to evaluate the subgrade stiffness accurately, the condition of the linear pavement response should be used in the analysis, and not any arbitrarily chosen deflections from the test results.

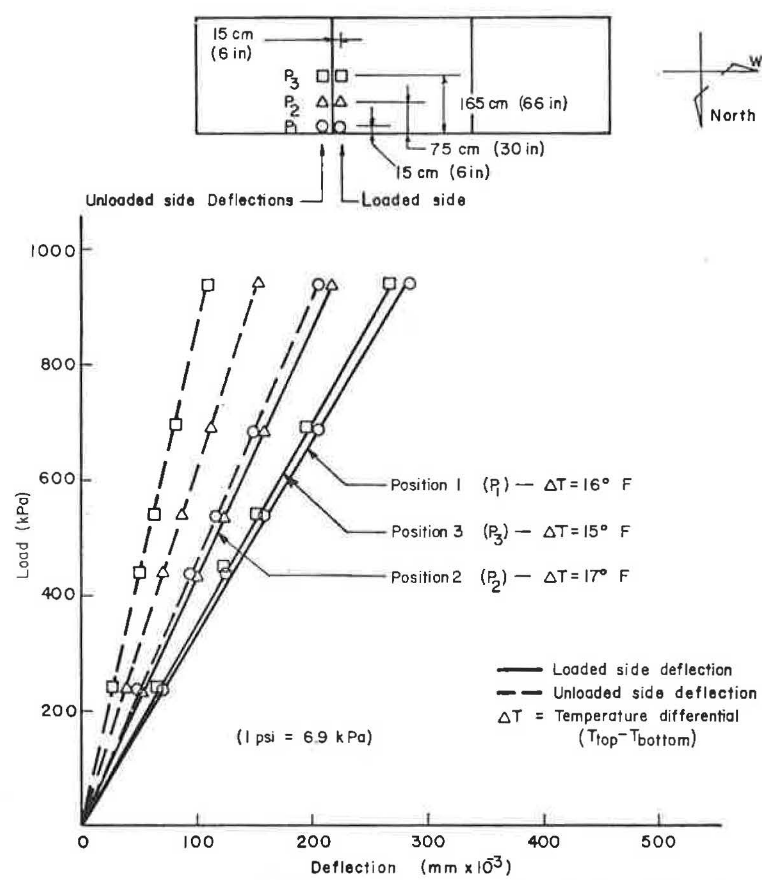

FIGURE 6 Linear load–deflection relations for three load positions along the undowelled Joint 4 of the test pavement.

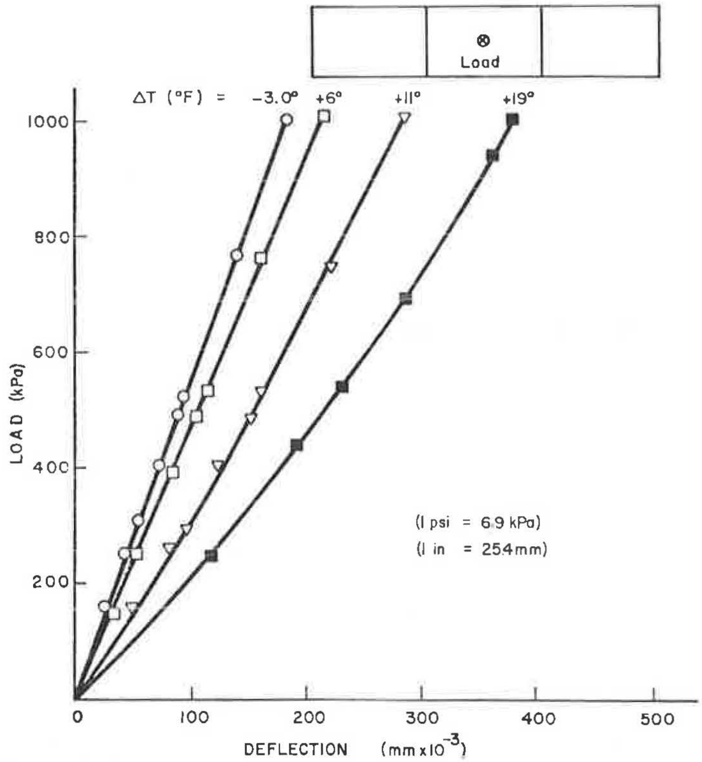

FIGURE 7 Typical load–deflection relations at the slab center.

RESULTS OF FEACONS III ANALYSES

Subgrade Stiffness of the Pavement

The predicted deflections that correlated best with the measured deflections from the summer and winter tests are shown in Figure 8. There appears to be a variation in the subgrade stiffness (K_s) between summer and winter. As shown in Figure 8, the K_s for summer was 0.35 pci and 0.25 pci for winter.

Different values of K_{EG}, K_L, and K_R were tried in the FEACONS III program. Results of the analytic solution showed no change in the values of the deflections at the slab center. This indicates that deflections in the slab center are not affected by changes in the joint and edge stiffnesses.

Edge Stiffness

Predicted deflection basins that correlated very closely with the actual deflection basin along the slab edge are shown in Figure 9. The deflection basin, representing K_s of 0.25 pci and K_{EG} of 10 psi, correlated very well with the actual deflection. Edge spring stiffness values of 15 ksi and 5 ksi were also tried in the program, but correlated poorly with the actual deflection basin as shown in Figure 8. Various combinations of K_L and K_R were also assumed, but showed no effect on the deflection basin along the joint.

Joint Stiffness

Joint stiffness was evaluated at two thermal conditions, A and B, for the summer test, and at two other seasons, fall and winter. Figures 10–13 show evaluations of the shear and moment stiffnesses at three positions along the undowelled joint for Thermal Condition A of the summer test. It is evident from the analyses that the stiffness along the joint varied at a ΔT 16°F. From Load Position 1 to Load Position 3, there were sharp reductions in the values of K_L and K_R as shown in Figures 10 to 13.

An examination of the joint stiffnesses in Figures 14 and 15 for Thermal Condition B indicates a uniform, constant stiffness along the joint. For this thermal condition the K_L and K_R remained constant at values of 10 ksi and 2,500 kips/in., respectively, regardless of load position along the joint.

Joint stiffness evaluations for the fall and winter conditions are shown in Figures 16 and 17. Compared with summer (Figures 10 and 11), the joint stiffness decreased in fall and winter. For K_s of 0.25, the value of K_L decreased from 750 ksi in the summer to 60 ksi in the fall to 10 ksi in the winter, and the K_R decreased from 5,000 kips/in. in the summer and fall to 2,500 kips/in. in the winter.

DISCUSSION OF RESULTS

Joint Stiffness

In this paper, the joint stiffness was evaluated by comparing predicted and measured deflection basins. No attempt was made to relate the joint stiffness to the joint efficiency that had been used in some previous studies (*2*, *3*). Joint efficiency was defined (*2*) as the percent ratio of deflections of the unloaded to the loaded sides of the joint. However, it was concluded from analyzing the test data for the present study, that relating joint stiffness to joint efficiency may be inaccurate and misleading

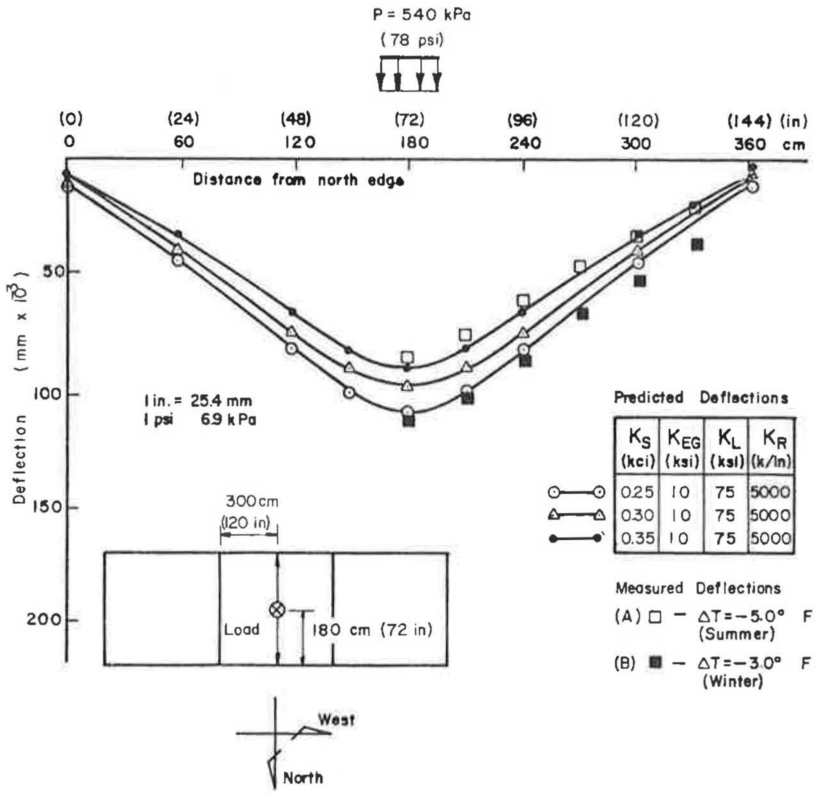

FIGURE 8 Deflection basin, center of slab, transverse direction.

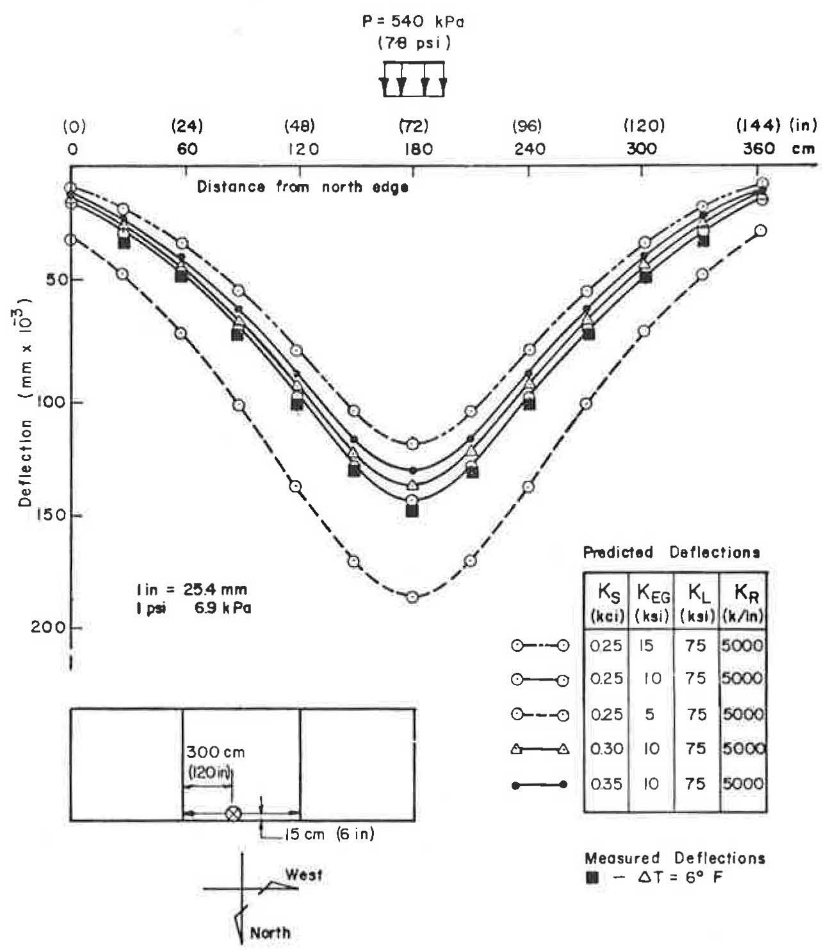

FIGURE 9 Deflection basin, slab edge on the longitudinal direction.

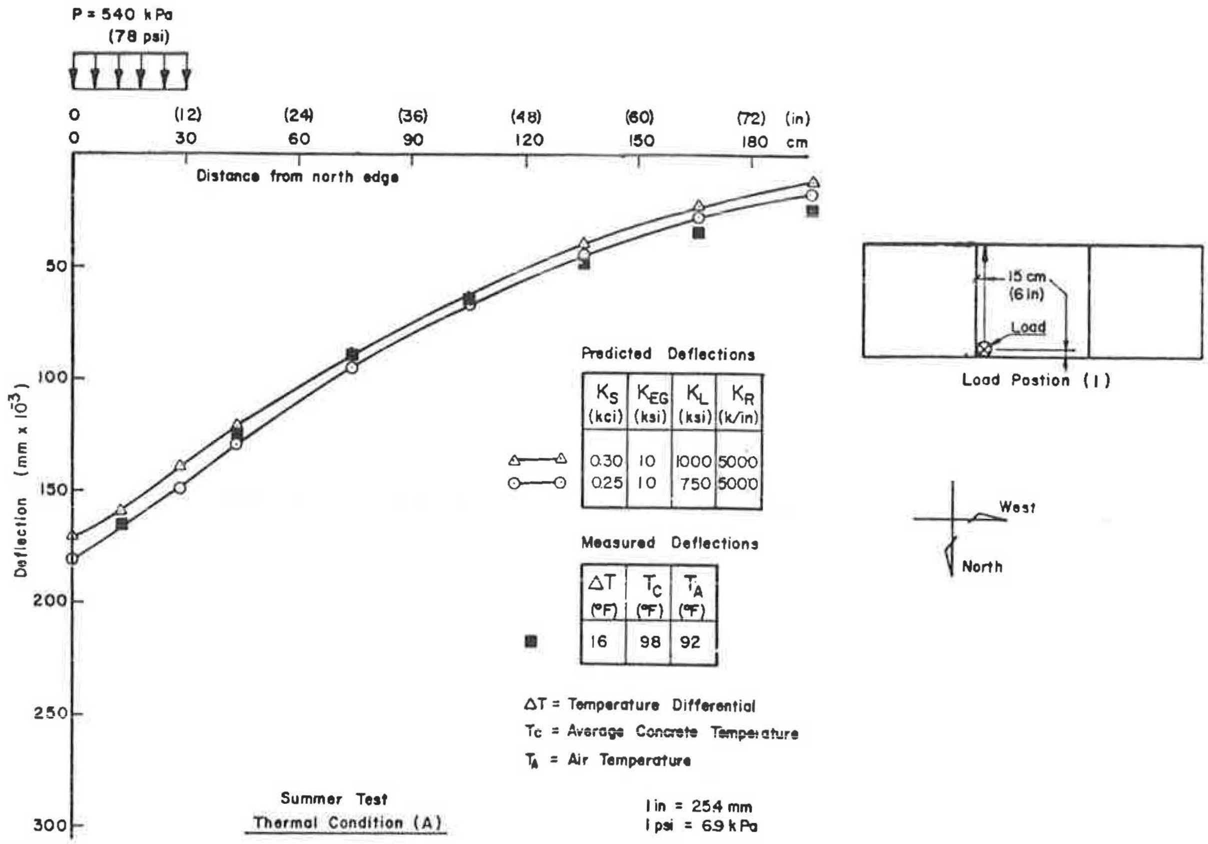

FIGURE 10 Deflection basins on the loaded side of undowelled joint, transverse direction.

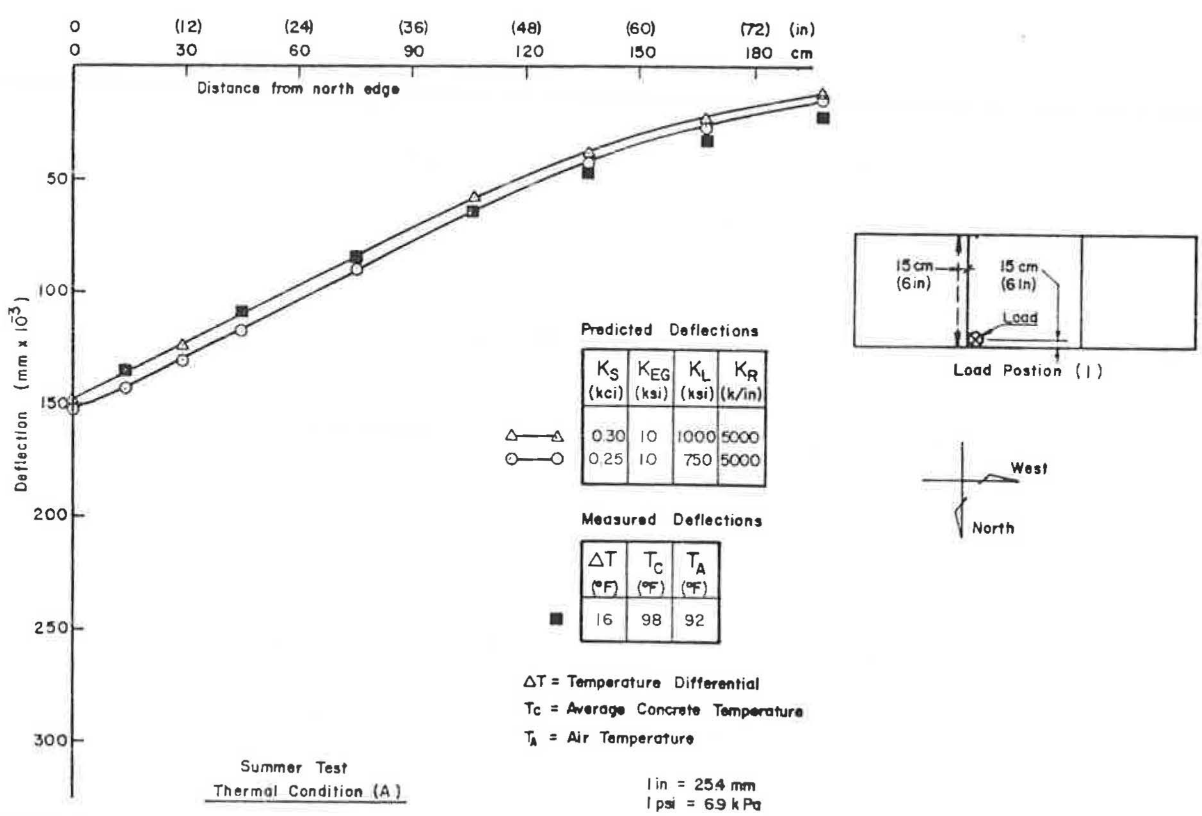

FIGURE 11 Deflection basins on the unloaded side of undowelled joint.

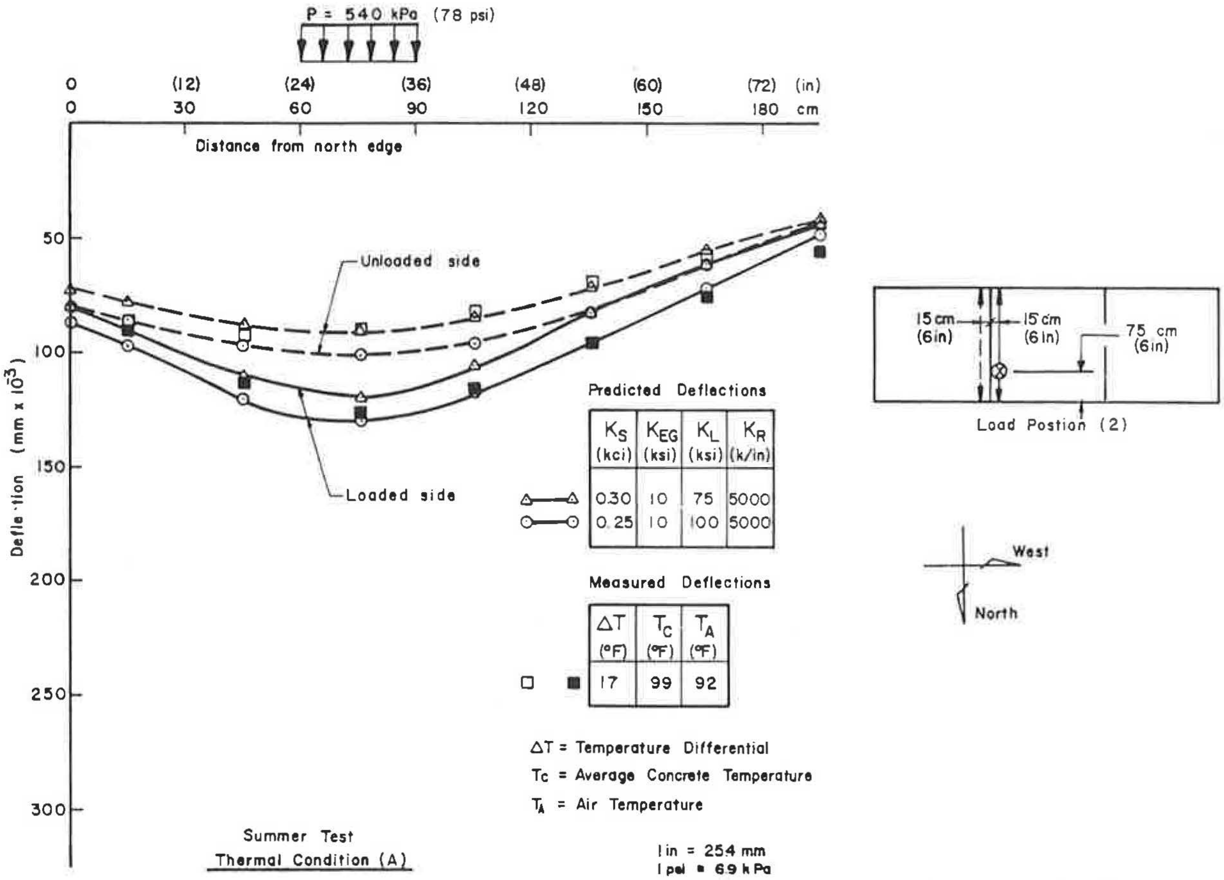

FIGURE 12 Deflection basins on the loaded and the unloaded sides of the undowelled joint, transverse direction.

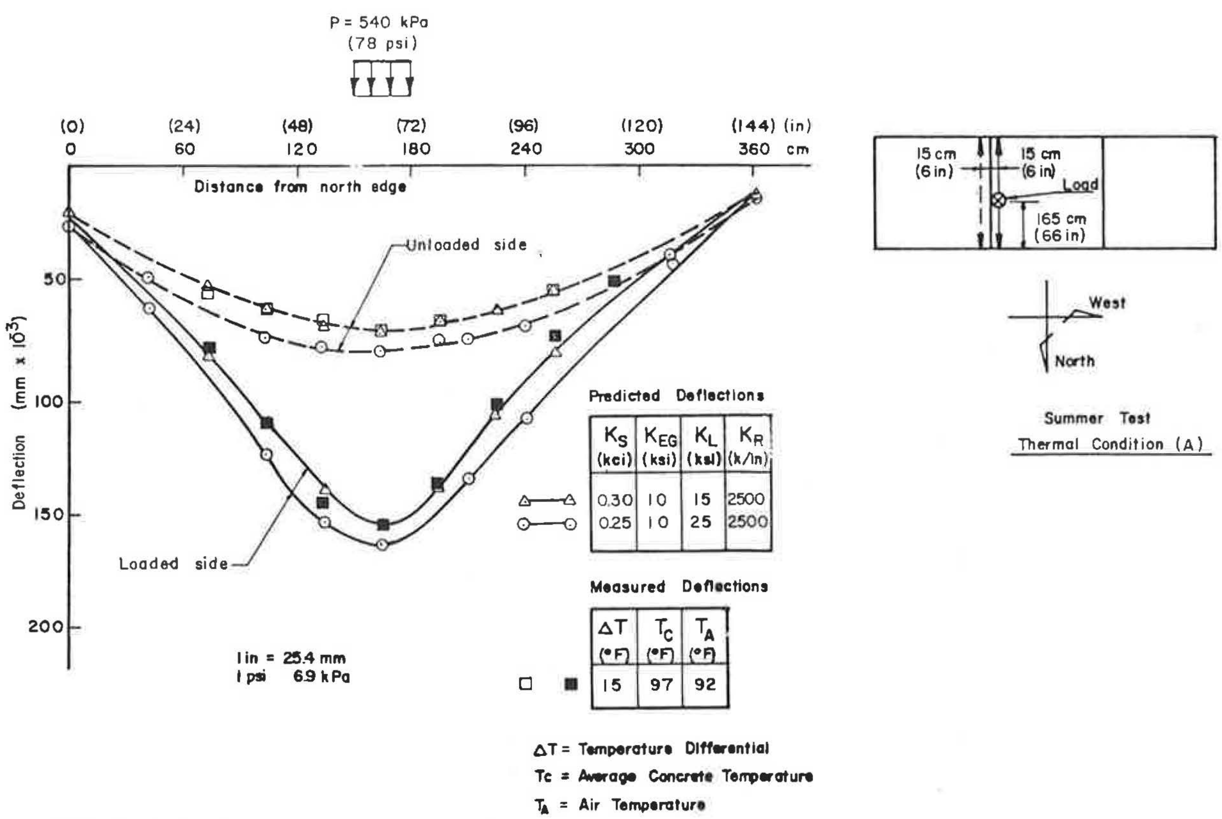

FIGURE 13 Deflection basins on the loaded and the unloaded sides of the undowelled joint, transverse direction.

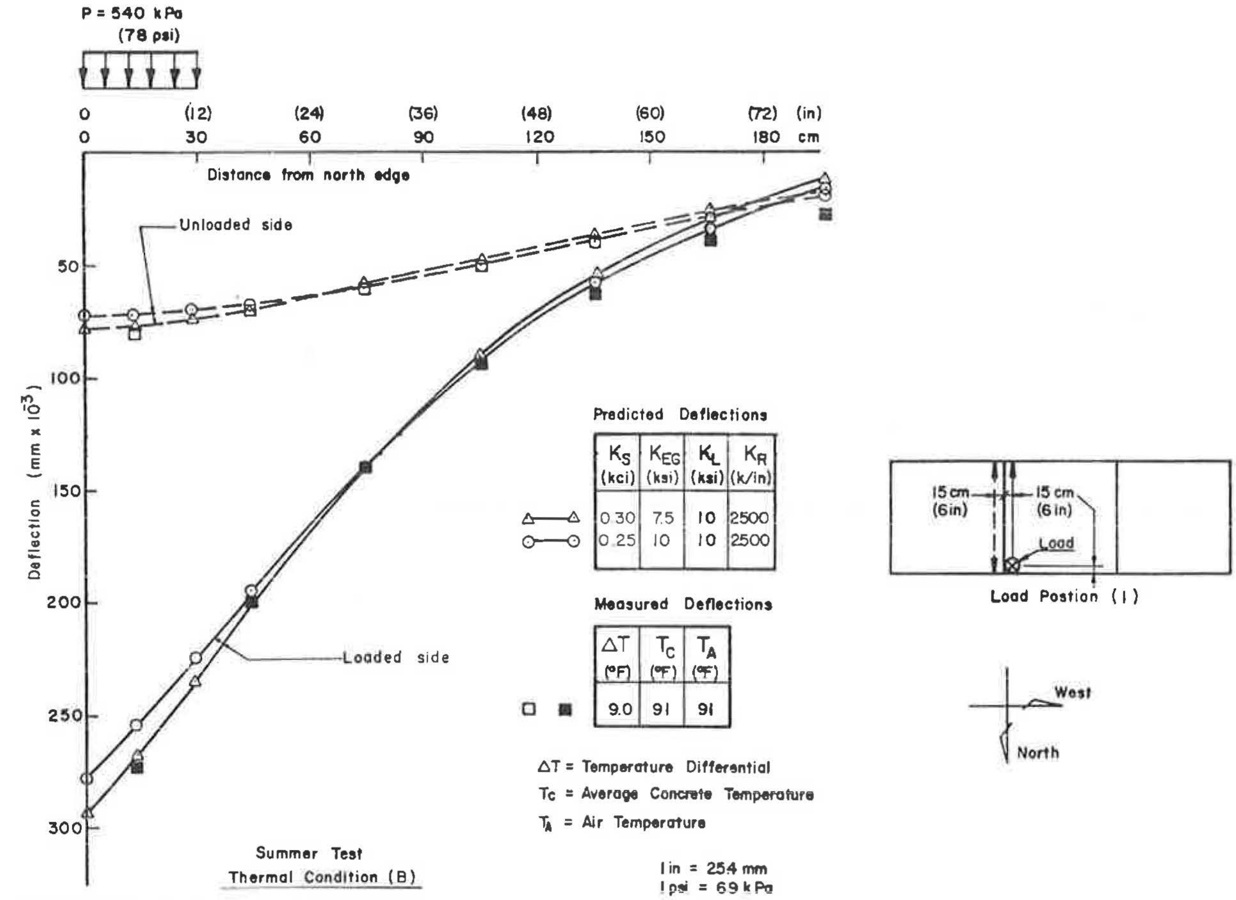

FIGURE 14 Deflection basins on the loaded and the unloaded sides of the undowelled joint.

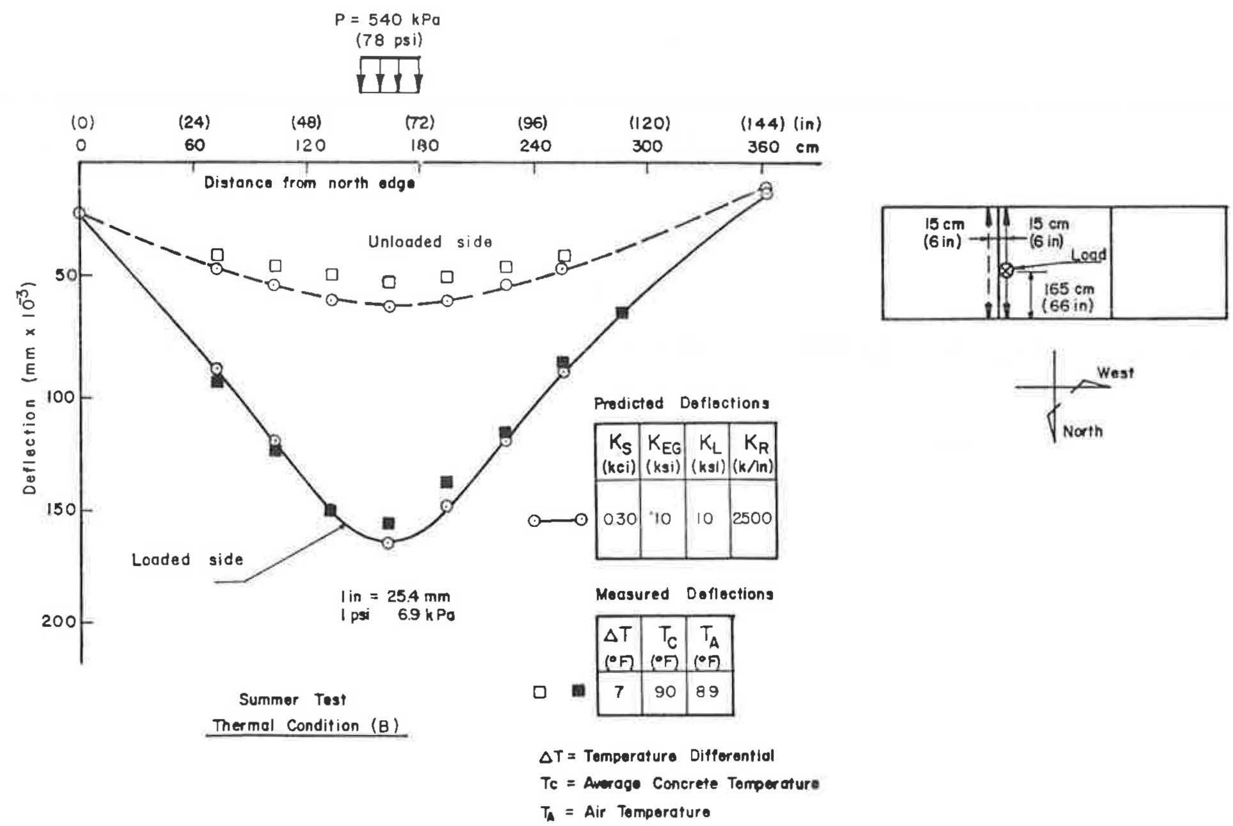

FIGURE 15 Deflection basins on the loaded and the unloaded sides of the undowelled joint (summer test).

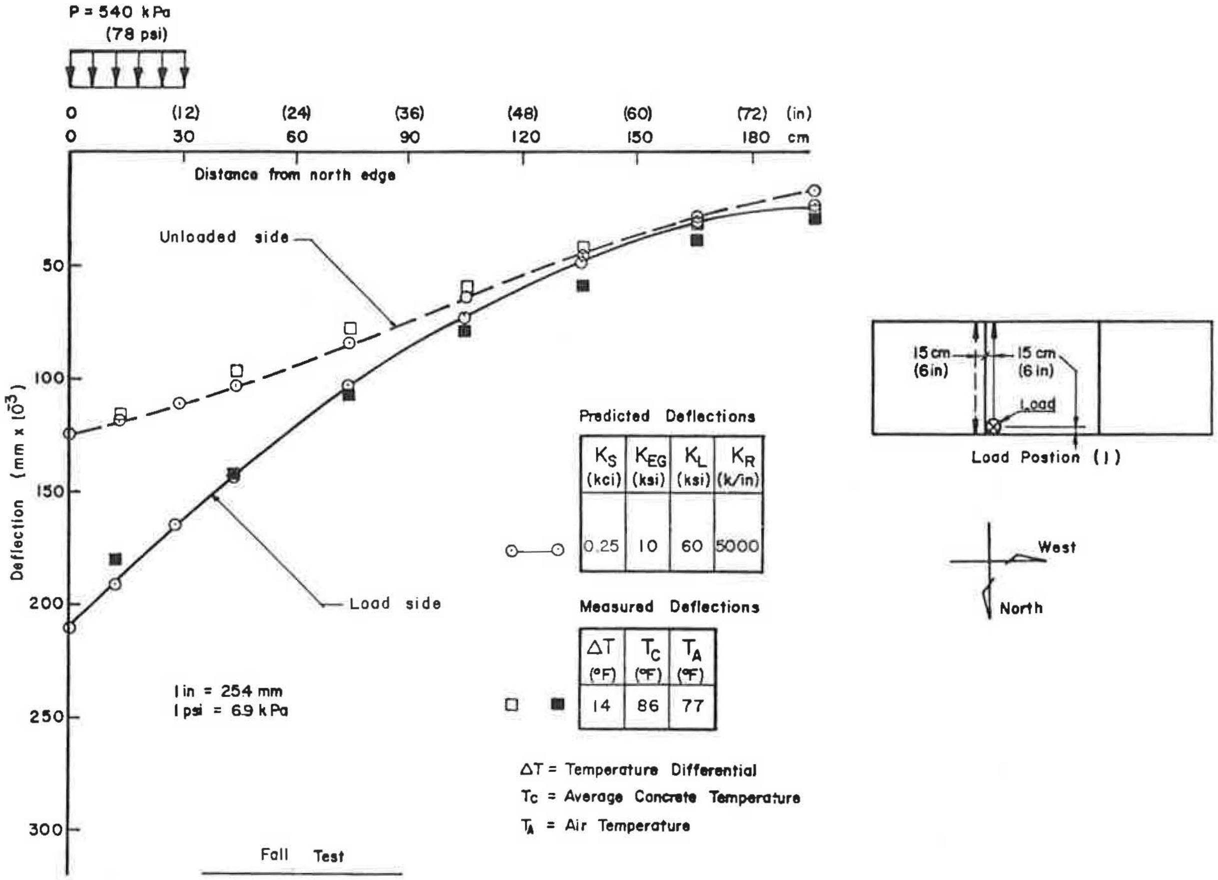

FIGURE 16 Deflection basins on the loaded and the unloaded sides of the undowelled joint (fall test).

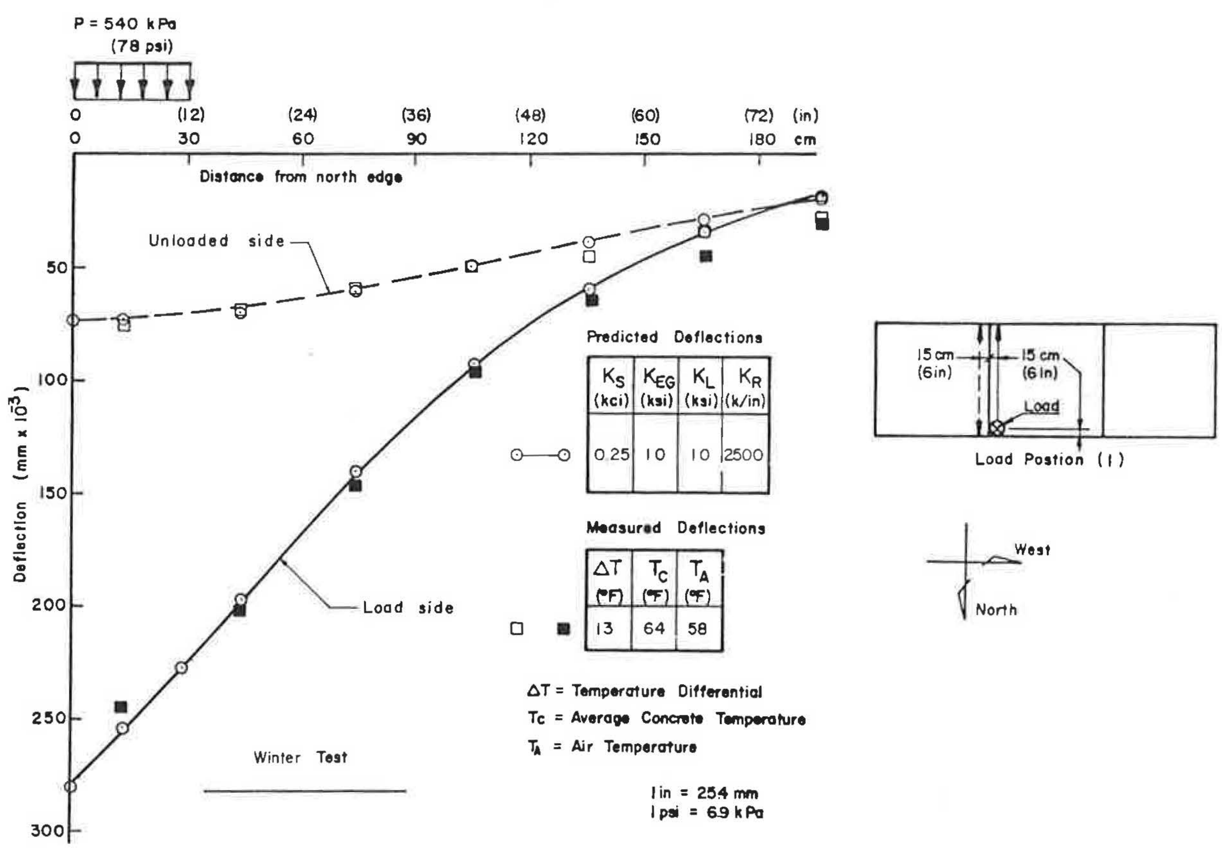

FIGURE 17 Deflection basins on the loaded and the unloaded sides of the undowelled joint (winter test).

TABLE 1 JOINT EFFICIENCIES ALONG THE JOINT FOR THREE LOAD POSITIONS

Distance From North Edge cm (in)	Load Position (1) Deflection (mm x 10^{-3}) Loaded Side	Unloaded Side	Joint Eff.%	Load Position (2) Deflection (mm x 10^{-3}) Loaded Side	Unloaded Side	Joint Eff.%	Load Position (3) Deflection (mm x 10^{-3}) Loaded Side	Unloaded Side	Joint Eff.%
15 (6)	165	136	82	89	86	97	-	-	-
45 (18)	124	110	89	107	92	86	-	-	-
75 (30)	90	86	96	127	88	69	77	56	73
105 (42)	67	66	99	115	81	70	111	62	59
135 (54)	50	49	99	96	69	72	147	67	46
165 (66)	37	37	100	77	59	77	153	69	45
195 (78)	28	28	100	57	49	86	132	67	51
225 (90)	-	-	-	-	-	-	105	63	60
255 (102)	-	-	-	-	-	-	72	56	78

Note: Load = 540 kPa (78 psi). 1 psi = 6.9 kPa, and 1 in. = 25.4 mm. Thermal conditions: $\Delta T = +17°F$, and $T_c = 99°$. Joint efficiency = (deflection, unloaded side/Deflection, loaded side) × 100. Load Positions 1, 2, & 3, see Figure 6.

as illustrated in Table 1. In Table 1 the values of joint efficiency changed from the 82 percent at Load Position 1 to 99 percent at 90 cm (36 in.) away from the load center. The joint efficiency measured at Load Positions 1, 2, and 3, also changed from 82 percent (Position 1) to 69 percent (Position 2) to 45 percent (Position 3). As a result of the inconsistent values of joint efficiencies, the evaluation procedure of the shear and moment stiffnesses was based on deflection basins correlations and not on ratios of measured deflections at the joint.

Variability of Stiffness Along the Undowelled Joint

In Figure 18, the shear and moment stiffnesses along the joint for Thermal Condition A are shown to have varied considerably, whereas for Thermal Condition B the stiffnesses remained constant along the joint. The temperature differentials for Thermal Conditions A and B were 16°F and 9°F, respectively. In Figure 5, the deflection profiles for ΔT of +15°F and +17°F indicate a downward curling of the joint. This

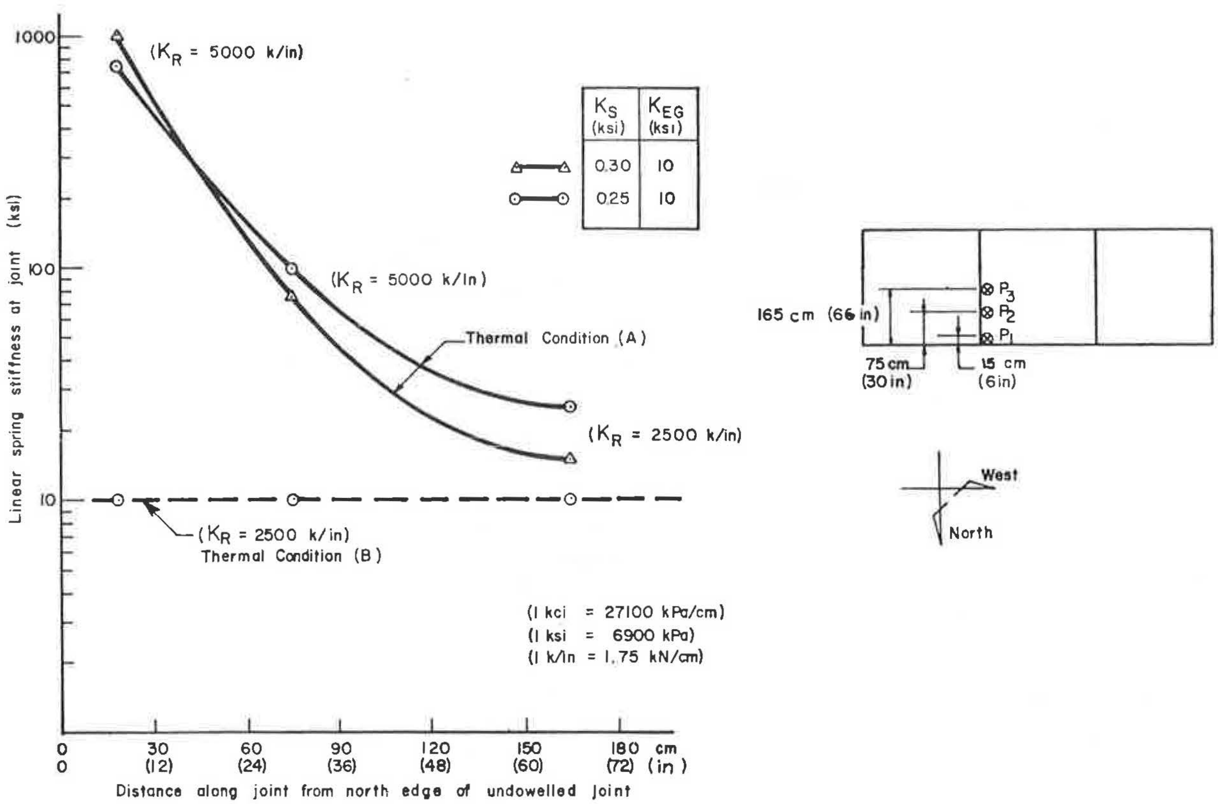

FIGURE 18 Effects of temperature differential of the concrete pavement on variability of joint stiffness along the undowelled joint.

curling along the joint may have caused variable joint opening and, consequently, may have induced a variable degree of aggregate interlock resulting in the variation of the stiffness along the joint.

In the case of Thermal Condition B, the temperature gradient ranged between +7.5°F and 10°F. As shown in Figure 5, the deflection profiles for this range of temperature differentials indicate an almost level surface or no warping condition along the joint. This thermal condition may have caused a uniform joint opening and subsequently a uniform aggregate interlock that in turn may have resulted in uniform shear and moment stiffnesses along the joint.

It should be noted from Figure 5 that the no warping or curling condition occurred at ΔT of +9°F and not at ΔT of 0°F. This may be a result of the effects of moisture in the concrete or the differential drying shrinkage that might have occurred in the slabs after placing the concrete.

Seasonal Changes in Joint Stiffness

Seasonal changes in the average temperature (T_c) of the concrete pavement resulted in the variability of the shear and moment stiffnesses. The variability in stiffness between summer, fall, and winter as T_c is decreased from 98°F in the summer to 64°F in the winter is shown in Figure 19.

The average concrete temperature affects the expansion or contraction of the pavement slabs and controls the degree of the joint locking. When T_c was reduced from 98°F to 64°F the joint between the adjoining slabs might have opened enough to cause the sharp reduction in the shear and the moment stiffnesses of the undowelled joint.

CONCLUSIONS

A procedure was presented to evaluate a test pavement, using the finite-element computer program FEACONS III and field deflection data from the FWD tests. Subgrade, edge, and joint stiffnesses were evaluated to correlate predicted and measured deflection basins. Based on the evaluation of the undowelled joint, the following conclusions were made:

1. The concept of joint efficiency has been determined to be an unrealistic measure of the joint stiffness due to its variability with changes in load positions and thermal conditions.

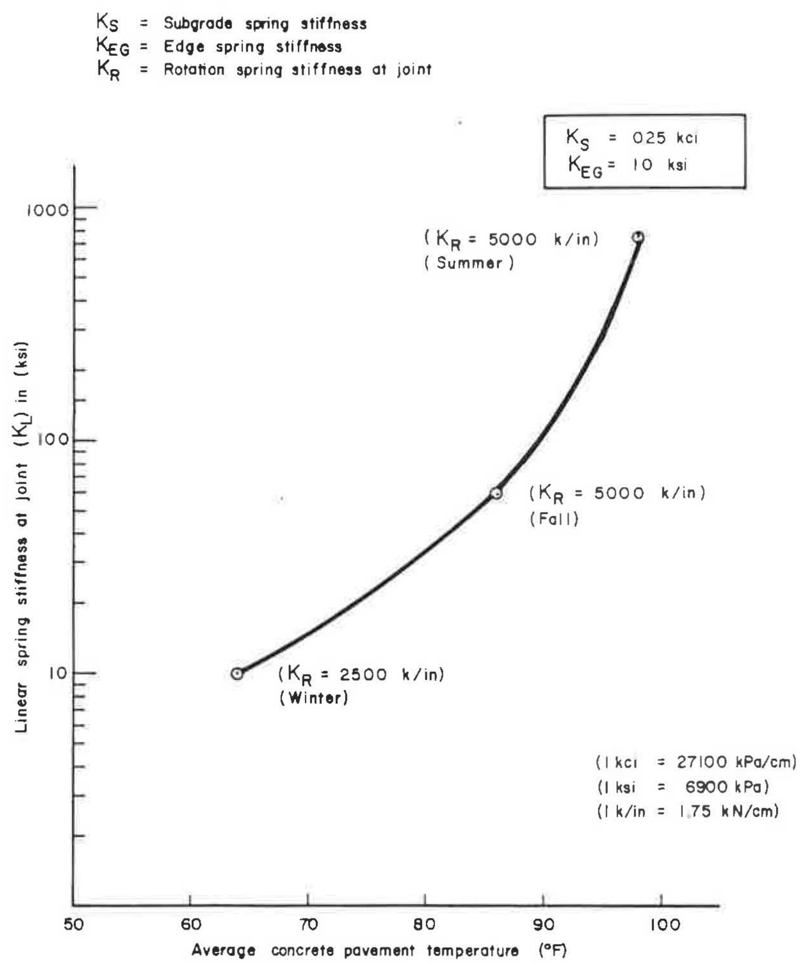

FIGURE 19 Effects of concrete pavement temperature on the joint stiffness of the undowelled joint.

2. The shear and moment stiffness varied along the joint when the deflection profile of the slab showed a condition of downward curling.

3. The shear and moment stiffnesses were constant when the deflection profile at the slab along the joint showed a condition of no warping or curling.

4. The shear and moment stiffnesses decreased as the average temperature of the concrete pavement decreased between the summer and the winter seasons.

FEACONS III will be further tested to determine its capability in modeling various joint types, slab conditions such as warping, and the presence of voids below the pavement. If all of the variables affecting pavement response can be modeled by this finite-element program, it should be equally applicable to the analysis of concrete pavements with different thicknesses, slab lengths, skewed joints, and so on. It is intended that charts, functions, or both be developed to predict the values of the K_s, K_{EG}, K_L, and K_R, which formulate the direct input into FEACONS III for use in the analyses or development of design charts for concrete pavements.

ACKNOWLEDGMENTS

This research has been sponsored by the Florida Department of Transportation. The technical assistance and suggestions of Mr. T. Larsen are gratefully acknowledged. The cooperation and effort of C. Davis and G. Padgett are highly appreciated.

REFERENCES

1. Y. T. Chou. Structural Analysis Computer Program for Rigid Multicomponent Pavement Structures with Discontinuities. Wesliquid and Weslayer. *Technical Report GL-80*, U.S. Army Waterways Experiment Station, Vicksburg, Mississippi, Sept. 1980.
2. A. M. Tabatabaie and E. J. Barenberg. "Finite Element, Analysis of Jointed or Cracked Concrete Pavements." In *Transportation Research Record 671*, TRB, National Research Council, Washington, D.C., 1978, pp. 11–19.
3. Y. H. Huang and S. T. Wang. "Finite Element Analysis of Concrete Slabs and Its Implication for Rigid Pavement Design." In *Highway Research Record 466*, HRB, National Research Council, Washington, D.C., 1973, pp. 55–69.
4. J. M. Lybas, M. Tia, and D. A. Twiddy. "Evaluation of a Concrete Test Pavement Using the FWD and WESLIQUID." *Proc., Third International Conference on Concrete Pavement Design and Rehabilitation*, Purdue University, LaFayette, Indiana, April 1985.
5. M. Tia, J. M. Armaghani, L. Lei, and K. L. Toye. "Development of FEACONS III Computer Program for Jointed Concrete Pavement Analysis." Unpublished paper.

Analysis of Concrete Pavement Performance and Development of Design Procedures

R. J. ROMAN, M. Y. SHAHIN, AND T. J. FREEMAN

A procedure to design concrete pavements based on local conditions and performance of existing pavements is presented. The procedure is used to develop design equations to determine required concrete thickness or terminal condition of the pavement for a number of design inputs. These inputs include subgrade support, concrete modulus of rupture, stress-to-strength ratio, traffic, concrete thickness, and the condition of the pavement at the end of the design period. The procedure utilizes the pavement condition index (PCI) survey procedures and nondestructive deflection testing to develop design equations for local conditions. Existing pavements are surveyed and evaluated to provide information for use in developing a design equation for local conditions.

A procedure to develop a performance-based concrete pavement design is described. In-service pavements with a range of traffic, age, thickness, and condition are used to develop design equations to determine the required thickness to adequately serve the projected traffic for the design period and desired terminal condition.

PROCEDURE

The steps involved in developing a performance-based design equation are shown in Figure 1. The primary steps to collect the necessary data and develop the equation include preliminary data collection, dividing the pavement into uniform sections, distress survey, nondestructive deflection testing (NDT), coring, and a traffic analysis. These steps are discussed in detail in the sections that follow.

Preliminary Data Collection and Pavement Identification

The first step is office data collection for information on construction history, design, materials and soils properties, and past and projected traffic. Any previous performance and maintenance data should also be obtained. Once this information has been collected, the pavements with the desired characteristics and range of variables such as thickness, traffic, or age are identified.

Division of Pavement Into Uniform Sections

After initial identification, the pavements are divided into uniform sections. A uniform section has consistent characteristics such as structural composition, construction history, traffic, and condition throughout its length. Once the uniform sections are identified, collection of additional information from coring, nondestructive deflection testing, and a distress survey can begin. As additional data are obtained from these activities, it may be necessary to modify the uniform sections. For example, if one uniform section has consistent construction history and structural composition but different levels of traffic or pavement condition, it is necessary to divide that section into two or more uniform sections. Definition of uniform sections is an iterative process throughout data collection.

Pavement Condition Survey

The condition of in-service pavements must be known to develop performance-based design equations. An objective measure of performance of existing pavement sections is the basis on which performance-based designs are developed. The pavement condition index (PCI) method developed by the U.S. Army Corps of Engineers (*1*) is used to determine the pavement section condition and provide a measure of its performance. The PCI is determined as a function of distress type, severity, and amount. The final calculated PCI is a number from 0 to 100, with 100 representing a perfect pavement. A summary of the PCI scale is shown in Figure 2.

Each uniform section is further subdivided into sample units for pavement inspection. Each pavement section may be surveyed in its entirety or by using sampling techniques. The PCI of each pavement section is determined and is used to develop a design equation.

Nondestructive Deflection Testing

NDT is used to measure the pavement system's structural response to simulated moving truck wheel loads, to evaluate subgrade support conditions, and provide information for use in materials characterization and fatigue analysis.

The NDT program is conducted using the falling weight deflectometer (FWD). The FWD is an impulse loading device capable of simulating a moving wheel load in both magnitude and duration of loading. The FWD is capable of producing loads from 1,500 to 24,000 lb force.

The NDT program should test slabs at both center slab and joint locations as shown in Figure 3. Results from center slab tests are used to determine the dynamic stiffness modulus of the concrete slabs and the dynamic modulus of subgrade reaction (k-value). Joint testing is used to determine load transfer efficiency. Load values used during testing should simulate the actual loadings expected for the pavement. A reference slab

R. J. Roman and T. J. Freeman, ERES Consultants, Inc., P.O. Box 1003, Champaign, Ill. 61820. M. Y. Shahin, 37 Maple Court, Lake Park, Champaign, Ill. 60656.

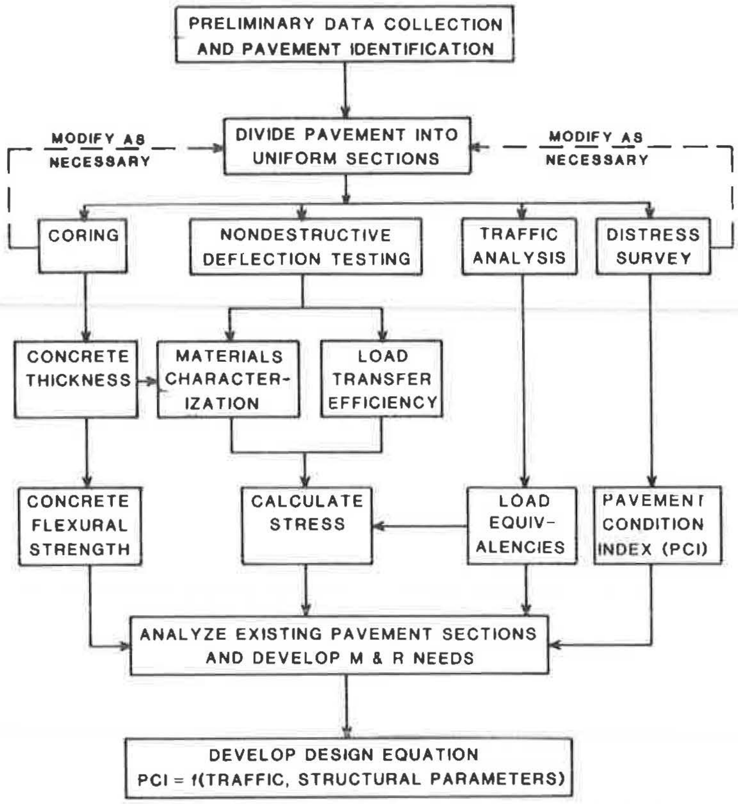

FIGURE 1 Steps to develop a performance-based concrete design equation.

should be chosen to measure the effects of temperature on deflection measurements. This is necessary to compensate for any environmental influences, such as slab curling, that may affect measured deflections or load transfer. Tests should be conducted at various times throughout the day at the same point at center slab and joint locations of the temperature reference slab.

Materials Characterization

Deflection data are used to evaluate the structural capacity of the pavement and subgrade properties. These properties include the dynamic modulus of elasticity of the concrete slab and the subgrade *k*-value. The NDT deflection basin results and layer thicknesses are used as inputs to a computer finite-element pavement model (*2*) to back-calculate the in-situ dynamic material properties. Both the dynamic slab modulus and subgrade modulus values are varied to obtain a grid such as that shown in Figure 4 for a given concrete pavement thickness and slab size. The basin area shown on the *x*-axis is obtained from deflection data as shown in Figure 5. Measured values obtained with the FWD are used as entrance points on this grid to determine both the dynamic subgrade *k*-value and the dynamic concrete modulus values simultaneously. Average values for the dynamic modulus of the concrete and subgrade *k*-value for each pavement section are determined in this manner. The existing concrete thickness must be known to develop

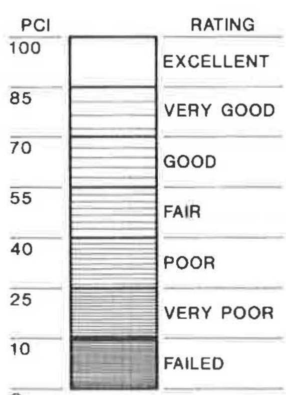

FIGURE 2 PCI rating scale.

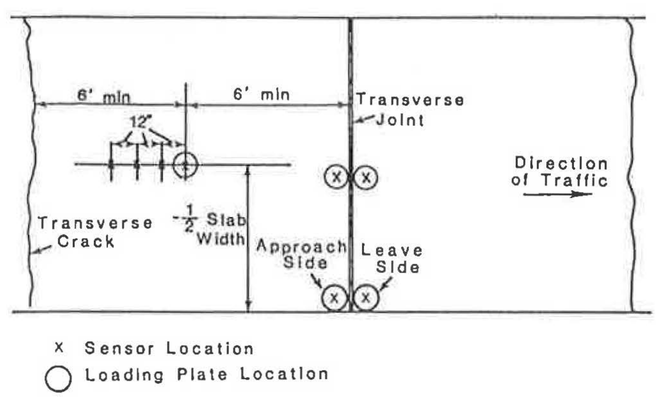

FIGURE 3 FWD test locations.

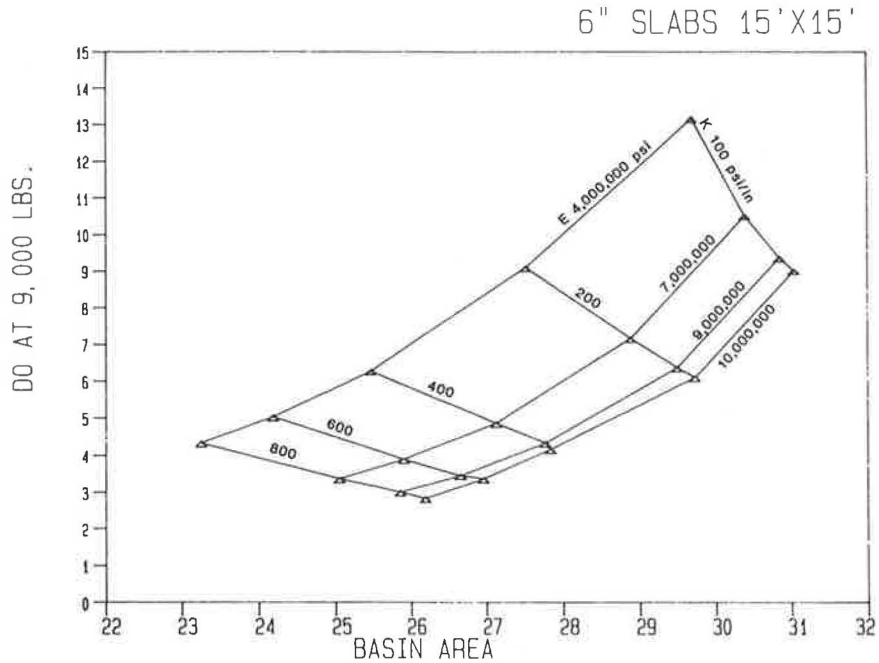

FIGURE 4 Example concrete modulus and k-value determination graph.

the grid system. Therefore, a coring program should be coordinated with the nondestructive deflection testing.

Load Transfer Across Joints

NDT is also used to determine the load transfer efficiency across joints. Load transfer efficiency is defined as the ratio of the deflection of the unloaded side of the joint to the deflection of the loaded side. Load transfer efficiencies in the range of 70 to 100 percent are considered good, whereas load transfer efficiencies below 50 percent are considered poor. A high degree of load transfer (greater than 70 percent) is effective in reducing the critical stress in the concrete slab due to the edge loading and corner loading conditions. Lower stresses will reduce the occurrence of load-related distresses such as corner breaks, spalling, and linear cracks.

Determination of Concrete Stresses

When material properties and the level of load transfer are determined, the stress in each pavement section is determined by using a number of models. The finite element program ILLI-SLAB (*2*), developed at the University of Illinois, is used to evaluate the structural response of the pavement and determine the concrete stresses. ILLI-SLAB is capable of analyzing jointed concrete pavements comprised of one or two layers with any specified level of load transfer at the joints or cracks and arbitrary loading conditions such as center, corner, or edge loading. The primary advantage of using ILLI-SLAB is that the actual load transfer conditions determined using nondestructive deflection testing are used when determining the concrete stresses for each pavement section under consideration. Required inputs to use ILLI-SLAB include slab size, thickness, modulus of elasticity, load transfer efficiency, dimensions of the loaded area, and amount of load. Therefore, traffic information and concrete thickness from a coring program are needed to determine the concrete stresses for each pavement section.

Coring

A limited destructive testing survey is necessary to determine the actual concrete thickness for each pavement section. The pavement thickness is used when back-calculating the dynamic concrete modulus of elasticity and dynamic subgrade *k*-value, and in determining the concrete stresses for each section.

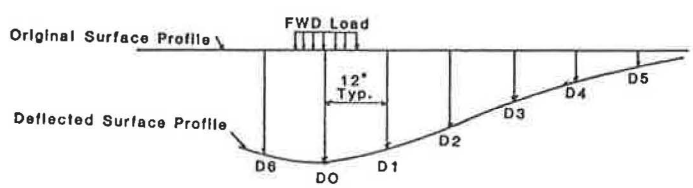

Deflection basin AREA1 is calculated using the formula:

AREA1 = [6/DO] x [Do + D1 + D6 + 2D2 + D3]

FIGURE 5 Determination of deflection basin area.

The flexural strength of each pavement section is determined by taking cores or cutting beams from the pavement and testing to determine the concrete modulus of rupture. The concrete flexural strength is used in the development of the design equation to relate the stress ratio for each pavement section to performance or condition of each section.

If concrete cores or beams are not available, the flexural strength can be calculated based on a correlation with a concrete dynamic stiffness modulus.

Traffic Analysis

Traffic data are necessary to provide information on traffic volume and loadings. This information is needed to define the uniform pavement sections and develop the design equation. Once the traffic volume and loadings are determined, the number of load equivalencies, such as 18-kip equivalent single axle loads, for each pavement section is determined.

Analysis of Existing Pavement Sections

Once the aforementioned steps have been completed, the pavement sections surveyed are analyzed and maintenance and rehabilitation needs are developed for each section. Maintenance and rehabilitation alternatives should be specified both to repair existing distress and to retard or prevent future deterioration of the pavement section. Loss of subgrade support should be evaluated. Results of nondestructive deflection tests at corner locations are used to determine the areas that are exhibiting loss of support (*3*).

Development of a Design Equation

A design equation is developed to determine the relationship between PCI, stress ratio (concrete stress/modulus of rupture), and traffic (*4*). The best general form of the equation was found to be $\mathrm{PCI} = 100 - 10^{a1} \times [\text{traffic} \times (\text{stress ratio})^{b1}]$.

Regression techniques are used to determine the coefficients $a1$ and $b1$. Once these coefficients are determined, the correlation between predicted PCI from the above equation and the measured PCI is determined. This equation is then used as a design equation to determine the required concrete slab thickness for some terminal PCI value at the end of the design period. The equation can also be used to predict the future PCI of existing pavements as a function of traffic and stress ratio.

EXAMPLE APPLICATION

The foregoing procedure to develop a design equation based on local conditions and pavement performance can be used in many applications. This example considers a large truck terminal. One-half of the truck terminal consists of a concrete pavement in various conditions. The other one-half of the terminal is currently asphalt concrete that is to be removed and replaced with a concrete pavement.

Preliminary Data Collection

The initial office data collection effort showed that the concrete pavements at the terminal could be categorized as follows:

1. A 6-in. jointed reinforced concrete pavement with Number 4 reinforcing bars in both directions placed on 6–9 in. of lime-modified subgrade. These areas were constructed in 1982.
2. An 8-in. jointed reinforced concrete pavement with Number 4 reinforcing bars in both directions on recompacted subbase material. These areas were constructed in 1982.
3. A 6-in. jointed reinforced concrete pavement constructed directly on top of 6–8 in. of lime-modified subgrade. This area was constructed in 1965.
4. A 6-in. jointed reinforced concrete pavement constructed directly on top of recompacted subbase. These areas were constructed in 1977.

Available traffic information included the number and weight of trucks that entered the terminal.

Results of the PCI Survey

Before conducting the PCI survey, the concrete pavement network was divided into uniform pavement sections and sample units. Sections were divided based on pavement areas that had consistent characteristics such as structural composition, construction history, traffic pattern, and function. Each section was further subdivided into sample units for pavement inspection. For pavements with joint spacings less than or equal to 30 ft, a typical sample unit consists of an area of approximately 20 slabs (± 8 slabs).

The PCI was determined from a visual survey in which distress type, severity, and quantity were recorded for the concrete areas. The PCI value calculated for each sample unit and the section PCI are shown in Figure 6. The PCI for each section was calculated by averaging the sample unit PCIs.

Nondestructive Deflection Testing

The program was conducted on pavement Sections 1 through 22. The objective of the NDT program was to (*a*) measure the pavement system's structural response to simulated moving truck wheel loads, (*b*) evaluate subgrade support conditions, and (*c*) provide information for use in materials characterization and fatigue analysis.

The NDT program was conducted using the FWD. Slabs were tested at both center slab and joint locations as shown in Figure 3. Results from center slab tests were used to determine the dynamic stiffness modulus of the concrete slabs and the dynamic subgrade *k*-value of the foundation.

Emphasis was placed on testing areas to provide information to evaluate the concrete and subgrade strength properties. A reference slab was chosen to evaluate the effects of temperature on deflection measurements. This is necessary to compensate for any environmental influences, such as slab curling, that may affect measured deflections or load transfer.

SECTION PCI SUMMARY

SECTION	PCI	SECTION	PCI
01	98	12	75
02	83	13	75
03	98	14	70
04	74	15	97
05	92	16	75
06	98	17	99
07	62	18	80
08	98	19	75
09	90	20	94
10	61	21	98
11	98	22	100

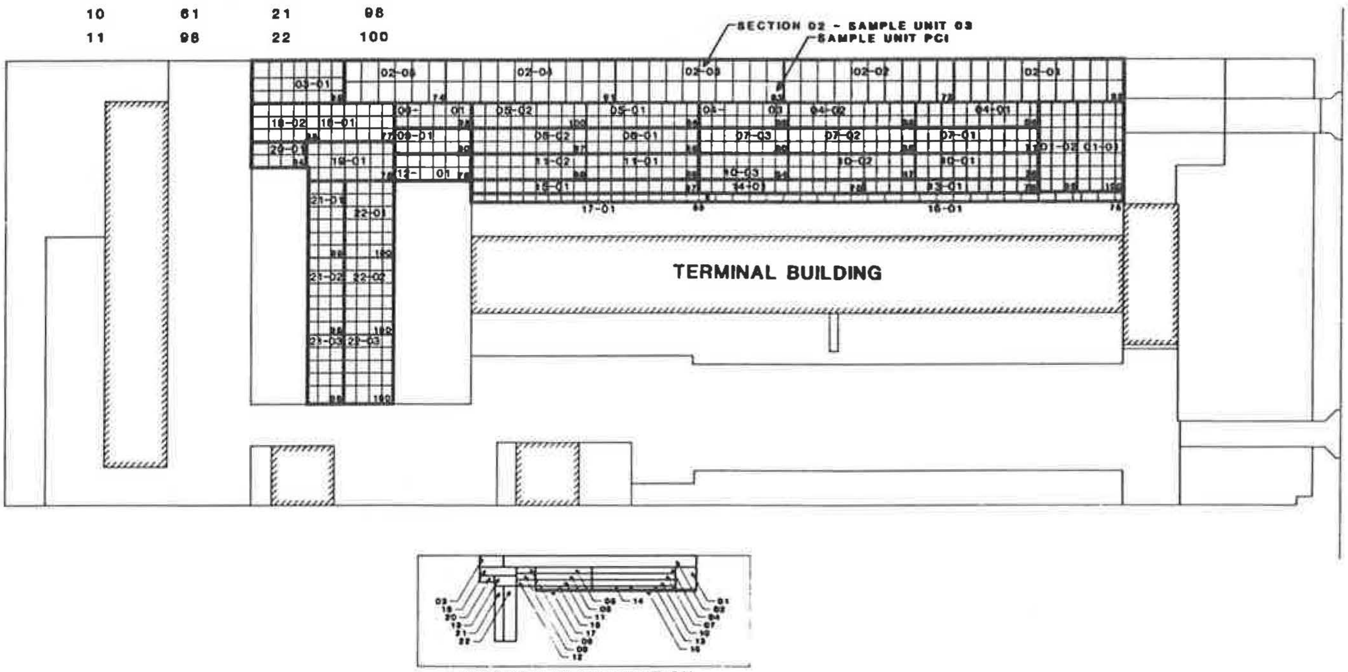

FIGURE 6 Section and sample unit PCI summary for truck terminal example.

Materials Characterization

Both the dynamic slab modulus and subgrade modulus values were varied to obtain a grid as shown in Figure 4. A grid was developed for both the 6-in. and 8-in. concrete sections. Measured values obtained with the FWD were used as entrance points on the grid to simultaneously determine the dynamic subgrade *k*-value and concrete modulus values. The average concrete modulus and *k*-values for each section are summarized in Table 1. The subgrade moduli values shown are dynamic moduli values that are approximately double the conventional static moduli values used in pavement design. The concrete moduli values are also dynamic moduli values that are approximately 1.4 times the conventional static moduli values.

The wide variance in back-calculated concrete moduli values suggests a significant slab thickness variation along the project in addition to varying strengths. The variation in concrete thicknesses and compressive strengths obtained from limited coring at the site support this. Results of test cores are given in Table 2. As the concrete thickness increases, the curves in Figure 4 will shift to the right along the subgrade *k*-value lines. Therefore, if the calculated slab modulus is 8×10^6 based on a grid system for a 6-in. thick slab, and the actual slab thickness is 7 in., the actual slab modulus would be reduced to 6×10^6,

TABLE 1 SUMMARY OF SLAB AND SUBGRADE MODULI VALUES

SECTION	Dynamic E_{pcc} ($x10^6$)	Dynamic k -value
1	7.83	373
2	8.76	224
3	6.80	223
4	8.42	347
5	7.73	219
6	8.87	290
7	7.36	282
8	9.50	400
9	7.30	337
10	7.12	288
11	7.85	405
12	8.00	350
13	9.25	305
14	7.50	285
15	8.00	377
16	6.37	217
17	7.70	330
18	6.36	306
19	7.80	333
20	8.40	340
Average	7.85	311
Standard Deviation	0.86	59
21*	6.65	278
22*	6.50	270
Average	6.58	274
Standard Deviation	0.11	6

* 8 inch slabs

TABLE 2 RESULTS OF TEST CORES

CORE NUMBER	PAVEMENT THICKNESS	UNCONFINED COMPRESSIVE STRENGTH	SLAB CONDITION
1	*5.29 inches	6460 psi	Shrinkage Crack
2	7.38	6530	No Distress
3	5.96	4560	Failed
4	5.35	--	Linear Crack
5	5.97	4440	Failed
6	6.32	--	At Joint
7	6.44	7100	No Distress

--Could not be tested

for example, if the grid system with the proper thickness had been used. The variation in k-values due to the thickness effects was found not to be significant. No attempt was made to correct the concrete modulus values for the variation in concrete thickness due to the wide range of thicknesses obtained during coring. Extensive coring would be required to accurately define the concrete thickness throughout the site. Ideally the concrete modulus and subgrade k-values should be back-calculated using center slab deflection data from slabs where the exact concrete thickness is known because the grid shown in Figure 4 is a function of concrete slab thickness. Therefore, center slab deflections should be taken at all slabs selected for coring.

Load Transfer Across Joints

The average load transfer for each section tested ranged from 32 to 100 percent and is given in Table 3.

TABLE 3 AVERAGE LOAD TRANSFER ACROSS JOINTS

	PERCENT LOAD TRANSFER JOINT CONDITION		
SECTION	LONGITUDINAL	TRANSVERSE	CORNER
01	95	68	66
02	40	66	55
03	*	94	98
04	89	90	64
05	96	95	*
06	82	*	*
07	83	96	*
08	91	*	*
09	78	*	*
10	32	83	*
11	80	50	*
12	71	*	*
13	64	76	82
14	47	79	41
15	94	100	*
16	56	43	*
17	90	95	*
18	81	*	*
19	60	*	*
20	70	94	*
21	67	*	*
22	*	75	*

* Not Tested

Development of Design Equation

A design equation was developed based on the results of the PCI survey, deflection testing, and available traffic information. This information was used to develop a relationship between PCI, the stress ratio (concrete stress/modulus of rupture), and traffic for Sections 1 through 22. The procedure followed to develop this relationship is described in the following sections.

Concrete Modulus of Rupture

The concrete modulus of rupture (MR) for each of the 22 pavement sections was determined using the average dynamic concrete modulus of elasticity (E) from each section as determined from deflection testing and the empirical relationship (5): $MR = 200E^{0.736}$. The modulus of rupture calculated using this equation is the dynamic modulus of rupture. This value is approximately 1.4 times the static modulus of rupture as determined from flexural tests of concrete beams. The dynamic modulus of rupture for each section is given in Table 4. Ideally, concrete cores or beams would have been taken to determine the concrete modulus of rupture. However, because of project constraints, this was not possible.

Determination of Concrete Stresses

The concrete stress for an edge loading condition with an 18-kip axle load and existing load transfer efficiency was determined for Sections 1 through 22. The concrete slabs were assumed to be 6-in. for Sections 1 through 20, and 8 in. for Sections 21 and 22, although the limited test cores show that this thickness may vary appreciably. The concrete stresses for each section are given in Table 4.

Traffic Analysis

The number of past and future traffic movements were estimated based on information from a typical 99-hr count that provides the number and weight of trucks due to arrive at the terminal during the next 99 hr. The same number of trucks were assumed to be leaving the terminal during this time span. This information was extrapolated over a period of 1 year to arrive at a total number of trucks entering and leaving the terminal during the year. Truck weights were also obtained from a 99-hr traffic count and extrapolated over the period of 1 year. The number of trucks was then converted to a number of 18-kip equivalent single axle loads (ESALs). Equivalent single load applications were determined to be approximately 33,200 per year. This number, along with a traffic factor, was used to calculate the past 18-kip ESAL applications for each uniform section.

A traffic factor was assigned to various sections of the terminal based on the terminal operations and the traffic patterns observed during on-site visits. Areas that were observed to carry the greatest number of traffic repetitions were assigned a traffic factor of 100 percent, areas that carried one-half of the greatest number of repetitions were assigned a traffic factor of 50 percent, and so on. This traffic information is an estimate, as several factors, such as the degree of traffic channelization and the number of interfacility movements, could not be adequately addressed. Past traffic information is given in Table 5.

TABLE 4 SUMMARY OF MATERIAL PROPERTIES

SECTION	DYNAMIC MR (psi)	DYNAMIC SLAB MODULUS (X 10^6)	DYNAMIC K-VALUE (pci)	EDGE STRESS (psi)
01	910	7.8	375	365
02	988	8.8	225	449
03	820	6.8	225	280
04	960	8.4	350	378
05	901	7.7	220	286
06	997	8.9	290	338
07	869	7.4	280	327
08	1049	9.5	400	293
09	864	7.3	340	330
10	848	7.1	288	442
11	911	7.9	405	398
12	924	8.0	350	369
13	1028	9.3	305	382
14	881	7.5	285	423
15	924	8.0	380	266
16	781	6.4	220	416
17	898	7.7	330	310
18	781	6.4	310	336
19	907	7.8	335	380
20	958	8.4	340	367
21	807	6.7	280	303
22	793	6.5	270	289

Note: All stresses in psi

Model Development

A linear regression was performed to determine the coefficients *a*1 and *b*1 in the regression equation. A second linear regression was then performed using the measured PCI values from the condition survey and the calculated PCI values from the aforementioned equation in the section on the development of a design equation. Results of this first regression indicated that several sections (Sections 05, 07, 16, and 17) could not be modeled with the equation. This was attributed to inaccuracies in estimating the traffic factor. These sections were omitted and the regression analysis was repeated. The final equation to predict PCI at the terminal is $PCI = 100 - 10^{-2.373}[\text{traffic (stress ratio)}^{3.7285}]$. The measured PCI versus the PCI predicted from the regression is plotted in Figure 7.

The effect of the stress ratio and traffic on PCI is shown in Figure 8. This graph was plotted using the preceding equation. Increasing traffic or stress ratio will greatly reduce the predicted PCI.

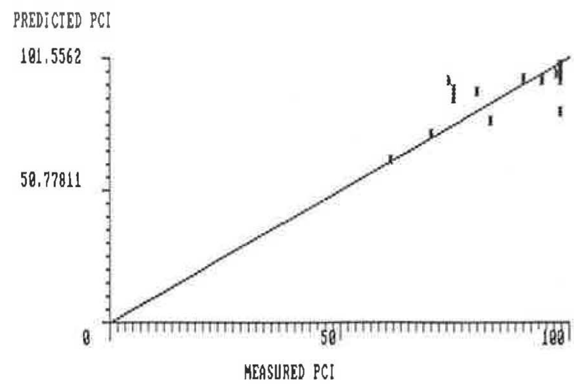

FIGURE 7 Relationship between measured PCI and predicted PCI.

TABLE 5 PAST TRAFFIC INFORMATION

SECTION	AGE (YEARS)	TRAFFIC FACTOR %	18-kip ESAL's
01	3	15	14,951
02	20	15	99,672
03	3	15	14,951
04	3	50	49,836
05	3	50	49,836
06	3	50	49,836
07	3	50	49,836
08	3	50	49,836
09	3	50	49,836
10	3	100	99,672
11	3	100	99,672
12	3	100	99,672
13	3	100	99,672
14	3	100	99,672
15	3	100	99,672
16	8	100	265,792
17	8	100	265,792
18	3	60	59,803
19	3	60	59,803
20	3	60	59,803
21	3	60	59,803
22	3	60	59,803

Thickness Design for a New Pavement

The west half of the terminal is currently asphalt concrete and was in need of pavement reconstruction. A concrete pavement thickness was determined for this area based on deflection testing and the PCI equation developed for the east half of the terminal.

Nondestructive deflection testing was used to evaluate the existing subgrade support conditions on the west half of the terminal. The design subgrade *k*-value was 225 pci.

The PCI equation was used to determine the required concrete thickness, for a range of terminal PCI values, after a 20-year period. The design inputs selected are as follows:

- Traffic: 35,000 ESALs/year with 20 years = 700,000 ESALs,
- Design modulus of rupture = 700 psi,
- Design concrete modulus of elasticity = 5.9×10^6 psi,

- Subgrade k-value = 225 pci, and
- Pavement thickness ranged from 6–12 in.

The concrete stresses for the edge loading condition were determined for each pavement thickness. A deflection load transfer of 40 percent was selected for an undowelled design, and deflection load transfer of 70 percent was selected for the dowelled pavement design. The concrete stresses are summarized in Table 6 and the stress ratio as a function of concrete thickness is shown in Figure 9. The concrete stresses, traffic, and design modulus of rupture were then used to determine the terminal PCI for each pavement thickness after 20 years. The terminal PCI after 20 years as a function of concrete thickness is shown in Figure 10 for both the dowelled and undowelled pavement sections. Figure 10 presents a performance-based design chart for the pavement conditions under consideration. For example, if a terminal PCI of 60 is desired after 20 years, a minimum concrete thickness of 8.5 in. dowelled or 9.5 in. undowelled will be required.

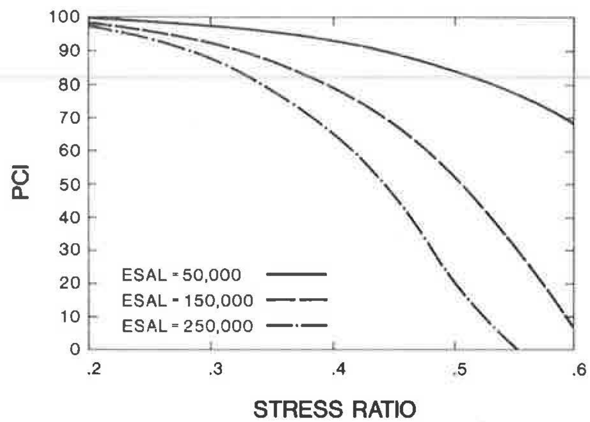

FIGURE 8 Effect of stress ratio and traffic on PCI.

TABLE 6 SUMMARY OF CONCRETE STRESSES FOR WEST HALF THICKNESS DESIGN

CONCRETE THICKNESS (in.)	EDGE STRESS NO DOWELS (psi)	EDGE STRESS WITH DOWELS (psi)
6	430	371
8	290	250
9	237	204
10	205	177
12	146	126

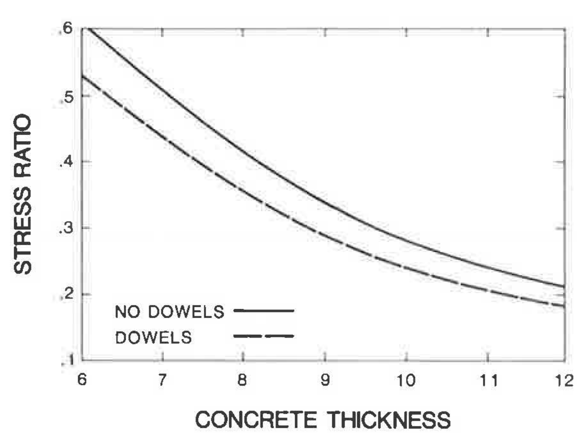

FIGURE 9 Stress ratio versus concrete thickness.

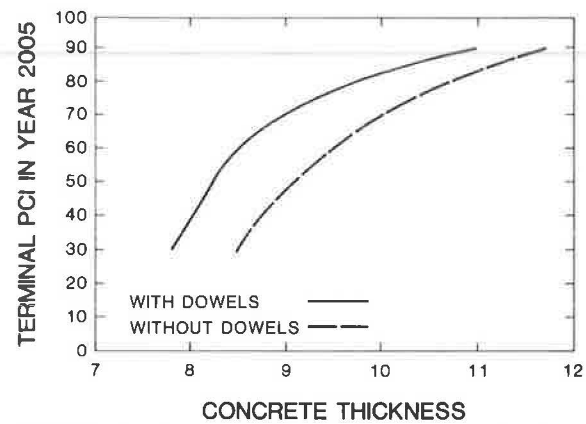

FIGURE 10 Terminal PCI after 20 years as a function of concrete thickness.

SUMMARY

Design equations can be developed based on local conditions to account for subgrade and material properties, traffic, and environment. Performance-based design equations based on local conditions provide the engineer with a tool to aid in the design of new pavements and the prediction of future performance of existing pavements. Equations developed using these procedures must be used within the range of variables from which they were developed. The models must not be used in some unusual situation caused by construction or materials problems that could invalidate the use of the design equation.

REFERENCES

1. M. Y. Shahin and S. D. Kohn. *Pavement Maintenance Management for Roads and Parking Lots.* Technical Report M-294. U.S. Army Construction Engineering Research Laboratory, Champaign, Ill., 1981.
2. A. M. Ioannides, E. J. Barenberg, and M. R. Thompson. Finite Element Model With Stress Dependent Support. In *Transportation Research Record 954*, TRB, National Research Council, Washington, D.C., 1984, pp. 10–16.
3. M. I. Darter, E. J. Barenberg, and W. R. Yrjanson. *NCHRP Report 281: Joint Repair Methods for Portland Cement Concrete Pavements.* TRB, National Research Council, Washington, D.C., 1985, 3 pp.
4. E. J. Barenberg and M. Y. Shahin. *1984 Report on Evaluation of Airfield Pavements at Dulles International Airport.* Crawford, Murphy & Tilly, Inc., Springfield, Ill.; ERES Consultants, Inc., Champaign, Ill., 1985.
5. J. W. Hall and D. R. Alelxander. *Comparative Study of Nondestructive Pavement Testing—Macdill Air Force Base.* Report WES/MP/GL-85-26. Pavement Systems Division, Geotechnical Laboratory, U.S. Army Engineer Waterways Experiment Station, Vicksburg, Miss., Sept. 1985.

Prediction of Subbase Erosion Caused by Pavement Pumping

A. J. VAN WIJK AND C. W. LOVELL

The characterization of the surface erosion of rigid pavement subbase and shoulder materials is described. Three testing methods were used in the study: (*a*) a jetting test for unstabilized (noncohesive) materials, (*b*) a brush test on the effect of six factors on the surface erosion of portland cement- and asphalt-stabilized materials. A statistically designed procedure was used to minimize the number of test samples and to model the interaction of material properties and climatic influences on surface erosion. A number of lean concrete samples were also tested using the brush test; and a rotational shear device was used to obtain the critical shear stress of portland cement-stabilized materials. The brush test provided relative erosion results in terms of weight loss. These results were used to investigate the effects of different variables on the weight loss of stabilized materials and to characterize the erosion of these materials. Brush test results were correlated with rotational shear test results, which were compared with conditions expected to develop under the pavement. The results show that unstabilized materials are not capable of resisting surface erosion in a concrete pavement. Curves were developed for stabilized materials to assist in the selection of subbases and shoulders with low erodibility using standard laboratory tests. These curves include the performance of stabilized materials in different climatic conditions.

Rigid pavement pumping is one of the leading causes of rigid pavement failure. Rigid pavement pumping is defined as (*a*) the ejection of water and subgrade, subbase or shoulder material through pavement joints, cracks, and edges; or (*b*) the redistribution of material underneath the slab. The major cause of material removal from the layer can be pore water pressure buildup or surface erosion. Fines are removed from stabilized layers and unstabilized shoulders mainly by surface erosion. In this process water is accumulated under curled slabs at joints. With the deflection of the approach slab the water is pushed toward the leave slab. The leave slab is then deflected very rapidly by the wheel load and the water is pushed back under the leave slab at a high velocity. Fines are then removed from under the leave slab and deposited under the approach slab. This causes the formation of voids and produces faulting.

Voids change the slab support from a uniformly supported to an unsupported condition at some points. Material removed from shoulders by surface erosion can either be ejected along the pavement edge or deposited under the slabs. This causes shoulder depressions and faulting. Fines are removed from unstabilized materials mainly through pore water pressure buildup.

Three conditions are necessary for pumping to occur: (*a*) high slab deflections (heavy wheel loads, thin slabs, or both); (*b*) water in the pavement; and (*c*) materials that are susceptible to pumping.

Department of Civil Engineering, Purdue University, West Lafayette, Ind. 47907.

Pumping has been a problem in the United States since the 1940s, with the increase in traffic loads during World War II. A number of remedies have been tried to eliminate or reduce pumping. Most of these methods used some type of subbase. Attempts to eliminate pumping include the placement of a granular subbase layer between the slab and the subgrade and the use of stabilized subbases. Stabilized subbases have been used since the 1950s in the United States. These subbases reduced, but did not prevent pumping (*1*). Lean concrete and asphalt concrete layers have also been used successfully in most cases to prevent pumping, because they are virtually nonerodible.

REVIEW OF EROSION TESTS

Erosion of soil is not only important as a factor in the design of rigid pavements, but also in the design of channels, earth dams, and soil slopes. Erosion occurs as a result of the shear stress induced by water flowing over the soil. Jetting and flume tests have been used extensively to investigate the erosion behavior of different types of soils subjected to flowing water.

The erosion of stabilized materials in channels and dam facings has been studied by subjecting cylindrical and beam samples to water overfalls (*2*) and jetting (*3*). Flumes, tube flows, and jetting tests (with jets at different angles) have been used to study the erosion of cohesive and noncohesive soils in geotechnical, hydraulics, and agricultural areas (*4–8*).

Espey (*9*) and Moore and Masch (*10*) developed a rotational shear device in the early 1960s, with which the erosion of cohesive materials could be tested. The apparatus basically consisted of water rotating around a stationary sample. Arulanandan et al. (*11*) also used a similar device in a study on the erosion of clay materials. Akky and Shen (*12*) and Akky (*13*) used such a device to investigate the erosion of soil–cement mixtures. Chapuis (*14*) improved the device and used it to measure mainly the erosion of cohesive materials.

Various tests have been conducted since the 1940s to investigate pumping. The majority of the U.S. testing programs investigating pumping used full-scale sections (*15 – 19*), scaled sections (*20*), and pavement models (*20, 21*). The emphasis was on the loss of fines from unstabilized subbase materials.

Although surface erosion is considered an important rigid pavement pumping mechanism, relatively little research has been conducted on the erosion of subbase and shoulder materials.

The California Department of Transportation uses a test referred to as the Surface Abrasion Test to measure the erosion or abrasion resistance of pavement materials (*1*). The test was initially developed to study the effect of water action on bituminous mixtures. Researchers in France conducted an extensive investigation on rigid pavement pumping in the late 1970s (*22*, *23*). Four tests were used to evaluate surface erosion: two brush tests, a jetting test, and a vibrating table.

TESTING METHODS

After evaluating a large number of testing procedures, the rotational shear apparatus, a jetting test, and a brush test were chosen to evaluate the erosion of rigid pavement subbases.

ROTATIONAL SHEAR DEVICE

Shear forces on the lateral surface of samples tested with the rotational shear device are uniform, can be calculated, and can be easily changed. The device has been used successfully in the investigation of the erosion of such diverse materials as clays and stabilized materials. The easy adjustment of uniform shear forces makes it applicable to a very wide range of subbase materials. It is the only test in which the shear stress that causes erosion can be measured accurately. The obvious disadvantage of this device is that noncohesive materials cannot be tested.

The rotational shear device was designed to accommodate samples compacted at the size specified in AASHTO T135 (*24*). The device was designed to have three annular spacings: 9.5 mm (0.375 in.), 13 mm (0.5 in.), and 16 mm (0.625 in.), by using cylinders with different inside diameters. The annular space is defined as the space between the outside of the sample and the inside of the cylinder. The maximum size of the aggregate was set at 9.5 mm (0.375 in.) to allow for the free movement of the eroded material at all times within the annular space. An air motor of 560 W (0.75 hp) was used to rotate the transparent cylinder at speeds of between 300 and 3,000 rpm. A strobe was used to measure the rotational speeds.

The sample was held in place by four 13-mm (0.5-in.) long tubes attached to a thin metal cap and penetrating into the sample. Epoxy was also used to secure samples to a smooth cap when the cap with the tubes could not be used. The sample rested on the bottom cap. Tape was used to protect the ends of the sample by placing it around the top and bottom ends of the sample covering the caps. The tape prevented water from entering the space between the caps and the sample ends. The top cap was connected to a shaft that transferred the rotation due to shear stress on the sample to a lever arm that pressed against a torque measuring device. A load cell, a string and pulley system, and a torque meter were used.

The amount of erosion was measured by recording the weight of the eroded material rather than weighing the sample after each test. This procedure was more cumbersome, but avoided inaccuracies produced by change in degree of saturation during the test, and prevented the sample from being disturbed. The base plate was modified to provide for easy removal of the eroded material. A schematic diagram of the rotational shear device is shown in Figure 1.

A number of tests were conducted to calibrate the equipment. For laminar flows on smooth surfaced samples the shear stresses can be calculated from the rotational speeds. However,

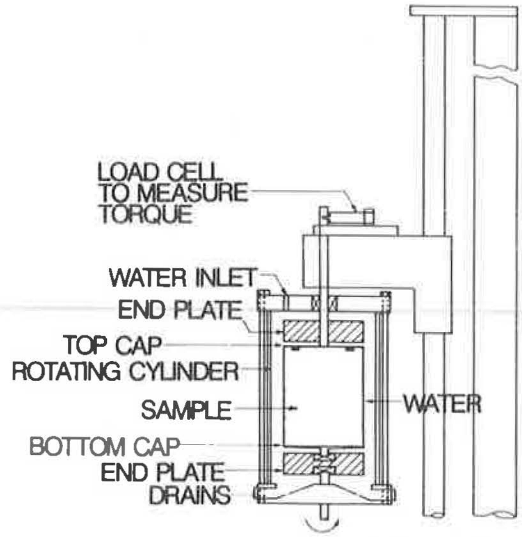

FIGURE 1 Schematic diagram of the rotational shear device.

this condition exists only at very low rotational speeds. The flow of the water in the annular space changes to turbulent flow when the critical Reynolds number (CRN) is reached. The speed at which the CRN is reached depends on the surface roughness of the sample and the annular space. The rotational speeds at which the flows change from laminar to turbulent are about 680 and 820 rpm for annular spaces of 9.52 and 12.5 mm (0.375 and 0.5 in.), respectively (Figure 2). The rate of increase in the shear stress with rotational speed during turbulent flow depends also on the annular space and the sample surface roughness.

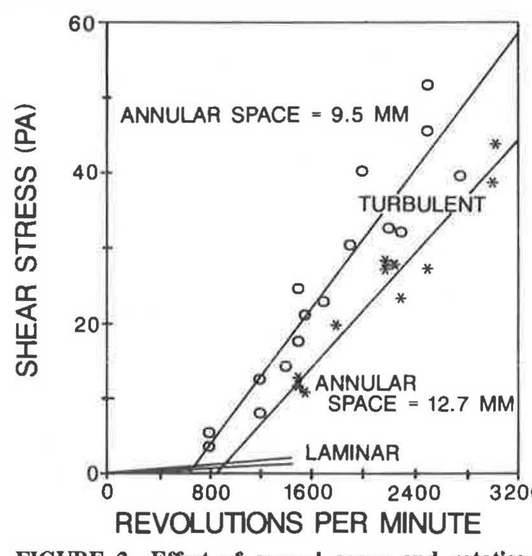

FIGURE 2 Effect of annual space and rotational speed on shear stress.

JETTING TEST

The jetting test (Figure 3) was used to evaluate noncohesive materials. The shear stresses on the sample are not uniform, and cannot be determined as accurately as with the rotational shear test apparatus.

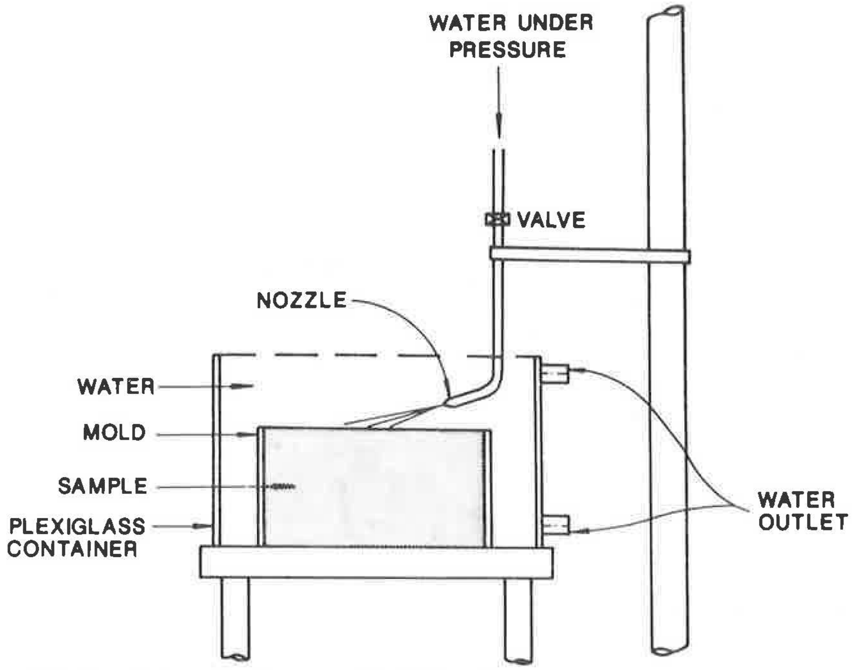

FIGURE 3 Schematic diagram of the jetting device.

The device consisted of a jet placed at an angle of about 20 degrees with the sample. Pressures of up to 345 kPa (50 psi) were provided by a pressure vessel. The sample was placed in a plexiglas container with water outlets at two different levels. Both the pressure vessel and the plexiglas container were built for the study.

The erosion of samples could be measured in the submerged or unsubmerged conditions by changing the water outlet level in the sample container. Samples could also be tested in or out of the molds. Eight spray nozzles with different orifices and spray angles were used. The shear stresses on the sample surface were approximated by dividing the forces at the sample surface by the area of contact. A uniform distribution over the area was assumed.

BRUSH TEST

A brushing test was also selected to evaluate the erodibility of materials, mainly stabilized materials. A brushing test is very simple and fast to use. A large number of samples can be tested, but the results are not correlated to the actual field conditions. The test was therefore selected to be used to investigate the effect of different factors on erosion and to compare the erodibility of materials, rather than trying to correlate the results directly with field conditions. The brush and brushing procedure specified in AASHTO T135 and T136 (*24*) were used because these procedures are the only standard ones available and are used in the evaluation of cement-stabilized materials.

EXPERIMENTAL PROCEDURES

The purpose of the testing program was to obtain information about the erosion of rigid pavement subbase and shoulder materials. The variables included in the testing program were chosen to include the properties of most of the subbases used in rigid pavements. This information was obtained from the results of the survey and rigid pavement design procedures, such as the Portland Cement Association (PCA) (*25*) and AASHTO (*26*). The results from a survey indicated that portland cement-stabilized, crushed stone, dense-graded, asphalt concrete, sand, and asphalt-stabilized subbases are the most widely used in the United States (*27*).

Two types of aggregate, pit-run gravel and crushed stone, were selected to represent the unstabilized materials. Portland cement- and asphalt-stabilized materials are most widely used as stabilized layers and were included in the testing program. A limited number of tests were also conducted on lean concrete materials. Asphalt concrete was not included because it is basically nonerodible. The n-value—n is the exponent in the equation $p = (d/D)^n$ where p is the percent passing size d and D is the maximum size—was used to characterize the gradations. Yoder (*21*) also used the n-value in pumping studies conducted in the 1950s.

The environmental conditions are important factors in determining the performance of all pavement layers. Environmental factors influence the strength, the durability, and the erosion potential of the pavement materials. The most important environmental factors are temperature and moisture content. Changes in temperature can cause freezing and thawing of the pavement materials, while changes in moisture content can cause alternate wet and dry conditions in the materials. Different materials are affected to different extents by these changes, as well as by the number of cycles of each change. The occurrence of the conditions and the number of cycles depend on the geographic location of the pavement and the position of the material in the pavement section. The effect of compaction effort (energy) is important to the strength of the material. The compaction effort would also have an effect on the erosion and was therefore included in the study.

A composite experimental design was selected as a testing procedure because it requires relatively few samples—only 32 samples for five main effects (variables) (*28*). The effects of the linear main effects can be assessed with an analysis of variants (ANOVA) procedure on the factorial part, and a regression equation can be developed relating the erosion with all main effects (*29*).

The composite design was used to test the effect of five variables at five levels each for the cement and asphalt-stabilized materials in two separate experiments. The five variables and the levels used are given in Table 1. The variables and levels were selected to include the important factors that influence erosion and the ranges of application of these factors.

A full experimental design was not used for the rotational shear testing; instead, results from the brushing test were used to identify important variables and ranges of these variables. The brushing test results indicated that portland cement content is the most important factor on the erosion. Samples were compacted at six different portland cement contents ranging from 1 to 7 percent because this is the range of portland cement contents at which the largest changes in erosion occur. The shear stresses on the sample are affected by the annular space and the surface roughness of the sample. The surface roughness is a function of the gradation. Samples were therefore also compacted using three different gradations with *n*-values of 0.3, 0.4, and 0.6.

A number of unstabilized samples were tested to investigate the effect of gradation, plasticity index (PI), and compaction effort on the erosion of these samples by means of the jetting test.

RESULTS

Jetting Test on Unstabilized Materials

The critical water velocity and the shear stress increased with increase in compaction energy, as expected. The compaction effort ranged from Standard Proctor to Modified Proctor. Both the critical water velocity and shear stress increased with an increase in PI. The PI ranged from 1 to 15. Although the jetting device could be used to compare different unstabilized materials, the shear stresses and the erosion cannot be determined very accurately. Assumptions, regarding mainly the area of application, had to be made to obtain some measure of the shear stresses. The calculated critical shear stresses ranged from about 1 to 6 Pa and the water velocities ranged from about 0.75 to 2.5 m/sec (2.5 to 8.2 ft/sec) for the materials tested.

Brush Test on Cement-Stabilized Materials

Although cement- and asphalt-stabilized materials were tested, only the results of the cement-stabilized materials are presented. Erosion was predicted from the average weight loss of the sample after two complete brushes after the last cycle. An analysis of variance was used to evaluate the statistical effects of the variables. All of the main effects and two-way interactions were significant at $\alpha = 5$ percent, except compaction energy and the interaction of gradation *n*-value and the number of freeze–thaw cycles, which were significant at $\alpha = 10$ percent. The variables are therefore all affected by each other.

TABLE 1 COMPOSITE DESIGN LEVELS

		Factor level					Unit
		-2	-1	0	+1	+2	
X1	CT	0.3	0.4	0.5	0.6	0.7	n-value
	AT	0.3	0.375	0.45	0.525	0.6	n-value
X2	CT	86	155	234	313	391	lb. in per in³
	AT	15	30	45	60	75	blows
X3	CT	4	7	10	13	16	% by weight
	AT	-1.5	-0.75	0	-0.75	-1.5	% from optimum
X4	CT	0	2	4	6	8	no. of cycles
	AT	0	1	2	3	4	no. of cycles
X5	CT	0	2	4	6	8	no. of cycles
	AT	0	1	2	3	4	no. of cycles

Note: *CT* = cement stabilized; *AT* = asphalt stabilized; *X1* = gradation *n*-value; *X2* = compaction effort; *X3* = cement or asphalt content; *X4* = number of freeze–thaw cycles; *X5* = number of wet–dry cycles; and *n* = exponent in $p=(d/D)^n$, where *p* is the percentage of material passing size *d*, and *D* is the maximum size.

Regression equations were developed to predict the erosion (weight loss) after 7 and 31 days.

A regression equation was also developed to predict the erosion with curing age as one of the variables. Erosion decreased with compaction effort and portland cement content. Erosion was a minimum at a gradation *n*-value of about 0.5. The erosion increased with the number of freeze–thaw cycles and the number of wet–dry cycles for low cement contents, low compaction efforts, and small gradation *n*-values. At high cement contents and high compaction efforts, the freeze–thaw and wet–dry cycles had no detrimental effect on the erosion. The variables used are given in Table 2 along with the coefficients, and other properties of the regression equations. The coefficients of all the variables are given to show the effect of all the variables in the model. Some of these variables can be omitted from the model without reducing the fit drastically. The following reduced equations were obtained:

$$\text{Eb7} = 758.39 - 698.86 \log(\text{X3}) \quad (R^2 = 60 \text{ percent})$$

$$\text{Eb31} = 459.88 - 436.59 \log(\text{X3}) \quad (R^2 = 72 \text{ percent})$$

$$\text{Ebage} = 3.88 - 1.37 \log(\text{X3}) - 0.865 \log(\text{age}) \quad (R^2 = 82 \text{ percent})$$

TABLE 2 REGRESSION COEFFICIENTS FOR PORTLAND CEMENT STABILIZED SAMPLES

VARIABLE	COEFFICIENTS		
	Eb31	Eb7	Ebage (log)
constant	1178.1814	1584.2571	2.9552
X1	-1459.7314	-1334.6571	-1.3965
X2	-0.8221	-1.1912	0.009515
$X1^2$	973.6656	1589.5526	5.8716
$X2^2$	-0.0011	0.0006	0.0000
log (X3)	-958.1171	-1455.1376	-1.7628
log (X4)	88.8042	-	-
log (X5)	17.2777	-	-
log (age)	-	-	-0.8727
X1X2	0.9210	-1.6583	-0.0198
X1X3	42.9041	36.6005	0.1836
X1X4	-23.0810	-	-
X1X5	-0.3667	-	-
X2X3	0.0939	0.1846	-0.0002
X2X4	-0.0025	-	-
X2X5	-0.0161	-	-
X3X4	-0.2540	-	-
X3X5	-0.2009	-	-
X4X5	0.7401	-	-
UCS	-	-	-
UCS^2	-	-	-
R^2	86%	73%	86%
Adj. R^2	81%	70%	85%
Std. error	67.25	152.88	0.125
Coef. var.	63.3%	76.4%	10.9%
n	68	84	194

Note: *Eb7* = brush erosion after 7 days moist curing (g/m²); *Eb31* = brush erosion 31 days after compaction (g/m²); *Ebage* = brush erosion with age as a variable (g/m²); *X1* = gradation *n*-value (0.3 to 0.7); *X2* = compaction energy (86 to 391) (lb-in./in.³); *X3* = Portland cement content (1 to 16) with percentage by weight; *X4* = number of freeze–thaw cycles (0 to 8); *X5* = number of wet–dry cycles (0 to 8); and *n* = exponent in $p = (d/D)^n$, where *p* is the percentage of material passing size *d*, and *D* is the maximum size.

where

Eb7	=	brush erosion after 7 days moist curing,
Eb31	=	brush erosion 31 days after compaction,
Ebage	=	brush erosion with curing age as variable,
X3	=	portland cement content, and
Age	=	curing age.

The 32 samples, tested as part of the composite design procedure used pit-run gravel as aggregate. A number of samples were also tested to investigate the effect on erosion of the use of crushed stone as aggregate. No difference in weight loss characteristics could be detected between gravel and crushed stone-stabilized samples, and the results were pooled in the development of the equations.

The unconfined compressive strength (UCS) of the samples was also obtained after 31 days. An equation was developed to predict erosion (as weight loss measured from the brush test) from the 31 day UCS:

$$\log(Eb31) = 2.9241 - 0.00085\ UCS + 0.000000112(UCS)^2$$

where

(Eb31)	=	brush erosion 31 days after compaction (g/m^2), and
UCS	=	unconfined compressive strength (psi).

Brush Test on Asphalt-Stabilized Materials

The erosion was predicted from the average weight loss of two brushings after the last cycle, with the sample in a semiwet condition.

The procedure of analysis used for the portland cement-stabilized material was also used for the asphalt-stabilized material. Of the main effects, compaction effort, asphalt content and number of wet–dry cycles were significant at $\alpha = 5$ percent. A number of regression equations to predict the erosion (weight loss) based on the test results were developed. Regression coefficients and ranges of variables used in the development are given in Table 3. A regression equation was also developed to predict the erosion with curing age as one of the variables (Table 3).

The following reduced models were obtained:

$$Eb4 = 209.69 - 116.98 \log(X2) + 149.44\ (X3) + 281.05\ (X1)^2 - 395.59\ (X1)(X3)$$
$$(R^2 = 72 \text{ percent})$$

$$Eb16 = 336.12 - 139.18(X1) - 140.8 \log(X2) + 3522277\ (X5)^2 - 15540.2\ (X3)(X5)$$
$$(R^2 = 61 \text{ percent})$$

$$Ebage = 290.17 - 92.86 \log(X2) + 72.10\ (X3) - 110.69 \log(age) - 192.49\ (X1)(X3)$$
$$(R^2 = 83 \text{ percent})$$

where

Eb4	=	brush erosion 4 days after compaction (g/m^2),
Eb16	=	brush erosion 16 days after compaction (g/m^2),
Ebage	=	brush erosion with age as variable (g/m^2),
X1	=	gradation *n*-value,
X2	=	compaction energy (Marshall hammer blows),
X3	=	asphalt content (percentage from optimum),
X5	=	number of wet–dry cycles, and
age	=	age after compaction (days).

The erosion (weight loss) reached a minimum at a gradation *n*-value of about 0.5. Low compaction efforts and small gradation *n*-values increased the erosion at all levels. The effect of the freeze–thaw cycles was in general small and not significant. At low asphalt contents the weight loss decreased slightly with an increase in the number of freeze–thaw cycles, while at high asphalt contents the weight loss increased slightly with an increase in the number of freeze–thaw cycles.

Asphalt-stabilized materials are subject to stripping, which increases the erosion. Asphalt stripping was simulated in the experimental program by wet–dry cycles because standard tests are not available to simulate stripping conditions with time. The results show that the weight loss of the samples is significantly influenced by these cycles, but it is not clear how well the wet–dry cycling simulated stripping conditions. The weight loss increased with the number of wet–dry cycles in all cases tested, but the rate of increase was higher at low asphalt contents, smaller size aggregates, and low compaction efforts. The weight loss (stripping) decreased as asphalt content increased. The erosion (weight loss) of the asphalt-stabilized samples decreased with age and asphalt content.

Rotational Shear Test on Portland Cement-Stabilized Materials

The erosion of portland cement-stabilized samples was evaluated with cement content as the only variable. A number of parameters may be obtained from the results. Typical results are shown in Figure 4 and the results of the tests are given in Table 4. A rate of erosion before the critical shear stress (T_c) is reached, and the rate after T_c can be obtained. The critical shear stress was defined as the shear stress of the water on the sample at which significant erosion begins. Two straight lines were visually plotted to obtain the erosion rates and the value of T_c. Exponential regression curves were also calculated. The exponential regression may be used to predict the erosion, based on the shear stress, but cannot be used to identify T_c.

The curing age obviously has an influence on the erosion. Samples were tested after different curing ages. Results of tests conducted at different curing times on one sample are shown in Figure 5. The critical shear stress increased with curing age. The erosion rates showed differences, but a statistical correlation could not be identified. The differences were small, in general, and the erosion rates appeared to be almost constant within the curing ages incorporated in the testing program (7 to 31 days).

TABLE 3 REGRESSION COEFFICIENTS FOR ASPHALT STABILIZED SAMPLES

VARIABLE	COEFFICIENTS		
	Eb16	Eb4	Ebage
Constant	646.5860	537.0200	511.6115
X1	-1775.8868	-1553.7052	-634.9318
X2	-	-5.9968	-
X3	47.9811	18.2000	69.2456
X4	61.2182	-	-
X5	25.1490	-	-
$X1^2$	1807.8486	1650.9968	707.6971
$X2^2$	-	0.0290	-
$X3^2$	9.2881	8.5796	3.6533
$X4^2$	-1.0083	-	-
$X5^2$	3.0548	-	-
log (X2)	-167.3990	-	-174.1663
log (age)	-	-	-102.2842
X1X2	4.1211	4.7099	1.9436
X1X3	-219.7609	-293.3122	-192.4926
X1X4	-76.9163	-	-
X1X5	-10.9880	-	-
X2X3	0.6593	0.2215	0.0635
X2X4	-0.4464	-	-
X2X5	-0.3365	-	-
X3X4	14.2844	-	-
X3X5	-18.6797	-	-
X4X5	-1.6376	-	-
R^2	90%	79%	66%
Adj.R^2	75%	71%	63%
Std. error	22.7994	22.5976	22.2979
Coef. var.	36.3%	29.5%	48.0%
number	33	33	109

Note: *Eb4* = brush erosion 4 days after compaction (g/m^2); *Eb16* = brush erosion 16 days after compaction (g/m^2); *Ebage* = brush erosion with age as a variable (g/m^2); *X1* = gradation *n*-value (0.3 to 0.6); *X2* = compaction energy (15 to 90) from Marshall hammer blows; *X3* = asphalt content (–1.5 to 1.5), percentage from optimum; *X4* = number of freeze–thaw cycles (0 to 4); *X5* = number of wet–dry cycles (0 to 4); and *n* = exponent in $p=(d/D)^n$, where *p* is the percentage of material passing size *d*, and *D* is the maximum size.

The effect of erosion time on erosion rate was also investigated. The erosion rate was found to be a function of a reference erosion rate and the logarithm of time. An erosion time of 10 min was selected as the reference time.

$$E_r = 1.095 + 0.88 * E_{10} + 1.0032 * \log (t)$$

R^2 = 84 percent, adjusted R^2 = 80 percent, and n = 11

where

E_r = erosion rate (g/m^2·min),
E_{10} = erosion rate after 10 min (g/m^2·min), and
t = erosion time (min).

The equation is only valid for erosion times of approximately more than 5 min. The weight losses of the samples at small

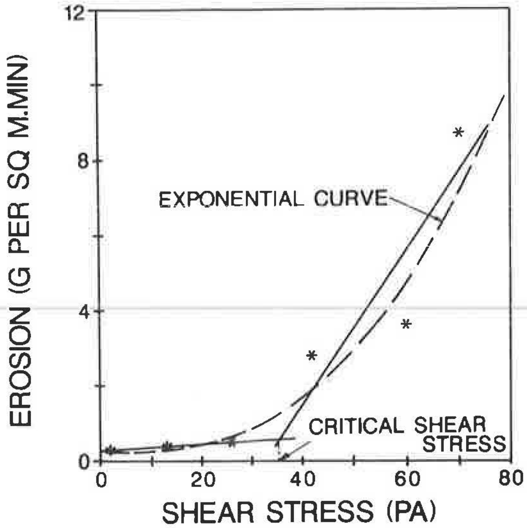

FIGURE 4 Typical rotational shear test results.

erosion times (approximately less than 5 min) were not measured, and therefore cannot be predicted by the equation.

All of the parameters given in Table 4 were compared with each other. The most useful and significant comparisons were critical shear stress and portland cement content. A regression equation was developed to relate the critical shear stress to the brush erosion (weight loss). Critical shear stresses are compared with brush weight loss results in Figure 6. The regression equation has an adjusted R^2 value of 61 percent and is given as follows:

$$T_c = 57.517 - 18.4 * \log (E_b)$$

$$R^2 = 64 \text{ percent}, n = 13$$

where

T_c = critical shear stress (Pa),
E_b = brush weight loss (g/m^2).

The materials tested included three different gradations, but no significant differences in T_c of the samples could be detected with the different gradations.

The rotational shear testing has a major limitation in that unstabilized cohesionless materials cannot be tested this way. For example, it was found that samples with cement contents of less than 1 percent had insufficient cohesion for testing in this device.

Brush Test on Lean Concrete Materials

Loss of weight of lean concrete materials depends largely on the portland cement content and the water–cement (W/C) ratio.

TABLE 4 RESULTS OF ROTATIONAL SHEAR TESTS ON PORTLAND CEMENT STABILIZED SAMPLES

Cement content (%)	Curing time (days)	Erosion rate 1	Critical Shear Stress	Erosion rate 2	Brush erosion (g/m² min)	a	b
1	7	-	4.5	2.04	817	-	-
2.5	7	-	5.5	0.074	265	-	-
	21	0.183	11.0	0.376	155	0.0508	-0.527
3.0	7	-	10.0	-	552	-	-
	31	0.108	13.0	2.76	331	0.0432	0.185
3.0	7	-	7.0	0.104	839	-	-
	31	0.167	12.0	4.0	486	0.1037	-0.683
4.0	7	-	6.0	0.18	309	-	-
	21	0.004	14.0	0.074	155	0.0174	-0.408
	31	0.019	24.0	0.19	66	0.0260	-0.804
7.0	7	-	6.0	0.18	199	-	-
	21	0.011	26.0	0.16	88	0.0229	-0.703
	31	0.011	33.0	0.16	66	0.0218	-0.627

Note: Erosion Rate 1 = erosion rate before T_c(g/m^2 · min/Pa); Erosion Rate 2 = erosion rate after T_c (g/m^2 · min/Pa); a,b = coefficients in log (erosion) = $a*T + b$; T_c = critical shear stress (Pa); T = shear stress (Pa); 1 kPa = 0.145 psi; 1 m = 3.281 ft; and 1 kg = 2.205 lb.

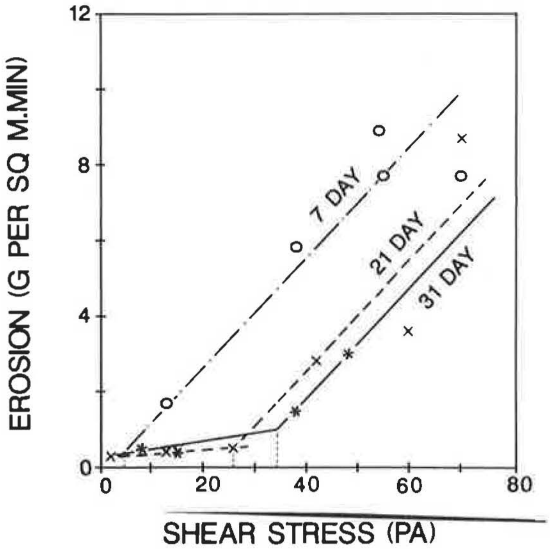

FIGURE 5 Change in critical shear stress with curing time.

The major advantage of lean concrete materials, with regard to erosion, is that loose particles are not as prevalent on the surface as in the case of portland cement-stabilized materials because of the type of compaction. The type of erosion caused by the bristles of the brush makes it impossible to detect differences due to compaction method on the surfaces of the samples. The weight losses induced by the brush bristles on the lean concrete samples were in the same order as those of the cement-stabilized samples.

CORRELATION WITH PAVEMENT CONDITIONS

The laboratory results need to be related to the actual behavior of the pavement to be useful in improving the design of subbases and shoulders. Water between the slab and subbase generates the surface erosion of the subbase or shoulder when the movement of the slab forces the water out of the void at high velocities that induce high shear stresses. Little is known about the flow characteristics of water between the slab and an essentially impervious subbase. The flow of the water under the slab is complex and influenced by a number of factors such as slab deflection velocity, the magnitude of the deflections, and void dimensions. At small void thicknesses, the water will resist the slab deflection.

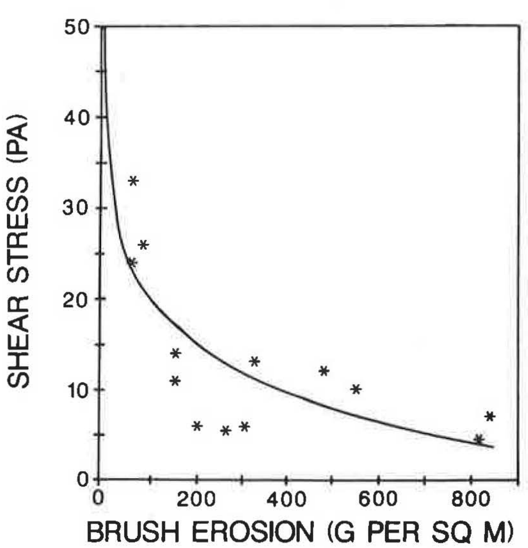

FIGURE 6 Critical shear stress versus brush erosion.

During the late 1970s, French researchers (*22*, *23*, *30*) investigated the flow of water on impervious subbases. In their theoretical calculations of the velocity of the water under the slab, they identified three void thickness zones in which water behaves differently. These zones were selected based on theoretical, laboratory, and in-situ observations.

1. Voids less than 0.5-mm (0.02-in.) thick—water behaves as a viscous fluid in these very thin layers.
2. Voids larger than 1-mm (0.04-in.) thick—water behaves as an ideal fluid in these voids.
3. Voids between 0.5- and 1-mm (0.02- to 0.04-in.) thick—this was identified as the transition zone where the fluid is neither ideal nor viscous.

The French results and hydraulic principles were used to obtain the water velocities and shear stresses induced by the water on the subbase under the slab. The slab movement was simulated by a flat, stiff plate rotating around an axis. This is a fair representation of the movement of the leave slab at the joint when the wheel load moves from the approach slab onto the leave slab. The water velocity was expressed as a parabolic distribution:

$$V = A(u/\delta)^2 + B(u/\delta) + C$$

At

$$y = 0,\ u = 0$$

Thus

$$C = 0$$

At

$$y = \delta,\ u = V_Z\theta \text{ (for small angles)}$$

Thus

$$B = V_Z\theta - A.$$

Further

$$\delta u/\delta x + \delta v/\delta y = 0$$

Thus

$$V = -\int (\delta u/\delta x)dy,$$

But

$$V = -V_Z \text{ (for small angles)}$$

Solving for A and B:

$A = -V_Z (3\theta + 1/\theta)$

$B = V_Z (4\theta + 1/\theta)$

The water velocity:

$\mu = A (y/\delta) + B (y/\delta)$

The shear stress:

$\tau = \mu\ [(2Ay/\delta^2) + B/\delta)]$

where

v = water velocity in the y-direction,
u = water velocity in the x-direction,
δ = void thickness,
θ = angle between the slab and the subbase,
μ = kinematic viscosity of water,
V_Z = speed of slab deflection, and
t = time.

These equations are true only when the water behaves as an ideal fluid. At very small void sizes the resistance of the water on the downward movement of the slab becomes important. Pnu (*23*) indicated that the minimum void thickness (after the slab deflection) for which the given equations can be used is about 1 mm (0.04 in.). As mentioned earlier, representative slab deflection velocities and void dimensions have not been established. The void dimensions and slab deflections depend on factors such as wheel load, temperature gradient, slab properties, and load transfer characteristics. The French researchers (*23*) speculated that the slab deflection velocities range from 1 to 100 mm/sec (0.04 to 4 in./sec).

The slab is not deflected at a constant velocity because it is accelerated from an initial stationary position by the wheel load until the reaction of the water becomes high enough to decelerate the slab to a position of equilibrium. At that position, the downward force of the wheel load is equal to the upward force of the water on the slab. This occurs at small void thicknesses where the viscous effect of the water becomes significant.

The French researchers (*23*) predicted a maximum water velocity under the approach slab, and between the approach slab and the shoulder of 2.8 m/sec (9.2 ft/sec). The maximum water velocity under the leave slab was predicted to be 4.4 m/sec (14.4 ft/sec). Materials erodible at a water velocity of 5 m/sec (16.4 ft/sec) were classified very erodible, and materials not erodible at a water velocity of 50 m/sec (164 ft/sec) were classified nonerodible. The influence of void size and slab deflection velocity on the shear stress is shown in Figure 7. These values are plotted from the equations for shear stress derived earlier (solid line), and from the French (22) results (dashed line). The shear stress induced by the water was used to describe the effect of the water on the subbase rather than the water velocity because the shear stress is better defined than the water velocity (average, bottom, maximum), and the rotational shear test provides shear stress values. The void length was taken as 0.75 m (2.46 ft), which can be considered a typical

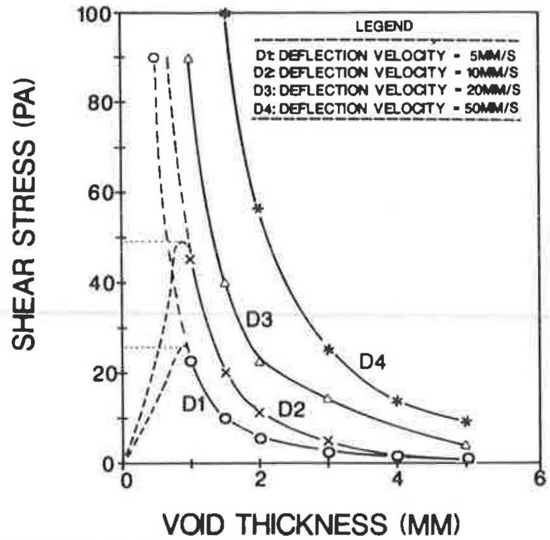

FIGURE 7 Effect of void size and velocity of slab deflection on the shear stress.

length of void at the joint. Both the water velocities and shear stresses increase rapidly at small void thicknesses. Infinitely high water velocities or shear stresses will not be reached because the reaction of the water at small void thicknesses will reduce the slab deflection and velocity of movement, as discussed previously.

Two shear stress values, 25 and 50 Pa (0.52 and 1.04 psf), were selected, based on the previously discussed experimental erosion results (Figures 6 and 7) data presented by the French researchers (22), to distinguish among erosion levels. A material that can resist erosion at a shear stress of 50 Pa (1.04 psf) should not show any signs of erosion during the life of the pavement. A material with a critical shear stress between 25 and 50 Pa (0.52 and 1.04 psf) should experience low erosion, while materials with critical shear stresses lower than 25 Pa (0.52 psf) should be subject to high erosion. The shape of the shear stress weight-loss curve (Figure 6) indicates that the weight loss drops off significantly at shear stresses of less than 20 to 25 Pa (0.42 to 0.52 psf). It must be emphasized that these values have not been verified and are provided only as a guideline.

DESIGN TO MINIMIZE EROSION

Unstabilized Materials

The shear stresses induced by the water (Figure 6) are likely to be higher than the T_c of the unstabilized materials. Therefore, any impervious unstabilized material used in rigid pavements will erode. The critical shear stress can be increased by increasing the compaction effort and the PI of the material, but it will probably not be sufficient to prevent pumping.

Unstabilized materials are subject to more than surface erosion. In most unstabilized materials, pumping is a combination of pore water pressure buildup and surface erosion. The more permeable the materials, the lesser the impact of surface erosion on pumping. The permeability at which the pore water pressure buildup becomes more important was not addressed in this study.

Stabilized Materials

Stabilized materials are usually relatively impervious and primarily subject to surface erosion. Stabilized materials can be strong enough to withstand surface erosion forces under the slab, depending on the composition of the material and environmental conditions.

The result of erosion testing will be most useful if the large number of variables and combinations of variables included in the testing program can be condensed to a few representative cases. This was done by identifying four climatic regions and four typical gradation-compaction effort combinations. The climatic regions were adapted from a map prepared by Carpenter et al. (*31*) and are shown in Figure 8. The laboratory tests were conducted to simulate four climatic conditions (warm dry, warm wet, cold dry, and cold wet) by using combinations of wet–dry and freeze–thaw cycles. The conditions in the wet regions (I) were simulated by eight wet-dry cycles and the freeze (A) and freeze–thaw (B) regions by eight freeze–thaw cycles.

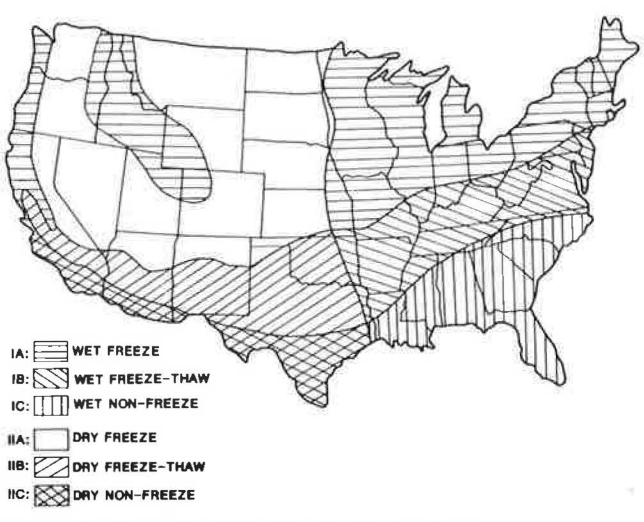

FIGURE 8 Climatic regions in the United States.

The weight loss or brush erosion was normalized to the erosion of a granular material stabilized with 3.5 percent cement, a gradation *n*-value of 0.5, and compacted with an energy of 234 lb-in./cu in. The erosion of this sample was chosen based on the study by Pnu and Ray (*22*). Results for the portland cement-stabilized materials are shown in Figures 9–12. From these relationships a portland cement content can be selected to ensure low erosion for each one of the four typical gradation-compaction effort combinations for each of the four climatic regions. The selection of a limiting shear stress or erosion level is still an open question. The value of 25 Pa (0.52 psf), recommended in the preceding section, can be used as a guideline in design of subbases and shoulders. A critical shear stress of 25 Pa (0.52 psf) corresponds with a brush erosion of about 60 $g/m^2 \cdot min$ and a normalized brush

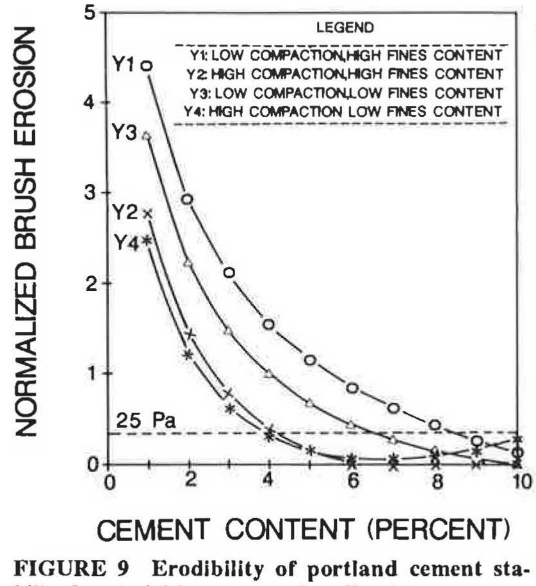

FIGURE 9 Erodibility of portland cement stabilized material in a warm, dry climate.

erosion of 0.33. A shear stress of 50 Pa (1.04 psf) corresponds to a brush erosion of about 3 g/m·min and a normalized brush erosion of 0.02. The curves can serve as a guideline in the design of rigid pavement subbases and shoulders.

Lean Concrete Materials

One of the characteristics of a stabilized layer is the existence of loose material on the surface after construction. These loose particles will erode regardless of the portland cement or asphalt content. Some of these particles can be removed by sweeping the surface of the subbase. The effect of construction on the erosion could not be included in the testing program, and is therefore not included in the erosion values presented in this paper. Indications are that the erosion of lean concrete materials will be approximately the same as the erosion of cement-

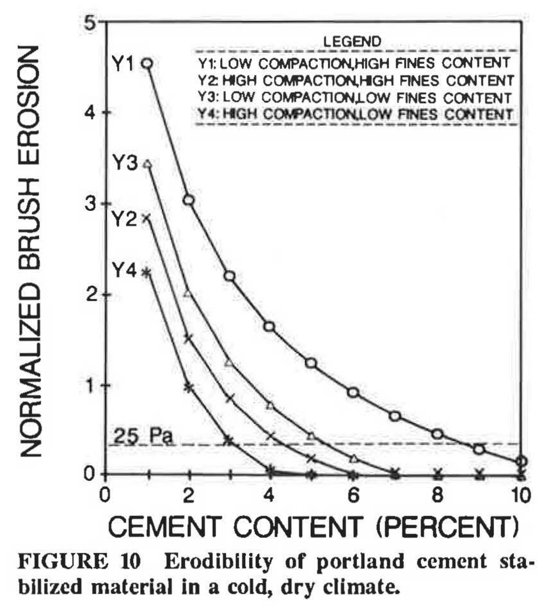

FIGURE 10 Erodibility of portland cement stabilized material in a cold, dry climate.

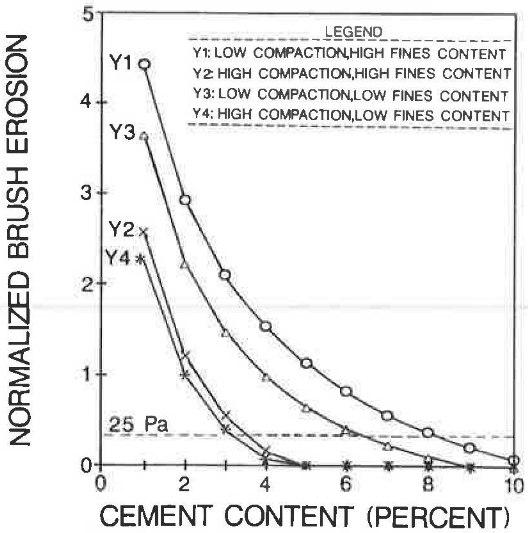

FIGURE 11 Erodibility of portland cement stabilized material in a warm, wet climate.

stabilized materials with the same portland cement content. Ray et al. (*32*) reported that a portland cement-stabilized material with 3 percent cement will be 7 times more erodible than a lean concrete material with 7 percent cement. The same order of difference in erosion between materials stabilized with 3.5 and 7 percent portland cement is shown in Figures 9–12.

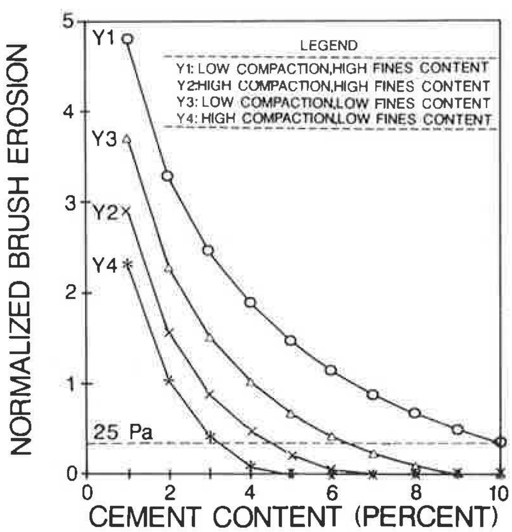

FIGURE 12 Erodibility of portland cement stabilized material in a cold, wet climate.

CONCLUSIONS

The brush test was appropriate for comparing the erosion of different lean concrete samples, but was inappropriate for comparing the effect of the different compaction efforts used in preparing lean concrete and cement-stabilized samples on erosion.

Use of the jetting test to characterize the erosion of unstabilized materials was the least successful. Although differences in erosion among unstabilized samples could be detected, the accuracy of the calculated and measured shear stresses are suspect.

Use of the rotational shear device was successful for determining the critical shear stresses and erosion rates of portland cement-stabilized materials. A relationship was developed between the brush erosion and the critical shear stress determined from the rotational shear test.

Portland cement content is the most important factor in the erodibility of cement-stabilized materials. The compaction effort and gradation are also important, but to a lesser extent. Environmental factors, such as freeze–thaw and wet–dry cycles, are only important when (*a*) the cement content is low, (*b*) the compaction effort is low, and (*c*) the material contains a large percentage of fines.

The results of the laboratory tests in asphalt-stabilized samples were not presented in this paper, but a summary of the main results is provided. The erosion of asphalt-stabilized materials is affected by the asphalt content, the compaction effort, and environmental factors. Wetting and drying have greater influence on the erosion of asphalt-stabilized materials than freezing and thawing.

The relationships of the brush erosion of asphalt and portland cement-stabilized materials to three material properties and two environmental factors were developed. These relationships can be used to predict the erosion of existing stabilized subbases or to design subbases with low erosion properties.

Indications are that the shear stresses induced by water under the slab are higher than the critical shear stress for unstabilized samples. Therefore, impervious unstabilized materials will always be affected by the pumping resulting from surface erosion. In less impervious unstabilized layers, the pore water pressure buildup is the controlling pumping mechanism.

Stabilized materials that may be eroded in a pavement, depending on their properties, are mainly the asphalt and portland cement contents. A family of curves was developed for four gradation-compaction effort combinations in each of four climatic regions, relating the normalized erosion to portland cement. These relations can be beneficial in the selection of rigid pavement subbase or shoulder materials to prevent pumping. Only the surface erosion is included in these curves. The strength and cost of these layers must be considered separately.

The guidelines presented for design have not been field verified, and should therefore be used with care. Further research is necessary, especially on the shear stresses present underneath the slab.

ACKNOWLEDGMENTS

The research was conducted under contract with FHWA with G. Ring as the project monitor. His assistance throughout the project is greatly appreciated. F. Glossic was responsible for building the equipment used in the study. The assistance and advice of Ross Duckworth during the experimental part of the study was invaluable.

REFERENCES

1. J. H. Woodstorm. Erodibility Testing and Development of Lean Concrete Base in California. Presented at International Seminar on

Drainage and Erodibility at the Concrete Slab–Subbase–Shoulder Interface, Paris, France, March 24–25, 1983.
2. L. L. Litton and R. A. Lohnes. Soil–Cement for Use in Stream Channel Grade-Stabilization Structures. In *Transportation Research Record 839*. TRB, National Research Council, Washington, D.C., 1982, pp. 33–37.
3. P. J. Nussbaum and B. E. Colley. Dam Construction and Facing with Soil-Cement. In *Research and Development Bulletin*, Portland Cement Association, Skokie, Ill., 1971.
4. R. N. Bhasin. *Erodibility of Sand–Clay Mixtures as Evaluated by a Water Jet*. MSCE thesis. Purdue University, West Lafayette, Ind., Aug. 1969.
5. U. Dash. *Erosive Behavior of Cohesive Soils*. Ph.D thesis. Purdue University, West Lafayette, Ind., Jan. 1968.
6. R. E. Passwell. *Special Report 135: Causes and Mechanisms of Cohesive Soil Erosion: The State of the Art*. TRB, National Research Council, Washington, D.C., 1973, pp. 52–74.
7. W. H. Graf. *Hydraulics of Sediment Transport*. McGraw–Hill Company, New York, N.Y., 1971.
8. V. A. Vanoni. Sedimentation Engineering. In *ASCE, Manuals and Reports on Engineering Practice, No. 54*, New York, N.Y., 1975.
9. W. H. Espey. *A New Test to Measure the Scour of Cohesive Sediment*. Technical Report HYD 01-6301. Hydraulic Engineering Laboratory, Department of Civil Engineering, University of Texas, Austin, Tex., April 1963.
10. W. L. Moore and F. D. Masch. Experiments of the Scour Resistance of Cohesive Siments. *Journal of Geophysical Research*, Vol. 67, No. 4, April 1962, pp. 1437–1449.
11. K. Arulanandan, A. Sargunam, P. Loganathan, and R. B. Krone. *Special Report 135: Application of Chemical and Electrical Parameters to the Prediction of Erodibility*. TRB, National Research Council, Washington, D.C., 1973, pp. 42–51.
12. M. R. Akky and C. K. Shen. *Special Report 135: Erodibility of a Cement-Stabilized Sandy Soil*. TRB, National Research Council, Washington, D.C., 1973, pp. 30–41.
13. M. R. Akky. *Erodibility of Soil-Cement*. Ph.D. thesis. Department of Civil Engineering, University of California at Davis, Davis, 1974.
14. R. P. Chapuis and T. Gatien. Quantitative Measurements of the Scour Resistance of Clays. *Canadian Geotechnical Journal*, May 1983.
15. W. T. Spencer, H. Allen, and P. C. Smith. Pavement Research Project in Indiana. *Bulletin 116*, HRB, National Research Council, Washington, D.C., 1952, pp. 1–56.
16. C. W. Allen and L. D. Childs. Pavement Research Project in Ohio. *Bulletin 116*, HRB, National Research Council, Washington, D.C., 1955, pp. 57–70.
17. F. N. Scrivner. *Special Report 73: Structural Deterioration of Test Pavements: Rigid*. HRB, National Research Council, Washington, D.C., 1962, pp. 186–197.
18. L. D. Childs, B. E. Colley, and J. W. Kapernick. Tests to Evaluate Concrete Pavement Subbases. *ASCE Journal of the Highway Division*, Vol. 83, No. HW3, July 1957, pp. 1297–1; 1297–40.
19. F. Burggraf. *Special Report 4: Test One-MD*. HRB, National Research Council, Washington, D.C., 1952, 142 pp.
20. B. J. Dempsey. Laboratory and Field Studies of Channeling and Pumping. In *Transportation Research Record 849*, TRB, National Research Council, Washington, D.C., 1982, pp. 1–11.
21. E. J. Yoder, J. A. Havers, W. P. Chamberlain, and R. D. Walker. *Base Course Requirements for Rigid Pavements*. Technical Report 183, Cold Regions Research and Engineering Laboratory, Hanover, N.H., Oct. 1966.
22. N. C. Pnu and M. Ray. The Erodibility of Concrete Pavement Sub-base and Improved Subgrade Materials. In *Bulletin de Liaison des Laboratoires des Ponts et Chaussées, Special Issue 8*, Paris, France, July 1979, pp. 32–45, (in French).
23. N. C. Pnu and M. Ray. The Hydraulics of Pumping of Concrete Pavements. In *Bulletin de Liaison des Laboratories des Ponts et Chaussées, Special Issue 8*, Paris, France, July 1979, pp. 15–31, (in French).
24. *Standard Specifications for Highway Materials and Methods of Sampling and Testing—Part II: Methods of Sampling and Testing*. 10th ed. AASHTO, Washington, D.C., 1970.
25. *Thickness Design for Concrete Highway and Street Pavements*. Portland Cement Association, Skokie, Ill., 1984.
26. *AASHTO Interim Guide for Design of Pavement Structures, AASHTO, Chapter III Revised*. AASHTO, Washington, D.C., 1981.
27. A. J. Van Wijk. *Design to Prevent Pumping: (1) Subbase Erosion and (2) Economic Modeling*. Ph.D. thesis. Purdue University, West Lafayette, Ind., May 1985.
28. W. G. Cochran and G. M. Cox. *Experimental Design*. 2nd ed. J. Wiley and Sons, New York, N.Y., 1957.
29. V. L. Anderson and R. A. McLean. *Design of Experiments: A Realistic Approach*. Marcel Dekker, Inc., New York, N.Y., 1974.
30. M. Ray. Drainage and Erodibility at Contacts Between Concrete Slab, Subbase and Shoulder. Presented at the International Seminar on Drainage and Erodibility at the Concrete Slab–Subbase–Shoulder Interface, Paris, France, March 24–25, 1983.
31. S. H. Carpenter, M. I. Darter, and B. J. Dempsey. *A Pavement Moisture Accelerated Distress (MAD) Identification System*. R/-81/079, FHWA, U.S. Department of Transportation, Washington, D.C., 1981.
32. M. Ray, J. Christory, and J. Poilane. Drainage and Erodibility: International Seminar Synthesis and New Research Results Related to Field Performance. *Proc., Third International Conference on Rigid Pavement*, 1985, pp. 609–624.

The contents of this paper reflect the views of the authors who are responsible for the facts and the accuracy of the data presented here.